2000

Hydrodynamics, Bottom Boundary Layer Processes and Sediment Transport on the South-Central Louisiana Inner Shelf: the Influence of Extratropical Storms and Bathymetric Modification.

David Alton Pepper
Louisiana State University and Agricultural & Mechanical College

INFORMATION TO USERS

This manuscript has been reproduced from the microfilm master. UMI films the text directly from the original or copy submitted. Thus, some thesis and dissertation copies are in typewriter face, while others may be from any type of computer printer.

The quality of this reproduction is dependent upon the quality of the copy submitted. Broken or indistinct print, colored or poor quality illustrations and photographs, print bleedthrough, substandard margins, and improper alignment can adversely affect reproduction.

In the unlikely event that the author did not send UMI a complete manuscript and there are missing pages, these will be noted. Also, if unauthorized copyright material had to be removed, a note will indicate the deletion.

Oversize materials (e.g., maps, drawings, charts) are reproduced by sectioning the original, beginning at the upper left-hand corner and continuing from left to right in equal sections with small overlaps.

Photographs included in the original manuscript have been reproduced xerographically in this copy. Higher quality 6" x 9" black and white photographic prints are available for any photographs or illustrations appearing in this copy for an additional charge. Contact UMI directly to order.

Bell & Howell Information and Learning
300 North Zeeb Road, Ann Arbor, MI 48106-1346 USA
800-521-0600

HYDRODYNAMICS, BOTTOM BOUNDARY LAYER PROCESSES AND SEDIMENT TRANSPORT ON THE SOUTH-CENTRAL LOUISIANA INNER SHELF: THE INFLUENCE OF EXTRATROPICAL STORMS AND BATHYMETRIC MODIFICATION

A Dissertation

Submitted to the Graduate Faculty of the
Louisiana State University and
Agricultural and Mechanical College
in partial fulfillment of the
requirements for the degree of
Doctor of Philosophy

in

The Department of Oceanography and Coastal Sciences

by
David A. Pepper
B.A., University of Windsor, 1994
M.A., University of Windsor, 1996
December, 2000

ACKNOWLEDGEMENTS

The author wishes to thank numerous individuals and agencies. Financial support for this research was provided by the United States Minerals Management Service under Contract #30660/19911. Personal financial support was provided through a Fellowship from the Louisiana State Graduate School and subsequently through a Research Assistantship from Dr. Gregory W. Stone of the Coastal Studies Institute. Supplementary data were supplied by the United States National Oceanic and Atmospheric Administration. Academic guidance was provided by an advisory committee that included Drs. Gregory W. Stone (Major Professor), John W. Day, Jr., Keith G. Henderson, Masamichi Inoue, Babak Naghavi, Robert V. Rohli, Lawrence J. Rouse, Jr., Ping Wang, Charles A. Wilson, and William J. Wiseman, Jr. Instrument design, construction, calibration and field deployment was facilitated by the Coastal Studies Field Support Group, which included: Rodney G. Fredericks (Director), Joel M. Chaky, J. Steven Dartez, Floyd A. DeMers, William J. Gibson, Mark W. Miller, and Walker D. Winans. Computer assistance was provided by Xiongping Zhang. Numerous friends and fellow students offered assistance throughout the project. Finally, the author wishes to thank his family, Barry, Lorraine, Jamie, Kristyn, and Rob Pepper for their continuing support throughout his academic career.

TABLE OF CONTENTS

LIST OF TABLES

LIST OF FIGURES

ABSTRACT

The south-central Louisiana inner shelf has several distinctive characteristics that are not well accounted for by common hydrodynamic and sediment transport models, including a high-frequency wave regime, low fair-weather hydrodynamic energy levels, a coastal orientation parallel to most storm approaches, and a prominent submerged sand body (Ship Shoal). To address these unique considerations, inner-shelf processes were studied using three instrumentation systems deployed on the seaward and landward sides of the shoal between November, 1998 and January, 1999. These instruments were designed to measure hydrodynamic characteristics, suspended sediment concentration, and bed level, which were used to calculate bottom boundary layer parameters and predict sediment transport.

Quasi-periodic extratropical storms were the most important forcing mechanism during the deployment, typically causing increases in wave height and frequency, mean and oscillatory current velocity, shear velocity, suspended sediment concentration, and sediment transport, which was predominantly offshore. One energetic event was not initiated by local storm activity but consisted of a group of high waves propagating from offshore. Some landward sediment transport also occurred during typical fair weather conditions.

Considerable inter- and intra-storm variability was noted and a storm classification system was established. Type 1 Storms were associated with anticyclonic activity, northeasterly winds, southerly waves, and southwesterly currents and sediment transport. Type 2 Storms were migrating cyclones that generated energetic, rotational, pre- and post-frontal winds and currents, and caused

high northerly swell that transformed into southerly sea. Overall, northwesterly winds during these events caused southeasterly currents and sediment transport. Aside from increases in wind speed, Type 3 Storms were similar to fair weather.

Ship Shoal influenced hydrodynamics significantly. Mean wave height and period on the landward side were 36% and 9% lower, respectively, than on the seaward side, due to attenuation. Across-shelf currents were offshore on the seaward side and onshore on the landward side, where flow speed was10% higher. Sediment flux across Ship Shoal appears to have been divergent during fair weather conditions and convergent during extratropical storms. It is clear, therefore, that winter hydrodynamic and sedimentary processes on the "low energy" Louisiana inner shelf are very dynamic, largely due to extratropical storms.

CHAPTER 1

INTRODUCTION

Geophysical systems are not comprised of a few easily identified processes that cause simple and predictable morphological responses—instead, innumerable variables are subtly interconnected by positive and negative feedback mechanisms over a range of spatial and temporal scales. Although the coastal environment is an ideal illustration of this, until recently, the geographical limit to "coastal processes" was often assumed to extend little beyond the surf zone, with waves and wave-driven currents acting as the primary, if not exclusive, agents of morpho-sedimentary change. In the past few decades, however, it has become increasingly apparent that coastal processes operate in much deeper water, and that inner shelves, which comprise the zone between the shoreline and a few tens of meters in depth, play an integral role in coastal dynamics. Far from being stagnant and uncomplicated, inner-shelf systems are instead driven by complex interlinkages of atmospheric, hydrodynamic, sedimentary and biotic processes and responses (Niedoroda et al., 1985; Wright, 1995).

There is a considerable body of research that deals with the fundamental physical processes that operate throughout the water column and at the seabed on inner shelves, much of which has been conducted in the laboratory or is based on theoretical considerations (overviews may be found in Soulsby, 1987; Nielsen, 1992, or Wright, 1995). Furthermore, the crucial influence of atmospheric storms and shelf bathymetry to hydrodynamics and sediment transport on inner shelves is clearly recognized (Wright, 1995). However, the role of these small- and large-scale processes on a particular shelf is complicated considerably by the influence of specific local and regional factors. Despite

this, many inner shelves, with a variety of unique characteristics, have never been studied, owing both to inherent technical and logistical difficulties, and to the fact that their importance within the coastal system has only recently been realized. As a result, the models of inner-shelf hydrodynamics and sediment transport that have emerged tend to be most applicable in a limited range of environments, with disparate results sometimes occurring at other locations. Specifically, the majority of studies have been conducted on exposed Atlantic or Pacific inner shelves, where hydrodynamic influences are more energetic, and long period swell waves are more influential, than in low energy environments such as the northern Gulf of Mexico.

This dissertation is an attempt to use extensive field data to address interactions between diverse meteorological, hydrodynamic and sedimentological variables on the Louisiana inner shelf. In particular, it will focus on the role of extratropical storms in generating waves, currents, bottom boundary layer responses and sediment transport in the region and the influence of bathymetric configuration in modulating their characteristics. This will allow models for inner-shelf processes to be extended to an oceanographic and bathymetric regime unique in comparison with most shelves that have been studied previously. To provide more detail regarding these points, the following section is designed to be a general review of the results of inner-shelf research, emphasizing the effect of meteorology, and particularly winter storms, on hydrodynamics, bottom boundary layer parameters and sediment transport. Chapter 2, on the other hand, discusses the specific, and unique, characteristics of the study area as they pertain to these parameters.

1.1 Previous Research

The inner shelf is the region adjacent to the coast where the entire water column is dominated by friction with the overlying atmosphere and the underlying seabed (Wright, 1995). In geographical terms, it lies between the shoreline and the mid-continental shelf, with the surf zone as its most landward portion (Niedoroda et al., 1985). The dominant hydrodynamic variables that operate in this environment are infragravity and wind waves, as well as currents generated by winds and tides. These hydrodynamic influences jointly exert stress on the water column and seabed, causing sediment to be mobilized and transported along the bed or in suspension (Soulsby, 1987; Wright, 1995; Kim et al., 1997). Given the importance of wind as a forcing mechanism, it follows that the passage of atmospheric storms often results in hydrodynamic responses, bottom boundary layer modification, and sediment transport on inner shelves. Not surprisingly, therefore, field research has often demonstrated that storm events can be responsible for transporting very large quantities of sediment in comparison with fair weather conditions.

The general model for inner-shelf sediment transport that has emerged from previous studies is one in which fair weather wave asymmetry gradually moves sediment onshore, while during storms, high wave orbital currents suspend sediment that is then transported offshore by downwelling mean flows (Niedoroda et al., 1985; Wright et al., 1991; Nittrouer and Wright, 1994). Furthermore, it is commonly assumed that along-shelf transport of suspended sediment during both fair weather and storm conditions is much higher than across-shelf transport, as a result of stronger along-shore mean flows. Considerable deviation from these general models results, however, from variability in meteorological conditions, local geology, bathymetry, and physical oceanography.

Additionally, a variety of complex and poorly-understood interactions and feedback mechanisms operate in the bottom boundary layer. For example, while it is sometimes assumed that waves provide the shear stress (or "stirring mechanism") that entrains sediment that is then transported by mean currents, recent research has demonstrated that waves and currents interact in a highly non-linear fashion, complicating sediment transport predictions (Grant and Madsen, 1979; Grant and Madsen, 1986). The following paragraphs are intended to serve as a discussion of field research conducted on inner shelves around the world, highlighting "typical" hydrodynamic, bottom boundary layer and sedimentary responses to meteorological forcing, as well as the sources of deviation from these responses.

A large proportion of research dealing with continental-shelf response to meteorological forcing emphasizes the importance of storms in generating high bed stress, due to the combined effects of waves and currents, and the concomitant increase in sediment transport, which is variable in direction. Nittrouer and Wright (1994) stated, for example, that sediment particles can be transported tens of kilometers seaward during storms, in contrast to fair weather conditions, when sediment transport may be landward, or may not occur at all. Lyne et al. (1990a, 1990b) estimated that 91% of sediment transport along the mid-continental shelf of the U.S. Atlantic coast occurs during storms due to strong bed stresses resulting from wave and current interaction. Niedoroda and Swift (1981) and Niedoroda et al. (1984) stated that winter storm activity provides an important contribution to the long-term retreat of the Long Island coast. They observed offshore and alongshore transport as a result of the combination of high wave energy and strong downwelling currents at the peak of a winter storm, while during the waning

phases of the storm, when upwelling occurred, the waves were generally too low to entrain sediment. Fair weather periods were characterized by wave asymmetry that transported sediment landward at depths shallower than 10 m. In contrast, Vincent et al. (1981) suggested that winter storms produce net onshore bedload sediment transport in the same region, accompanied by a shore-parallel transport of fine suspended sediment. The researchers did note, however, that offshore transport components were measured during one winter storm, and thus, that the study did not account for any variability in transport direction that may have depended on the specific wind conditions accompanying individual storms.

Despite well-documented differences in oceanographic regime, the continental shelf of the Pacific coast of North America seems to be characterized by similar storm-driven responses as the Atlantic. According to Cacchione and Drake (1990), over 50% of sediment transport during a one-year period on the northern California inner shelf occurred during that year's 20 stormiest days. The authors proposed that, during storms, sediment transport is predominantly offshore at depths less than 50 m, as a result of strong wave activity combined with downwelling, and alongshore in deeper water, due to oceanic currents. They noted that transport is almost always the result of an interaction between factors, most often mean and wave-orbital flows. Finally, they pointed out that transport rates and directions are strongly dependent upon the location and intensity of the storm, the regional pattern of wind stress, the magnitude of sea-level setup, and the bottom gradient. These results were corroborated by Cacchione et al. (1994), who calculated that offshore transport on the same shelf reached a maximum of 0.5 g $cm^{-1}s^{-1}$ during an early-March storm event. Cacchione et al. (1987) concluded that the repeated

occurrence of winter storms on the California coast generates high bottom stress due to the combined effects of waves and currents, which is ultimately a crucial factor in controlling the spatial distribution of bottom sediment.

Lynch et al. (1997) showed that sediment transport was dominated by large storms during an eight-week winter deployment in 90 m of water off the California shelf. Transport was predominantly along-shelf, although offshore, and occasionally, onshore components were recorded. Interestingly, although sediment concentrations of up to 0.75 g l^{-1} were measured, these did not necessarily correlate with high transport rates, since high concentrations were sometimes accompanied by weak mean currents. According to Gross et al. (1991), suspended sediment concentrations of 0.030 g l^{-1} over the California shelf are caused by high orbital velocities generated by winter storms, and as a result, 75% of the total annual sediment flux occurs between December and March. The researchers observed statistically-significant logarithmic current profiles, even under strong wave-orbital flows, and calculated apparent bottom roughness (z_{0c}) of up to 18 cm during winter storms. This was more than 25 times the typical non-storm value, and appears to have been the result of wave-current interaction. Similarly, Cacchione and Drake (1982) observed large increases in shear velocity and apparent bottom roughness (maximum values of 6.9 cm s^{-1} and 8.6 cm, respectively) at a depth of 18 m on the continental shelf of Alaska during a storm.

Research from Canada, New Zealand and the United Kingdom has also provided important contributions to the understanding of storm-induced bottom boundary layer and sedimentary processes. Li et al. (1997) measured two to threefold increases in shear stress, order of magnitude increases in apparent bed roughness, and two to three order of

magnitude increases in sediment transport on eastern Canada's Scotian shelf during storms. Although fair weather sediment transport in the region is determined almost exclusively by tidal flows, the researchers found that transport direction during storms is dependent on the direction of both waves and wind-driven currents, and showed a high degree of inter- and intra-storm variability. Amos et al. (1999) measured sediment transport maxima of 0.027 and 0.035 g $cm^{-1}s^{-1}$ at a 22-m deep location on the Scotian Shelf during two storms. Amos and Judge (1991) used the sediment transport model SEDTRANS in combination with field data to predict sediment transport at several sites on the eastern Canadian continental shelf. They concluded that long-term sediment transport varies over a range of temporal scales. At one site, for example, transport was dominated by storms of the longest return interval (32 years) and would thus not be well predicted using the patterns that occur during a "typical" winter storm. On the other hand, at more easterly sites, transport appeared to be dominated by waves and wind-driven currents generated by storms of a one-year return interval (a "typical" strong winter storm). Certain exceptions were noted in channels, however, where (semi-diurnal) tidal currents were shown to be the dominant long-term influence. Manighetti and Carter (1999) described a complex system in the Hauraki Gulf, New Zealand, in which sediment may be transported offshore at times, but remains in the shelf system as a result of rotating tidal currents, until it is ultimately lost through an adjacent channel to deep water. The authors stressed that storms are the dominant agents of sediment transport in the region, although the specific effect of an individual storm at a particular location is highly dependent upon local coastal geography. Green et al. (1995) discussed numerous responses to the passage of a severe winter storm from a 25-m deep site on the macrotidal

British North Sea shelf. They found that apparent bed roughness and sediment transport was two orders of magnitude higher during the storm than fair weather conditions. High suspended sediment concentrations resulted from incident wave and wave group activity, although transport resulting from wave orbital flows was minimal. Instead, net transport during the storm was largely due to sediment being suspended by waves and transported off- and alongshore by steady wind-driven flows that distorted the tidal ellipse.

A series of papers by Wright and others describes the influence of the passage of "Northeasters" (extratropical storms) over the inner shelf of the Mid-Atlantic Bight of North America in terms of distinct storm phases, or in certain cases, storm types. Wright et al. (1986) measured a net seaward flux of suspended sediment accompanied by a bed level change of 15 cm in the Middle Atlantic Bight during a single storm. Bed level response was characterized by four distinct stages: 1) negligible response to an initial peak in wind and current speed and suspended sediment concentration; 2) gradual erosion of the bed following this initial peak; 3) slow bed accretion during the second and stronger peak of the storm; 4) rapid bed accretion during the waning phases of the storm. Green et al. (1988) expanded on results from the same deployment. They stated that tidal currents prior to the storm and wind-driven offshore flows during the storm's initial phases controlled the transport direction, while later in the storm, transport turned onshore, against the mean flow direction, as a result of wave asymmetry.

Madsen et al. (1993) and Wright et al. (1994) reported maximum suspended sediment concentrations of 1.0 g l^{-1} within the lowest meter of the water column during a severe Northeaster. Suspended sediment transport during this event was highly dependent on the phase of the storm. During the storm's main phase, sediment flux was seaward as a

result of strong downwelling, in response to onshore winds. The later, swell-dominated, phase of the storm was characterized by the deployment's highest shear velocity as well as high suspended sediment concentration, although only low onshore fluxes occurred, owing to the presence of weak mean flows. Kim et al. (1997) characterized a Northeaster over the Mid-Atlantic Bight in terms of four phases: 1) an initial calm period when non-diffusive sediment transport was confined to the thin wave boundary layer (WBL); 2) the storm's onset, when the WBL thickened dramatically and suspended sediment transport increased; 3) the storm's peak, when bed stress, WBL thickness, and suspended sediment transport were at a maximum, causing the onset of sheet flow; and 4) the post-storm phase, when suspended sediment transport was confined to the thick WBL, owing to low current shear. Wright et al. (1991) summarized results from three years of field deployments in 7-17 m water depths on the Middle Atlantic Bight. They found that measurable contributions to sediment transport were made by mean flows, infragravity oscillations and incident waves. During storms, downwelling mean flows caused sediment to be transported offshore, while during fair weather and moderate energy conditions, mean currents transported sediment both on- and offshore. During all conditions, incident waves were the primary source of shear stress, and fluxes at both wind- and infragravity-wave frequencies were just as commonly onshore as offshore. Xu and Wright (1998) identified two significantly different storm types and their associated currents on the North Carolina shoreface. Southerly storms caused coastal set-down and upwelling, while northeasterly storms were associated with coastal set-up and downwelling. This appears to be one of the few references to coastal upwelling induced by winter storms in the region. It is clear from this research, therefore, that considerable

variability may occur during various stages of an individual storm as well as between different storms.

In addition to the complications to bottom boundary layer response and sediment transport introduced by local geographic, geological, and oceanographic differences, important influences are exerted by negative feedback, and other non-linear mechanisms, some of which will be introduced briefly in the following paragraphs. Glenn and Grant (1987) demonstrated by means of a sophisticated mathematical model that storms may result in enhanced turbulent mixing owing to wave-current interaction. This can, in turn, cause a reduction in shear stress owing to stable stratification of the water column by suspended sediment (Villaret and Trowbridge, 1991). Bed armoring occurs when sediment in size classes with a low critical entrainment stress is winnowed from the bed, leaving a higher bed concentration of less-easily-entrained size-fractions. Both sediment stratification and bed armoring have been shown to reduce sediment transport on the inner shelf during high-suspension events such as storms (Lyne et al., 1990b; Wiberg et al., 1994).

The morphology of the bed is also an important factor influencing bottom boundary layer characteristics and sediment transport. Li et al. (1996) described feedback between bed forms and suspended sediment transport during various meteorological conditions in the Middle Atlantic Bight. They found that during fair weather, bed ripple roughness, shear stress, and the amount of sediment suspended by vortices were directly related. During moderate storms, bed roughness reached a "breakoff point" where it, and hence vortex activity, began to decline with increasing shear stress. During severe storms, ripples on the bed were completely washed out, vortex activity was eliminated, and sheet

flow prevailed. These results are supported by more recent research at a 39-m deep location on the Canadian continental shelf by Li and Amos (1999). They observed the disappearance of large wave ripples during the strong combined wave and current flows that accompanied storm activity, and their subsequent re-formation as sediment fell out of suspension following the peak of the storm. Vincent and Green (1990) demonstrated that wave vortices had unpredictable effects on sediment transport over a rippled bed on the tide-dominated inner shelf of north Norfolk, U.K. Vortices were responsible for phase differences in sediment concentration and flow at various levels above the bed. As a result, sediment transport was onshore near the bed, slightly offshore between five and 10 cm above the bed, and onshore higher in the water column, indicating that measurement of many levels of a suspension profile may be necessary not only to accurately estimate sediment transport rate, but its direction as well. Boon et al. (1996) highlighted an interesting shallow-water (d~11.5 m) phenomenon in which interacting wave trains at swell and sea frequencies in an estuary caused an enhancement of sediment transport by a factor of $2^{0.5}$. Clearly, therefore, bottom boundary layer responses to hydrodynamic forcing are seldom simple or linear and researchers must be cognizant of a variety of potentially-complicated interactions.

Three general conclusions of the research discussed in the previous paragraphs are evident. First, storm-induced sediment transport is often so high that it dominates total long-term transport on inner shelves, despite the fact that storm activity typically accounts for only a small fraction of time. Second, certain responses to storm conditions on the continental shelf are fairly universal and are to some degree predictable. Common bottom boundary layer responses include changes in bed form morphology and apparent

bottom roughness, and increases in shear velocity and suspended sediment concentration. Sediment transport rate during storms tends to increase considerably over fair weather values, while transport direction is largely determined by, wind-driven, barotropic and tidal currents, as well as wave asymmetry non-linear wave-current interaction. Finally, hydrodynamic, bottom boundary layer and sedimentary responses to storm events are extremely sensitive to the duration, intensity, track, and wind structure of the storm, as well as to the characteristics of the coastal environment itself, including its geology, bathymetry, coastal orientation, and physical oceanography. These responses are further complicated by poorly-understood interactions between variables and complex negative feedback mechanisms such as stratification and changes in bed morphology. Thus, the general model of large off- and alongshore fluxes of sediment resulting from the passage of storms, while useful in some cases, must be applied with caution in the context of a specific inner-shelf site, such as, in the case of this dissertation, the Louisiana coast. It is in this framework that the unique characteristics of the study area will be considered in the subsequent section.

CHAPTER 2

THE STUDY AREA

The study area is located on the south-central Louisiana inner shelf, seaward of the Isles Dernieres, in water depths of six to nine meters (Fig. 2.1). Two deployment sites were chosen so as to occupy both the seaward and landward margins of Ship Shoal, the area's most prominent bathymetric feature. The coordinates of the seaward location (Site 1) are 28° 50.68 ' N, 91° 07.52 ' W, and those of the landward site (Site 2) are 28 ° 55.74 ' N, 91° 01.73 ' W. Supplemental data were obtained from two additional sites operated by the National Oceanic and Atmospheric Administration (NOAA). These were the Grand Isle C-Man station (GDIL1) located at 29° 16.20 ' N, 89° 57.60 ' W and National Data Buoy Center (NDBC) buoy #42002 at 25°52.50' N, 93°34.05' W. This chapter will discuss the specific characteristics of the deployment sites and provide a brief overview of pertinent regional considerations.

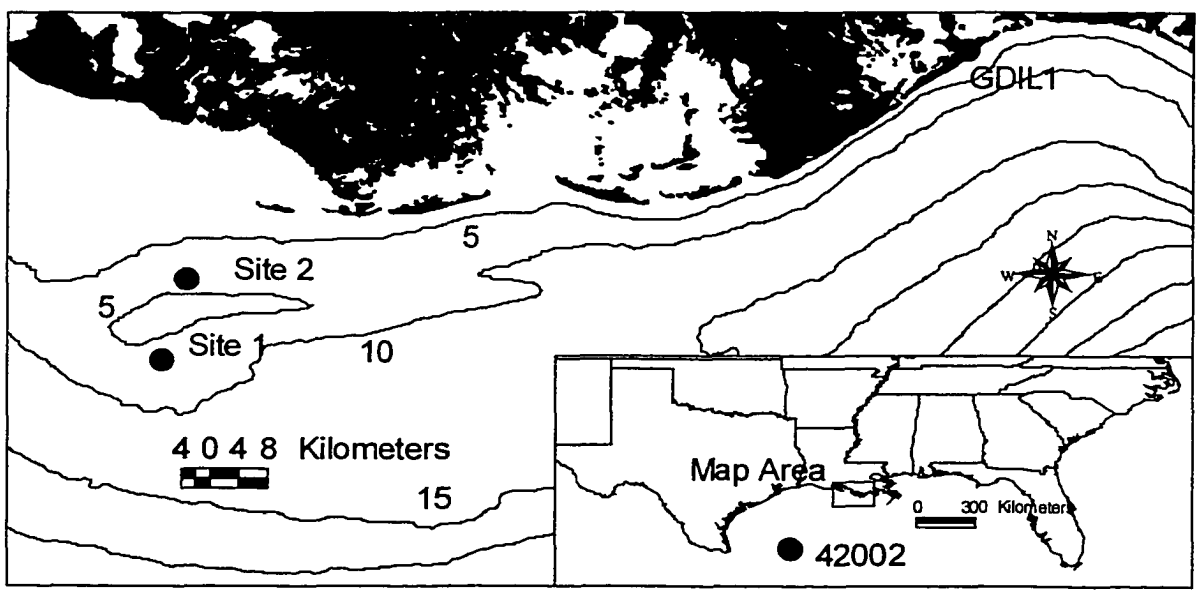

Figure 2.1: The study area. The co-ordinates of the sites are: Site 1: 28° 50.68 ' N, 91° 07.52 ' W; Site 2: 28 ° 55.74 ' N, 91 ° 01.73 ' W; GDIL1 (Grand Isle C-Man station): 29° 16.20 ' N, 89° 57.60 ' W; and NDBC #42002: 25°52.50' N, 93°34.05' W. All contours are in meters.

2.1 Meteorology

A primary focus of this dissertation is to investigate the influence of meteorological conditions, and in particular, winter extratropical storms, on inner-shelf processes in Louisiana. Annually, mean wind speed in coastal Louisiana is approximately 4.9 m s^{-1} (NOAA, 2000) and winds blow most frequently from the southeast, although they are strongest from the north and northeast (Dingler et al., 1993). The present study was conducted during a year in which the El Nino/Southern Oscillation (ENSO) occurred, however, and it is unclear exactly how this may have influenced the prevailing weather patterns. Since wind conditions vary considerably over the course of the year, storm climatology is most conveniently represented in terms of two "seasons"—a winter season lasting from November to April, and a summer season comprising the remainder of the year (DiMego et al., 1976).

During the summer months, coastal Louisiana's weather is dominated by Maritime Tropical air masses centered over the Gulf of Mexico. This almost always results in uniformly hot, humid, and calm weather, aside from localized convectional thunderstorm activity. Infrequent but often very powerful tropical cyclones (tropical storms and hurricanes), do occur, however, during this time. Tropical storms and hurricanes have made landfall on the Louisiana coast during the past century once every 3.3 and 4.0 years, respectively, with the highest frequency in September (Stone et al., 1997). Tropical cyclones can obviously be extremely high-energy events; for example, sustained winds during Hurricane Camille, which struck the Louisiana coast in 1969, were in excess of 100 m s^{-1} (Neumann et al., 1993). The impact of such storms on a particular section of coast, while potentially dramatic, is highly variable, and depends

upon the intensity, duration, and track of the individual cyclone. Since no tropical cyclones influenced the study area during the deployment period, however, no further discussion of such events is included.

From approximately November to April, extratropical, or mid-latitude, meteorological systems dominate coastal Louisiana's weather. Since mid-latitude meteorology is controlled by a complex interrelationship between air masses, cyclones, anticyclones and fronts, only a brief overview is offered here, although more detailed references are abundant (e.g. Moran and Morgan, 1994; Aguado and Burt, 1999). Ultimately, extratropical storms are the result of Rossby waves generated by heat transfer along the polar front, which forms the global boundary between tropical and polar air masses (Henderson-Sellers and Robinson, 1986; Aguado and Burt, 1999). Synoptic-scale storms are initiated along this front through cyclogenesis, a regular sequence of events that commences when an area of strong divergence in the upper atmosphere causes a drop in surface air pressure and the formation of a low-pressure cell, or "Low" (Moran and Morgan, 1994). In the Northern Hemisphere, counter-clockwise, or cyclonic, circulation develops around this Low, and the cyclone begins to migrate eastward. As this occurs, the portion of the polar front to the east of the Low moves northward as a warm front, while the portion to the west moves southward as a cold front. The process of cyclogenesis, as described above, tends to occur in particular geographic locations, and although there are several such source regions in North America, the most important for coastal Louisiana are on the lee side of the Rocky Mountains and in the western Gulf of Mexico (Chaney, 1999).

Since any portion of a mid-latitude system may impact the Louisiana coast during any stage of development, the general term *extratropical storm* is used in this dissertation to include all meteorological phenomena that originate in the mid-latitudes and generate high, sustained, wind speeds in the study area for several hours. It should be noted, however, that authors have used different nomenclature to identify such events. For example, the terms "cold front" (Roberts et al., 1987; Roberts et al., 1989; Chaney, 1999), "cold air outbreak" (Chuang and Wiseman, 1983), "episodic atmospheric forcing" (Armbruster et al., 1995), "Nor'easter" (Wright et al., 1986), "winter storm" (Drake and Cacchione, 1992) as well as "mid-latitude/ extratropical" cyclone (Hsu, 1993), refer to phenomena labeled extratropical storms in this dissertation.

Extratropical storms have been amply demonstrated to be important meteorological forcing mechanisms in a variety of environments in the northern Gulf of Mexico (Crout and Hamiter, 1981; Roberts et al, 1987; Dingler and Reiss, 1990; Murray et al., 1993; Armbruster et al., 1995; Stone and Wang, 1999). While they tend to be less intense than tropical storms, they are much more frequent, occurring roughly 20 to 30 times per year, with a maximum frequency in January (Roberts et al., 1987; Roberts et al., 1989). Given their complex evolution and their spatial and temporal variability, it is not surprising that individual extratropical storms that pass a particular location may differ widely in terms of their meteorological characteristics. While wind speed may exceed 25 m s^{-1}, as estimated for the "Storm of the Century" in 1993 (Chaney, 1999), it may be only slightly above average for weaker events. Generally, extratropical storms are characterized by a wind field that veers from south to north, with high wind speeds occurring prior to, and especially, following the passage of its associated cold front

(Chaney, 1999). This results in a general shift from onshore to offshore winds along the coast of the Gulf of Mexico, a phenomenon that does not occur in the same way on the Atlantic or Pacific coasts, which are aligned north-south. This presumably has implications for wave growth and propagation, current flow, and sediment transport. The semi-predictable sequence of wind velocity shifts introduced above will be discussed in greater detail in Chapter 5.

2.2 Hydrodynamics and Bottom Boundary Layer Regime

The northern Gulf of Mexico is a microtidal environment characterized by low hydrodynamic energy, except during storms (Penland et al., 1988; Wright and Nittrouer, 1995; Wright, 1995; Jaffe et al., 1997, Wright et al., 1997). Average significant deep-water wave height and peak period are approximately 1 m and 5-6 s, respectively, while the dominant angle of wave approach is from the southeast (Penland et al., 1988; Jaffe et al., 1997). Wave dissipation and refraction occur across the shallow Louisiana shelf, however, modifying these parameters closer to shore causing, most notably, a decrease in wave height. According to Ritchie and Penland (1988) the average wave height seaward of the Isles Dernieres (immediately landward of the present study area) is only about 0.6 m. On the other hand, wave characteristics during storms tend to be markedly different from those measured during fair weather. During extratropical storms, for example, significant wave heights of 2-3 m may occur (Dingler et al., 1993). A typical, although variable, sequence of wave responses to these events can be placed in a temporal framework based on the passage of the cold front that typically accompanies their passage. During the pre-frontal phase, high, long-period waves typically propagate from offshore, while during the post-frontal phase, sea-like conditions, with variable wave

heights, periods and directions, generally prevail (Roberts et al., 1987). During the summer, occasional tropical storms and hurricanes generate a variety of wave conditions depending upon their track and intensity, including waves several meters in height and greater than ten seconds in period (Stone et al., 1997).

Tides in the study area are diurnal, with a tropic range of roughly 0.4 m, resulting in only weak tidal currents (Wright, 1995; Wright et al., 1997). On the other hand, storm surges associated with wind events play a significant, but highly variable, role in modulating sea level over the shelf and in nearshore environments (Chuang and Wiseman, 1983; Biocourt et al., 1998). For example, water level set-up along the coast may reach 0.9 m during extratropical storms (Ritchie and Penland, 1988) and 7.0 m during hurricanes (Stone et al., 1997).

As would be expected from the hydrodynamic regime, only low-energy processes operate the majority of the time in the bottom boundary layer of the Louisiana continental shelf (Wright, 1995; Wright et al., 1997). Several field studies conducted on the mid- and outer shelf have indicated that mean near-bottom flows and bed stresses are not strong enough to re-suspend sediment during typical conditions (Adams et al, 1987; Halper and McGrail, 1988). Even on the inner shelf, in depths of 15-20m, Wright et al. (1997) estimated a mean combined wave-current shear velocity of less than 0.7 cm s^{-1}, an apparent bottom roughness of 0.011-0.015 cm, and a mean drag coefficient of 3.6×10^{-3}, during fair weather conditions. They concluded that variations in suspended particulate concentration are generally the result of the advection of sediment plumes from nearby rivers. On the other hand, a few authors have evaluated field data with mathematical models that suggest that bottom stress may be large enough to suspend bottom sediment

under certain conditions. For example, Crout and Hamiter (1981) analyzed pressure transducer data from a 10-m deep location on the inner shelf of western Louisiana using the model of Komar and Miller (1975), and estimated that summer storms, winter cold front passages, and southeasterly wind events during the spring can generate sufficient stress to suspend bottom sediment. Jaffe et al. (1997) used the Grant-Madsen-Glenn model (Grant and Madsen, 1979; Glenn and Grant, 1987) to predict sand resuspension on the shoreface adjacent to the Isles Dernieres during a variety of conditions. They concluded that the measured bottom stress is incapable of suspending a significant amount of sediment except during storm conditions. Specifically, they emphasized that sediment transport rates on the Louisiana inner shelf during normal fair weather conditions is more than 10^3 times lower than during large storms, such as major cold front passages, and more than 10^4 times lower than during hurricanes. This analysis indicated that extreme events are probably responsible for the vast majority of long-term sediment transport in the region, even considering their relative infrequency. In summary, therefore, the few studies conducted on the Louisiana shelf have indicated that its bottom boundary layer is characterized by low hydraulic energy, except during storms, when bed stresses may increase to a level capable of suspending and transporting bottom sediment.

2.3 Geology/Geomorphology

The geology of the Louisiana continental shelf is extremely complex, and includes features as diverse as diapirs, salt domes, and any number of muddy, silty and sandy sedimentary structures. It is also one of the most extensively studied environments in the entire field of marine geology, and a comprehensive discussion is therefore clearly beyond the scope of this dissertation. However, excellent reviews may be found in Kolb

and Van Lopik (1958), Scruton (1960), Frazier (1967) Worzel and Burk (1978) and Coleman et al. (1998).

The geology of the Louisiana inner shelf has been largely dominated during the past several thousand years by the influence of the Mississippi River system and its associated delta cycle (Scruton, 1960). This cycle consists of quasi-periodic delta-switching, which occurs roughly every 1000 years, and smaller-scale switching associated with subdeltas, bayfills, and crevasse splays, which occur with frequencies from a few decades to hundreds of years (Coleman et al., 1998). During this cycle, coastal progradation of up to 100m yr^{-1} takes place while a delta or lobe is active (i.e. during regression). Following abandonment, the delta gradually becomes submerged due to subsidence, and the shoreline retreats (transgression). This cycle has created an alternating succession of transgressive and regressive sedimentary features that dominate Louisiana's coastal geology. Only two areas of Louisiana's coast, the Birdfoot and Atchafalaya/Wax Lake Deltas, are presently experiencing the regression phase of this cycle, while the majority of the coast, including the study area, is undergoing relative sea level rise at a rate of roughly 1.0-1.1 cm yr^{-1} (Penland and Ramsey, 1990).

Ship Shoal is a sand body that is approximately 50 km long and 12 km wide at its western end, where the minimum overlying water depth is 3 m. It is asymmetric in profile, with steep landward slopes of 1:90 to 1:750 and shallower seaward slopes of 1:900 to 1:2,000 (Penland et al., 1988). Penland et al. (1988) attempted to account for coastal features associated with deltaic transgression in Louisiana in terms of a three-stage model that included the development of: 1) an erosional headland with flanking barriers; 2) a transgressive barrier island arc; 3) an inner shelf shoal. According to this

classification, Ship Shoal is a typical stage 3 feature that formed from the transgression and submergence of a former barrier shoreline, while the adjacent Isles Dernieres chain is a transgressive barrier island arc (Penland et al., 1988). Bathymetric surveys suggest that Ship Shoal is migrating landward across deposits from the abandoned Maringouin Delta at a rate of between 15 m yr^{-1} in the west, and 7 m yr^{-1} in the east (Penland et al., 1988).

The sedimentary composition of Ship Shoal is somewhat unique in a regional context. Unlike many of Louisiana's coastal environments, which are dominated by silt and mud, bed sediment in the study area is clean quartz sand with a mean grain diameter of 0.12-0.13 mm. Complete results of the analysis of bottom sediment from both study sites are shown in Figs.2.2 and 2.3.

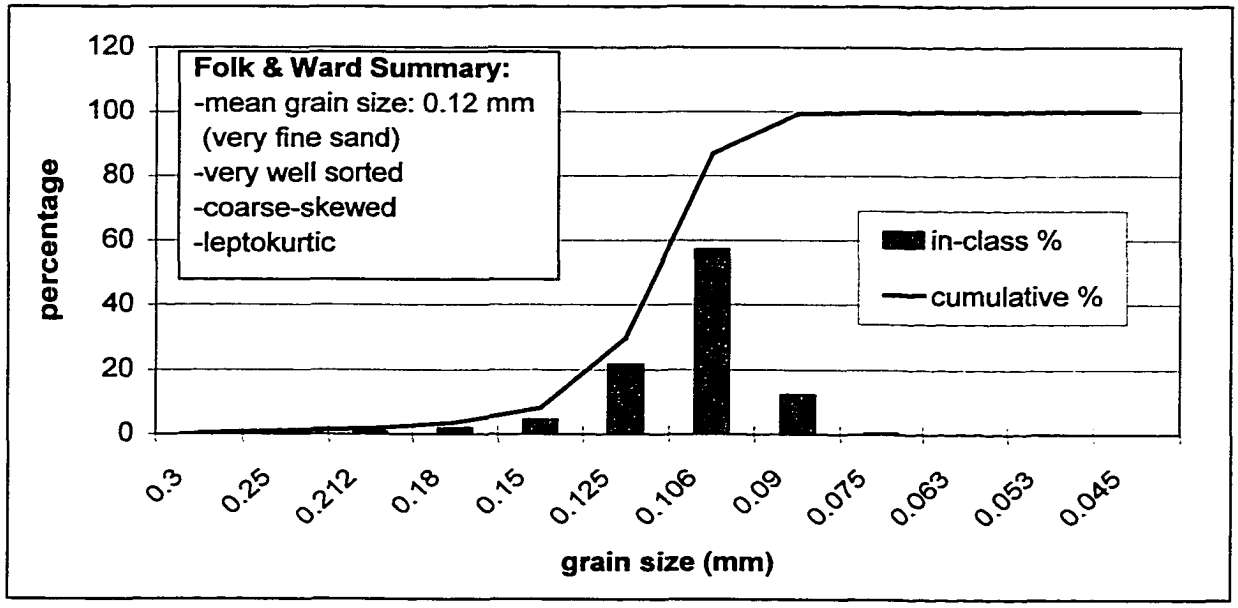

Figure 2.2: Results of sediment analysis from Site 1 (the offshore site).

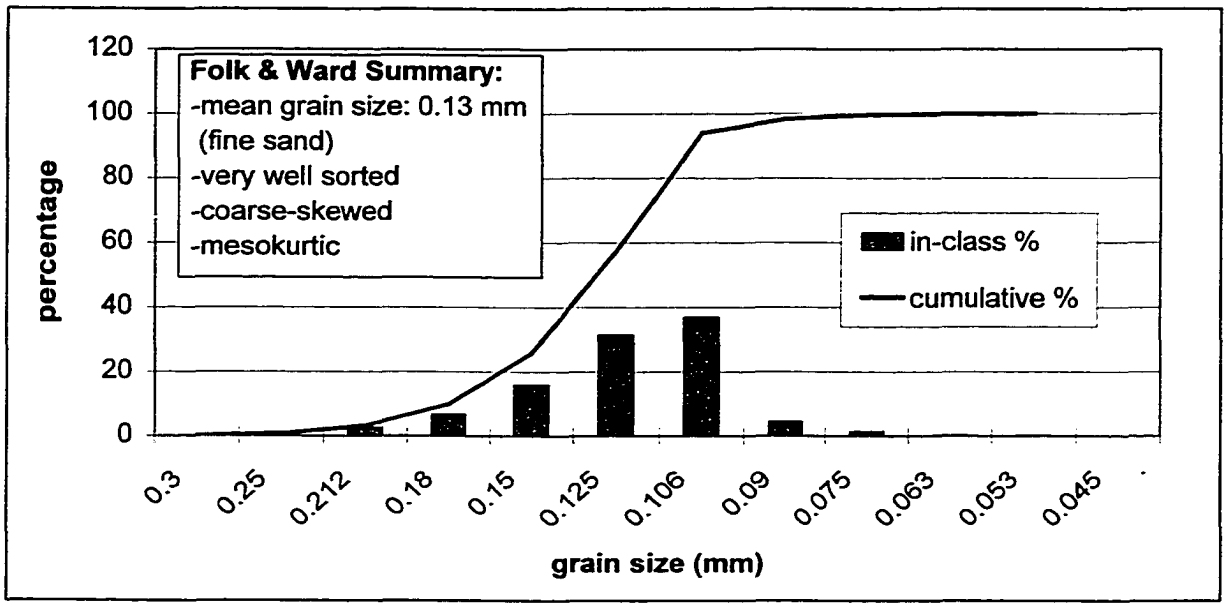

Figure 2.3: Results of sediment analysis from Site 2 (the nearshore site)

2.4 Practical Concerns

The unique characteristics of the Louisiana coastal zone have been widely discussed in the literature, including, but not limited to oceanographic, geological, ecological, geographical, and policy-oriented sources. Obviously, relative sea level rise and coastal land loss are primary concerns. One prominent proposal has been to artificially maintain the volume of eroding offshore barrier island chains to act as a protective barrier against wave energy for the adjacent coast (Stone and Xu, 1996). The possible means by which to do so include the implementation of hard structures, such as breakwaters, and artificial nourishment using sediment from distant sources. Ship Shoal, with its large quantity of clean, quartz sand, is considered a viable source for this sediment (Stone and Xu, 1996). Unfortunately, the shoal's influence on waves, currents, bottom boundary layer dynamics, and sediment transport in the region is not well-understood. Clearly, therefore, a knowledge of hydrodynamic and sedimentary processes on the south-central Louisiana inner shelf is of great practical, as well as theoretical concern.

CHAPTER 3

CONCEPTUAL BASIS FOR THE RESEARCH

It has been demonstrated in preceding chapters that many issues regarding hydrodynamic, bottom boundary layer and sedimentary responses to meteorological forcing on inner shelves are poorly understood. Further, it has been noted that the response of a particular inner-shelf environment is sensitive to a variety of local and regional factors. The inner shelf of Louisiana is unique in comparison with many previously-studied oceanic shelves in that it is exposed to a much lower mean level of hydrodynamic energy, it is dominated by higher frequency waves, and it has a different orientation relative to prevailing and storm wind directions. Furthermore, it is an important component of a system that is experiencing some of the highest rates of land loss in the world, providing not only theoretical reasons for its study, but very pragmatic ones.

Ultimately, the goal of this dissertation is to describe and quantify hydrodynamic variables, bottom boundary layer parameters, and directional sediment transport on the south-central Louisiana inner shelf. Although many factors will be considered, particular emphasis will be given to wave height and period, mean and orbital flow velocity, current and combined wave-current shear velocity, and across-shelf (i.e. on and offshore) sediment transport. These variables will be discussed in the context of three general themes: 1) the influence of meteorological forcing, and particularly of winter storms; 2) the effect of Ship Shoal; and 3) the implications of these data for Ship Shoal's evolution. To do so, the following specific objectives will be addressed:

1. To establish a general, but quantitative, winter "climate" for the Louisiana inner-shelf that incorporates meteorological, hydrodynamic, bottom boundary layer, and sedimentary variables.

2. To illustrate the episodic nature of inner-shelf processes in the region during the winter by quantifying the variability in these processes during a deployment lasting several weeks. Causes of this variability will then be identified, with a particular emphasis on the role of extratropical storms as a forcing mechanism.

3. To outline a classification system for extratropical storms in the region, in terms of their influence on the Louisiana inner shelf, and to identify the sequence of processes and responses associated with these extratropical storm classes, stressing the observed differences between storm phases.

4. To discuss the role of additional winter forcing mechanisms on the inner shelf that are not directly related to local extratropical storm activity.

5. To evaluate the influence of Ship Shoal on regional hydrodynamics, bottom boundary layer processes, and sediment transport.

6. To estimate the overall flux of sediment across Ship Shoal over a short time scale. This will permit a quantitative evaluation of event-scale erosion, accretion, and migration of the shoal, and will allow forcing mechanisms to be identified and placed within the context of the shoal's long-term evolution.

The fulfillment of these objectives will provide a unique and useful evaluation of the important forcing mechanisms, and their responses, on the Louisiana shelf during the winter. Additionally, it will provide information regarding the present influence of Ship Shoal on regional inner-shelf processes, as well as the shoal's temporal evolution. Given the unique characteristics of the study area, it is hoped that this analysis will ultimately enhance overall understanding of bottom boundary layer and sediment transport processes on inner-shelves worldwide, where research has been somewhat limited in both quantity and geographical coverage.

CHAPTER 4

DATA ACQUISITION AND PROCESSING

4.1 Instrumentation and Field Methods

The primary component of the field research was the deployment of instrumentation during a period of several weeks, beginning November 24, 1998, at the two sites discussed in Chapter 2. Three bottom-mounted instrumentation systems were used, two of which (Systems 1A and 1B) were deployed a few meters away from each other at Site 1, while the other (System 2A) was deployed at Site 2. System 2A was retrieved on January 12, 1999, while the others remained at Site 1 until February 2, 1999. Due to memory constraints, however, System 1A ceased logging on January 20, 1999. During each deployment and retrieval, divers collected sediment from the bed, and water samples from the water column, and observed and measured any visible bed forms.

The instrumentation consisted of two types of frame-mounted system, both of which included a self-contained data recorder module. The primary components of Systems 1A and 2A (Fig. 4.1) were SonTek$_{TM}$ downward-looking Acoustic Doppler Velocimeters (ADV's) that measured seabed elevation, relative particulate concentration and three-dimensional currents at an elevation of approximately 20 cm above the bed. Additionally, both included internal compasses and tilt and roll sensors to enable directional measurements to be rotated into a planetary frame of reference. System 1A was programmed to sample at 25 Hz, the maximum rate achievable by the sensor, since such a high sampling rate had seldom, if ever, been used in an inner-shelf environment (see Table 4.1, at the end of this section, for all instrument sampling rates). However, storage of these high-frequency data necessitated the use of a sampling interval of only

81 seconds every three hours. It was thought at the time that since System 1B was deployed in the immediate vicinity, potential gains achieved by (possibly) detecting high-frequency turbulent fluctuations that had not previously been reported in this environment would outweigh losses incurred by using a short burst interval. Unfortunately, this did not prove to be the case. Since System 2A was deployed alone, it included a Paroscientific pressure sensor in addition to the ADV, and was programmed to sample at 4 Hz for 8.5 minutes every three hours.

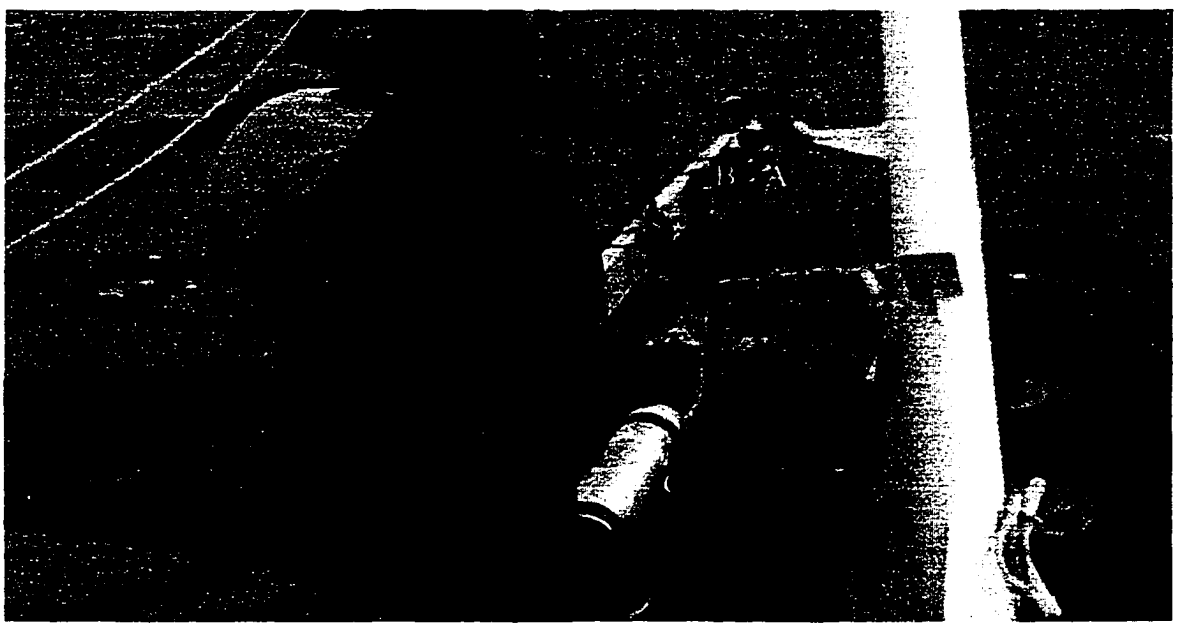

Figure 4.1: System 2A during deployment at Site 2. Key: A) Acoustic Doppler Velocitmeter (ADV) B) Pressure Sensor C) Enclosed cylinder containing recorder module, compass and power supply. System 1A was identical except that it did not include a pressure sensor.

System 1B was a unique multi-sensor package nicknamed WADMAS (Fig 4.2). It consisted of a Paroscientific pressure sensor, a sonar altimeter, and a vertical array of three co-located Marsh-McBirney electromagnetic current meters and Seapoint optical backscatter sensors (OBS's). This instrumentation enabled WADMAS to measure water level, directional wave parameters, and seabed elevation, as well as current velocity and

suspended sediment concentration at heights of 20, 60, and 100 cm above the seabed. To conserve battery power and recorder memory, all of the sensors on WADMAS were programmed for burst-mode (i.e. discontinuous) sampling. Specifically, the sonar altimeter collected one measurement every 15 minutes, while all other sensors sampled for 8.5 minutes per hour at a frequency of 4 Hz.

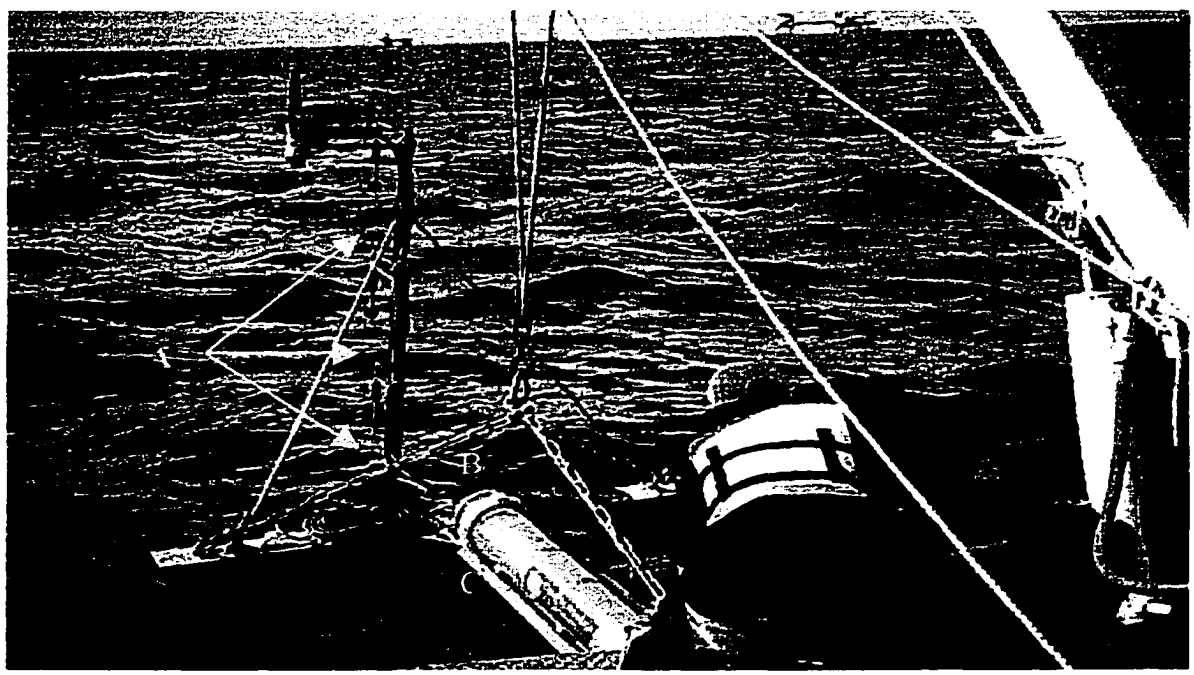

Figure 4.2: System 1B during deployment at Site 1. Key: A) Stacked array of co-located electromagnetic current meters and optical backscatter sensors B) Pressure Sensor C) Water-tight cylinder containing recorder module, compass and power supply D) Sonar altimeter.

Unlike many comparable instrumentation packages that have been deployed on inner shelves, the systems used in this study are notable in that they do not employ a traditional tripod or tetrapod-type frame design. Instead, sensors are supported by thinner, less-obtrusive, metal supports that allow them to remain separated from the heavy bottom-mounted frames. The intent of this design was to minimize the interference of the equipment with the parameters being measured. In particular, design of System 1B

allowed the sonar altimeter to measure bed elevation at a distance of nearly 1 m from the main section of the frame so that bed level changes relative to it could, in certain cases, result from localized effects that did not influence the entire instrument, such as ripple formation or migration.

Hourly wind data for the deployment period were obtained from the National Oceanographic and Atmospheric Administration (NOAA) station located on Grand Isle, Louisiana (GDIL1). These measurements were supplemented by daily national weather maps obtained from the National Weather Service, which were inspected visually to verify the occurrence of extratropical storm passages.

Table 4.1: Sampling schedules used in data collection. * Note: Sampling schedule shown for the meteorological station refers to GDIL1 data selected for use in this study, and not the entire data set collected by NOAA, which was more comprehensive.

System	*Sensor/ Measurement*	*Hours between Bursts*	*Samples/ Burst*	*Burst Duration (min)*	*Rate (Hz)*
1A (ADV)	Pressure	3	2048	8.5	4
	3-D Current	3	2048	8.5	4
	Suspended Sediment Concentration	3	2048	8.5	4
	Bed Level	3	1	-	-
2A (ADV)	3-D Current	3	2048	1.35	25
	Suspended Sediment Concentration	3	2048	1.35	25
	Bed Level	3	1	-	-
1B (WADMAS)	Pressure	1	2048	8.5	4
	Current	1	2048	8.5	4
	OBS	1	2048	8.5	4
	Sonar Altimeter	0.25	1	-	-
GDIL1 (NOAA)	Wind	1*	1	10	-

4.2 Laboratory Methods

Laboratory procedures for this project included two components: 1) instrument calibration, testing and preparation; and 2) analysis of sediment and water samples from the field site. All instrumentation was calibrated, prior to deployment, by the Louisiana State University Coastal Studies Institute Field Support Group in their testing facilities. Since optical backscatter sensors are more sensitive to fine than to coarse sediment, while the reverse is true for acoustic systems, appropriate field conversion factors were established using bottom sediment from the study sites. This procedure consisted of exposing the sensors to a series of uniformly-stirred mixtures of distilled water and known concentrations of field sediment. The voltage output from the sensors was then related to the sediment concentration by using linear regression analysis to fit a calibration curve to a scatter-plot of these variables. Since the field data from the optical backscatter sensors were ultimately found to be faulty, apparently due to rapid bio-fouling, OBS calibration results will not be discussed. Field data from the ADV's appeared to be reliable, however, and as such, the electronic signal strength was converted from the calibration curve obtained in the laboratory, which, as suggested by SonTek (1997), took the form:

$$C=k\,(10^{\,0.043SS}) \tag{4.1}$$

where C is the volumetric concentration of sediment, k is an empirically-determined constant with a value of 7.20197×10^{-10} and SS is the ADV signal strength.

Dry sieving at 0.25 ϕ intervals was conducted to determine the grain-size composition of the samples of bottom sediment. The water samples, collected at the surface and at 0.5, 2 and 4 m above the bed, were filtered through 0.7μm paper using a

pump-operated filtration system, dried in an oven at 60°C, and weighed to determine the sediment concentration.

4.3 Data Processing and Analytical Methods

4.3.1 Spectral Analysis

An initial discussion of spectral analysis is warranted since it played a prominent and varied role in this dissertation. Spectral plots of individual variables and cross-spectral plots of paired variables were generated on several time scales. In addition, plots of coherence and phase spectra were derived from the cross-spectra of the paired variables. Matlab® software was used to conduct this analysis. Generally speaking, the purpose of spectral, or frequency-domain, representation is to identify periodicities (essentially recurrence intervals) over which phenomena fluctuate. Power spectra indicate the frequency ranges over which an individual variable fluctuates, whereas cross-spectra do the same for the cross-product of two variables. Coherence spectra illustrate, on a scale of 0 to 1, the correlation between two variables, while phase spectra show the lead or lag of one variable in relation to a second, in both cases, at different frequencies (Jenkins and Watts, 1968).

Spectral analysis generally involves the application of smoothing, segmenting, or windowing techniques to increase the confidence level of the results (Jenkins and Watts, 1968). The Welch method, in which a single data series is initially subdivided into several shorter segments with a specified overlap length, was used in this study. A Hanning window was then applied to smooth these series, and Fourier series expansion was used to convert these series from the frequency to the time domain. Because spectral techniques have been applied in this dissertation in situations where sampling schedules

and record lengths have varied widely, the details of analysis techniques are summarized in Table 4.2.

Table 4.2: Segment, window, and overlap lengths used in spectral analysis.

System	*Series Length*	*Samples*	*Frequency*	*Segment Length*	*Window Length*	*Overlap Length*
1A	8.5 min	2048	4 Hz	256	256	128
1B & 2A	8.5 min	2048	4 Hz	256	256	128
1A	56 d	448	8 day^{-1}	64	32	0
1B & GDIL1	65.5 d	1574	24 day^{-1}	256	256	128
2A	49 d	392	8 day^{-1}	64	32	0

4.3.2 Directional Wave Processing

Directional wave parameters were calculated from the pressure and current-meter data by using the spectral approach of Earle et al. (1995) to generate the first five coefficients (a_0, a_1, b_1, a_2, and b_2) of the directional Fourier series. To compensate for the effect of depth attenuation, wave-pressure and horizontal-velocity-amplitude correction factors (Rp and Ru, respectively) were applied to the coefficients. These correction factors were calculated for each frequency (f) using:

$$Rp(f) = \frac{\cosh[k(z_d + d)]}{\cosh(kd)} \tag{4.2}$$

$$Ru(f) = \frac{\cosh[k(z_d + d)]}{\sinh(kd)} \tag{4.3}$$

where z_d and d are the mean sensor and total water depths, and wave number (k) was calculated iteratively using the dispersion equation:

$$(2\pi f)^2 = (gk)\tanh(kd) \tag{4.4}$$

The five Fourier coefficients were calculated by generating all possible combinations of the cross-spectra (Cxy) of the pressure (p) and horizontal velocity components (u_c and v_c), and using the following formulas:

$$a_0(f) = \frac{Cpp(f)}{Rp^2(f)\pi} \qquad (4.5)$$

$$a_1(f) = \frac{Cpu_c(f)}{Rp(f)Ru(f)(2\pi f)\pi} \qquad (4.6) \qquad b_1(f) = \frac{Cpv_c(f)}{Rp(f)Ru(f)(2\pi f)\pi} \qquad (4.7)$$

$$a_2(f) = \frac{(Cu_c u_c(f) - Cv_c v_c(f))}{Ru^2(f)(2\pi f)^2\pi} \qquad (4.8) \qquad b_2(f) = \frac{Cu_c v_c(f)}{Ru^2(f)(2\pi f)^2\pi} \qquad (4.9)$$

It should be noted that the correction factors *Rp* and *Ru* are frequency-dependent, and thus will approach zero as the frequency increases. As such, a high-frequency "cut-off" value of 0.35 Hz was selected on the basis of research conducted by Long and Oltman-Shay (1991). Mean and principal wave direction (θ_1 and θ_2) were calculated using:

$$\theta_1 = \arctan(b_1/a_1) \qquad (4.10)$$

and

$$\theta_2 = 0.5 \arctan(b_2/a_2) \qquad (4.11)$$

These Cartesian directions were converted to geographical directions on the basis of the instrument orientation measured by the compasses included on the systems.

Peak wave period (*Tp*) and significant wave height (H_{mo}) were calculated using the non-directional wave spectrum, *Czz*, which is equal to the product of a_0 and π. Peak period is simply the reciprocal of the spectral frequency at which the highest energy occurs (i.e. where *Czz* is the highest). Significant wave height was computed from

$$H_{mo} = 4.0\sqrt{m_0} \qquad (4.12)$$

where the zero moment of the non-directional spectrum (m_0) is the summation of spectral energy over the total number (*Nb*) of frequency bands of bandwidth *df*:

$$m_0 = \sum_{n=1}^{Nb} Czz(f)df \qquad (4.13)$$

This calculation is commonly used in wave analysis, although it may yield estimates 5-10% higher than the traditional definition of significant wave height ($H_{1/3}$), calculated using the highest one-third of the waves in the wave field (Longuet-Higgins, 1980).

4.3.2 Calculation of Bottom Boundary Layer Parameters and Sediment Transport

This section describes the procedures used to calculate bottom boundary layer parameters and predict flow, sediment suspension and sediment transport. Since it is a lengthy and detailed section, a few initial notes of explanation are warranted to clarify how each technique relates to the overall structure of the research.

Two methods were used to calculate an initial value of shear velocity, depending on the instrumentation system from which the data were obtained. Values from Systems 1A and 2A were computed using the Reynolds Stress technique (RS), while values from System 1B were calculated on the basis of the logarithmic profile (LOG) method. Sediment transport was calculated using essentially three techniques, called, for the purposes of this dissertation: 1) the GMR, or Grant-Madsen-Rouse method (Grant and Madsen, 1979, 1986; Rouse, 1937); 2) the MPM, or Meyer-Peter and Muller (1948) method; and 3) the SCP spectral cross-product method (Vincent et al., 1999). The first two of these (GMR and MPM) were based on the concept of shear velocity, while the SCP method was based on instantaneous field measurements of flow and particulate concentration. It was assumed in this study that sediment transport could be subdivided into bed and suspended load modes, as is commonly done, despite the somewhat arbitrary nature of this classification scheme (Davies and Li, 1997). Bed load is generally defined as all sediment that maintains occasional contact with the bed, while moving horizontally at a measurably slower rate than the flow, while suspended sediment is assumed to

remain above the bed at all times and to be transported horizontally at approximately the fluid velocity (Fredsoe and Deigaard, 1992). In this study, the MPM method was employed to calculate bed load transport, while the GMR and SCP methods were used to calculate suspended sediment transport. Table 4.3 summarizes the methods used to calculate shear velocity and sediment transport. A final point to note is that although the relevant equations in this section are presented sequentially, the reader should bear in mind that the actual physical processes they represent are interrelated by feedback mechanisms, and therefore, calculations were often performed iteratively.

Table 4.3: Summary of methods used to calculate shear velocity and sediment transport.

Abbreviation	*Full Name*	*System*	*Mode*	*Basis*
Shear Velocity				
LOG	Logarithmic profile	1B		-
RS	Reynolds stress	1A, 2A		-
Sediment Transport				
GMR	Grant-Madsen-Rouse	All*	suspended	shear velocity
SCP	Spectral cross product	All*	suspended	sensor
MPM	Meyer-Peter and Muller	All*	bed	shear velocity

4.3.2.1 Bottom Boundary Layer (BBL) Parameters

Two important parameters in bottom boundary layer modeling, particularly with respect to sediment transport, are the apparent bottom roughness length, z_{0c} and the shear velocity, defined in units of cm s^{-1}, as $u_* = (\tau/\rho)^{0.5}$, where ρ is the density of seawater (1.025 g cm^{-3}), and τ is the shear stress. Two approaches were used to calculate these parameters in this study. For System 1B (WADMAS) data, velocity profiles were initially estimated from log-linear regression of the burst-averaged current meter velocities (the "log-profile" method). Two conditions were initially satisfied for a profile to be considered logarithmic in a statistically significant sense: first, the correlation coefficient

(r^2) was equal to or greater than 0.994 (Drake and Cacchione, 1992); second, the variation in mean direction between current meters was less than 20°. Shear velocity and apparent bottom-roughness length were calculated for all logarithmic profiles using the von Karman-Prandtl equation:

$$u(z) = \frac{u_*}{\kappa} \ln\left[\frac{z}{z_{0c}}\right] \tag{4.14}$$

where $u(z)$ is the horizontal velocity at height z above the bed, and κ is von Karman's constant (0.4).

The Reynolds stress, or eddy correlation, technique was used to estimate bottom boundary layer parameters from the ADV data (Systems 1A and 2A). The total horizontal and vertical velocities (u and w) were represented as the sum of mean ($\bar{u}$ or $\bar{w}$), periodic (u_p or w_p), and turbulent (u' or w') components:

$$u = \bar{u} + u_p + u' \tag{4.15}$$

and

$$w = \bar{w} + w_p + w' \tag{4.16}$$

which is based on the assumption that turbulent and mean velocities are uncorrelated at all frequencies. The turbulent velocity was isolated by subtracting the periodic (wave-orbital) velocity component from the total-velocity-power spectrum (Green, 1992). To do so, wave orbital velocity was defined as the portion of the velocity spectrum (P_{UU}) that was coherent with pressure:

$$P_{u_w u_w}(f) = \gamma^2 U_p(f) P_{UU}(f) \tag{4.17}$$

where $P_{u_w u_w}$ is the wave-driven component of the velocity spectrum and $\gamma^2 U_p$ is the coherence between pressure and velocity (note that the same was done for the vertical, w, component). Obviously, this also has the effect of removing any turbulence that is

coherent with pressure, including wave-induced secondary flows. Although such flows were not directly observed during this study, they may have been present at certain times. However, it is assumed that their influence can be neglected in calculating shear stress and bed roughness, since these parameters are based on diffusive, rather than convective processes. Furthermore, there are difficulties inherent in using this method to remove all wave-induced turbulence in the presence of complex wave fields (Kitaigorodskii et al., 1983). Given these caveats, however, and also assuming that field measurements were taken in the constant stress layer, shear velocity is defined as:

$$u_* = -\sqrt{\overline{u'w'}} \tag{4.18}$$

Bottom roughness was calculated by applying these results to Equation 4.14.

4.3.2.2 The Combined Effect of Waves and Currents

Numerous field studies have demonstrated that the superposition of waves and currents enhances bottom shear stress and apparent bottom roughness (Wiberg and Smith, 1983; Cacchione et al., 1987; Lyne et al., 1990a; Drake and Cacchione, 1992; Kim et al., 1997). Wave-current interaction is a highly non-linear phenomenon that is understood primarily at a theoretical level, and as such, various approaches have been applied to apply it empirically. According to Dyer and Soulsby (1988) the following four categories of models are commonly used in combined wave and current situations: 1) Prescribed mixing-length distribution 2) Prescribed eddy viscosity distribution 3) Momentum deficit integral 4) Turbulent kinetic-energy closure. These model categories differ widely, not only in their assumptions and inputs, but also in the results they typically produce. Since a field comparison of these model-types, not to mention all available models within each category, would constitute a dissertation unto itself, the Grant-Madsen (prescribed eddy-

viscosity distribution) model (1979, 1986) was used in this study, owing to its widespread familiarity and high level of empirical verification (Larsen et al., 1981; Cacchione et al., 1987; Huntley and Hazen, 1988; Lyne et al., 1990a). According to the model, a wave boundary layer (WBL) of thickness (δ_w) develops during wave activity within the lower extremity of the current boundary layer, as discussed in the previous section, and the velocity profile is defined separately within and above this layer as:

$$u_c = \frac{u_{*c}}{\kappa}\left(\frac{u_{*c}}{u_{*cw}}\right)\ln\frac{z}{z_0}, \qquad z \le \delta_w \tag{4.19}$$

$$u_c = \frac{u_{*c}}{\kappa}\ln\frac{z}{z_{0c}}, \qquad z \ge \delta_w \tag{4.20}$$

where u_{*c} and u_{*cw} are the current-, and combined wave-current-induced shear velocities, z_0 is the roughness length produced by the sand grains, defined as D/30, where D is the mean grain diameter, and z_{0c} is the apparent bottom roughness length experienced by the current above the wave boundary layer. Wave boundary layer thickness is defined by:

$$\delta_w = \mathrm{n}\, u_{*cw}\, \omega \tag{4.21}$$

where n has a value of 2 (Grant and Madsen, 1986) and ω is the wave radian frequency, 2π/Tp. Apparent bottom roughness, z_{0c}, is used because the current experiences drag due to the combined influences of physical elements (grain roughness and bed forms) as well as non-linear interaction with the wave boundary and mobile bedload layers (Grant and Madsen, 1982; Gross et al., 1991). Equation 4.14 was used to determine u_{*c} and z_{0c}, and u_{*cw} was calculated using an iterative procedure involving the following equations:

$$u_{*cw} = u_{*wm}[1 + 2(u_{*c}/u_{*wm})^2\cos\phi + (u_{*c}/u_{*wm})^4]^{1/4} = \sqrt{C_R}\,u_{*wm} \tag{4.22}$$

where u_{*wm} is the wave shear velocity, ϕ is the acute angle between the waves and the current (waves were considered to be bi-directional, thus $\phi \leq 90°$), and C_R is a coefficient initially assumed to equal unity. A wave friction factor (f_w) was then defined through:

$$u_{*wm} = \sqrt{C_R}\sqrt{f_w / 2}u_b \tag{4.23}$$

$$\frac{1}{4\sqrt{f_w}} + \log\frac{1}{4\sqrt{f_w}} = \log\left(\frac{C_R u_b}{z_0 \omega}\right) - 1.65 + 0.24(4\sqrt{f_w}) \tag{4.24}$$

where u_b is the maximum near-bottom orbital velocity per wave period.

The current-induced shear velocity, u_{*c}, was assumed to act in the same direction as the mean current, while the direction of u_{*cw} was expected to oscillate during the course of the wave cycle. When the wave orbital velocity was at a minimum (near zero) the direction of u_{*cw} was the same as that of the current; when it was at its maximum, its direction ($\varphi_{\max}$) was between the wave and current directions, specified by the equation (modified from Cacchione et al., 1994):

$$\varphi_{\max} = \arctan\left(\frac{\sin\phi}{\cos\phi + \frac{u_b}{u}}\right) \tag{4.25}$$

Obviously, the direction of u_{*cw} has implications for sediment transport within the wave boundary layer, which will be discussed in greater detail in a subsequent section.

4.3.2.3 Sediment Suspension, Flow Stratification, and Bed Armoring

Sediment transport occurs when the shear stress (τ) exerted by the fluid on sediment grains exceeds the critical shear stress (τ_{crit}) required to initiate sediment motion. In practice, determination of the critical shear stress of seabed sediment is problematic, as a result of three general factors outlined by Drake and Cacchione (1986).

First, the grain-size distribution of shelf sediment may be quite broad, second, the presence of even a small fraction of clay-sized sediment may cause cohesiveness, which increases τ_{crit} and finally, benthic organisms exert a significant, but poorly understood, influence on the properties of bed sediment. Fortunately the first two of these considerations do not appear to have been important for the study area (recall Figs. 2.2 and 2.3), although the third may have. Not surprisingly, various methods may be used to determine τ_{crit} under combined flows, including a modified Yalin technique outlined by Li et al. (1996), which was used in this study. The dimensionless Yalin parameter (Ξ) is defined by:

$$\Xi = [(\rho_s - \rho) g D^3 / \rho \nu^2]^{0.5} \tag{4.26}$$

where ρ_s and ρ are the densities of sediment (2.65 g cm^{-3}) and seawater (1.025 g cm^{-3}), respectively, D is grain diameter, and ν is kinematic fluid viscosity (0.013 cm^2 s^{-1}). The Yalin parameter was used to calculate a critical Shield's criterion (θ_{crit}), and τ_{crit} using:

$$\log \theta_{crit} = 0.041(\log \Xi)^2 - 0.356 \log \Xi - 0.977 \tag{4.27}$$

and

$$\tau_{crit} = \theta_{crit} (\rho_s - \rho) g D \tag{4.28}$$

Critical shear velocity was then simply calculated by: $u_{*crit} = (\tau/\rho)^{0.5}$. Since sediment at the study site was fairly uniform in size, it was assumed that a single value could be applied. The equations outlined above showed that the appropriate value for u_{*crit} was 0.81 cm s^{-1}. An additional parameter derived from critical shear velocity that was employed in this study was the normalized excess shear stress (S'):

$$S' = \left(\frac{\tau - \tau_{crit}}{\tau_{crit}} \right) \tag{4.29}$$

where τ is the observed shear stress.

The sediment suspension profile over a sandy bottom was shown by Lynch et al. (1997) to be well represented by the standard Rouse (1937) equation, even under combined wave and current flows. This profile is the result of a balance between the upward-diffusive and downward-settling fluxes of sediment. It is represented by:

$$C(z) = C\ (z_a)\left(\frac{z}{z_a}\right)^{-\alpha}, \qquad \text{where} \qquad \alpha = \frac{\gamma w_s}{\kappa u_*} \tag{4.30}$$

$C(z_a)$ is the reference concentration at height z_a, γ is the ratio of the eddy diffusivity of sediment to that of momentum (~1), and w_s is the sediment fall velocity. These equations are based on the somewhat vaguely defined concept of a reference concentration of sediment near the bed. The concentration $C(z_a)$ is commonly defined by the equation from Glenn and Grant (1987):

$$C(z_a) = C_{bed}\frac{\gamma_0 S'}{1+\gamma_0 S'} \tag{4.31}$$

where C_{bed} is the sediment concentration in the bed (~0.65) and γ_0 is a dimensionless empirical constant with a value, according to Hill et al. (1988) and Gross et al. (1991) of approximately 1.3×10^{-4}.

Under certain conditions, suspended sediment may cause the water column to become stable-stratified, increasing the vertical velocity gradient, but inhibiting the upward diffusion of mass and momentum (Smith and McLean, 1977; Adams and Weatherly, 1981; Glenn and Grant, 1987; Huntley et al., 1994). Some authors have suggested that this phenomenon should be represented numerically by modifying von Karman's constant (Adams and Weatherly, 1981; Gust and Southard, 1983). The more conventional approach, however, is to apply a stratification correction to the velocity profile based on the predicted sediment concentration, and this technique was therefore

used in this study. As suggested by Glenn and Grant (1987), the correction was applied only above the wave boundary layer and took the form:

$$u_z = \left(\frac{u_{*c}}{\kappa}\right)\left[\ln\left(\frac{z}{z_0}\right) + \beta z / L\right] \tag{4.32}$$

where β is an empirical constant with a suggested value of 4.7 (Glenn and Grant, 1987), and L is the Monin-Obukhov length scale, defined by:

$$L = \frac{u_{*c}^{\ 3}}{z\kappa g((\rho_s - \rho)/\rho) w_s C} \tag{4.33}$$

where C is sediment concentration.

Bed armoring occurs when sediment in size classes with a low critical entrainment stress is winnowed from the bed, leaving a higher bed concentration of less-easily-entrained size-fractions. This phenomenon, which serves as a negative feedback mechanism for sediment transport, has been observed on the inner shelf during high-suspension events such as storms (Lyne et al., 1990b; Wiberg et al., 1994). Its possible effect was accounted for in this analysis by incorporating the mixing-depth limitation (δ_{mix}) suggested by Green et al. (1990):

$$\delta_{mix} = 2.5\ S'/(\rho_s - \rho)g \tag{4.34}$$

4.3.2.3 Sediment Transport

Suspended sediment transport is represented mathematically by time- and depth-integrating the product of the horizontal velocity of the fluid and the suspended sediment concentration. As simple as this may seem, it is a very complex problem in combined-flow regimes, owing to phase differences in velocity and concentration, and the possible occurrence of secondary flows including ejected vortices (Agrawal and Aubrey, 1992; Osborne and Greenwood, 1993; Davies, 1995). As a result, the time-scale chosen for this

integration procedure is of great importance. In fact, Osborne and Vincent (1996) indicated that not only may the magnitude of transport vary on the basis of averaging period, but in some cases the direction may be completely reversed. On the other hand, the use of instantaneous measurements is problematic, since the time scales of velocity- and suspended-sediment-profile development are different (Davidson et al., 1993). Lesht (1980) and Shauer (1987), for example, recommend scales of several minutes for the establishment of logarithmic velocity profiles. As such, two approaches were employed in this study, the first based on time-averaged values and the second on instantaneous field measurements.

The first technique, which was earlier labeled the GMR approach, was to multiply the burst-averaged velocity and concentration profiles as calculated on the basis of the shear velocity. This approach has often been employed in wave-dominated environments (e.g. Vincent et al., 1981; Kim et al., 1997) despite the fact that it assumes temporally-uniform values, a condition that may not be satisfied during unsteady oscillatory flow. The profiles were integrated both within and above the WBL using:

$$Q_{sn} = \frac{1}{t}\int_{z=\delta_w}^{z=\eta}\int_0 uC_n\, dzdt \qquad \text{for} \qquad z > \delta_w \qquad (4.35)$$

$$Q_{sn} = \frac{1}{t}\int_{z=z_0}^{z=\delta_w}\int_0 uC_n\, dzdt \qquad \text{for} \qquad z < \delta_w \qquad (4.36)$$

where η is the sea surface elevation.

The cross-product of instantaneous values (i.e. every 0.04 s or 0.25s) of velocity and concentration from Systems 1 and 2A were also used to calculate suspended sediment transport. This had the advantage of accounting for time-varying effects of waves on the sediment suspension and velocity profiles as well as allowing transport to

be analyzed according to frequency components. In many instances during this dissertation, for example, sediment transport (Q) calculated using this method will be presented on the basis of mean, low-frequency (LOW), wind-wave (wind), and turbulent (turb) components, which represent time periods of >81s, 10.24-80s, 2.34-10.23s, and <2.33s , respectively. It should be noted that the high-frequency cut-off for the low-frequency component used in the study (i.e. 0.09 Hz) was much lower than has often been used in marine environments, since the peak frequency of waves at the study site was always below this. Total transport (Q_t) is the sum of the individual components:

$$Q_t = Q_{mean} + Q_{LOW} + Q_{wind} + Q_{turb} \tag{4.37}$$

Unfortunately, quantitative assessments of sediment transport made using this method may not have been particularly precise, since it was necessary to assume (very simplistically) that the mean sediment concentration and flow velocity throughout the water column were equal to the burst-averaged values measured at the sensor.

Bed load transport rate (Q_{bl}) was calculated by using the combined wave-current shear stress as an input to the empirical formula of Meyer-Peter and Muller (1948) as adapted by Wiberg et al. (1994):

$$Q_{bl} = 8\frac{(\tau - \tau_{crit})^{3/2}}{(\rho_s - \rho)g} \tag{4.38}$$

The direction of bedload transport under the combined flow of waves and currents is as yet an inadequately resolved issue. Cacchione et al. (1994) assumed that bedload transport would occur in same direction as that of the maximum shear stress (φ_{max}) within the wbl. Although this seems to be a somewhat simplistic assumption since the direction of stress may vary up to 180° over the course of a wave cycle, these workers were able to

reasonably represent observed trends of bed form migration. As such, this method was adopted for this study.

A wide variety of methods have been presented in this chapter, many of which involve important assumptions that have not necessarily been well-tested in the field. The uncertainties inherent in the calculation of shear velocity using either the logarithmic profile or the Reynolds Stress method are compounded by those involved in attempting to account for combined wave-current interaction using mathematical models. Sediment transport estimates are even less certain quantitatively, given their dependence on several poorly-known factors. Owing to this, results from several of the methods are presented in many cases, and as will become apparent in later chapters, the trends they produce are similar in most instances. Furthermore, all have a solid grounding in the literature. Nonetheless, since all methods have their strengths and weaknesses the choice of the most reliable, must, to some degree, be left to the discretion of the reader.

CHAPTER 5

METEOROLOGICAL CONDITIONS DURING THE DEPLOYMENT

5.1 Classification Systems for Meteorological Events

One objective of this dissertation is to differentiate between various meteorological conditions that occurred during the study period and to associate these with hydrodynamic, bottom boundary layer and sedimentary responses. It is useful, therefore, to establish a classification system by which to characterize atmospheric conditions, specifically those related to winter extratropical storms and fair weather in the northern Gulf of Mexico. Numerous classification schemes have been proposed to categorize atmospheric conditions in a variety of environments—however, since meteorological processes are inherently complicated, these are of necessity based on criteria that suit a particular purpose. Depending on the requirements of a specific study, for example, a classification scheme may be based on local atmospheric measurements, on synoptic or global-scale atmospheric circulation, or on the effect of atmospheric forcing on some aspect of the physical or human environment. The system employed in this chapter was ultimately designed to differentiate between: 1) fair weather and storm conditions; 2) different phases of extratropical storms; and 3) extratropical storms of different intensities and synoptic types. As such, it draws upon several classification systems suggested in the literature, as well as criteria specific to the research, and employs both hourly wind velocity data and visual observations from daily national weather maps.

Storm magnitude scales, such as the Saffir-Simpson scale for hurricanes and the Fujita scale for tornadoes, are a fairly simple and familiar type of meteorological classification system based largely on wind speed and barometric pressure (Moran and

Morgan, 1994). Although magnitude scales for extratropical storms are somewhat less familiar, several have been proposed. One example is the Northeast storm scale of Halsey (1986), who ranked storms in the Atlantic qualitatively, on the basis of their effect (damage potential) on coastal beaches. More recently, Dolan and Davis (1992a, 1992b) suggested a scale for Atlantic coast Northeast storms (Nor'easters) that was also based on coastal damage potential, but included, in addition, a quantitative index of storm power calculated as the square of the significant wave height times the duration of the storm. Hsu (1993) proposed a classification system for extratropical cyclones in the Gulf of Mexico. This scale is based on the minimum central pressure of a Gulf cyclone and the predicted maximum wind speed, and is thus more fundamental meteorologically than the scales proposed for Atlantic storms. Chaney (1999) used a simple measure of magnitude for Gulf Coast storms known as the V-square or Power-V value, which is based on the sum of the squares of the hourly wind speed during a storm event, thus incorporating the influence of both wind speed and duration. A variation of this simple scale will be applied extensively during this dissertation.

Synoptic-scale classification systems have also been applied to the meteorology of the northern Gulf of Mexico. Notably, Muller (1977) subdivided New Orleans weather into eight synoptic types that included both storms and fair weather. Roberts et al. (1987) identified two end member types of extratropical storms in coastal Louisiana: the migrating cyclone, characterized by the passage of a cold front aligned oblique to the coast; and the Arctic surge, in which a front is aligned parallel to the coast. Chaney (1999) subdivided characteristic synoptic weather patterns responsible for extratropical storms over the northern Gulf of Mexico into seven categories: 1) Primary Front (P); 2)

Secondary Front (S); 3) Secondary Gulf Front (SG); 4) Secondary Gulf Low (SL); 5) Gulf Front (GF); 6) Gulf Low (GL); and 7) Primary Low (PL). Different synoptic types were shown to be associated with unique meteorological conditions capable of generating a range of hydrodynamic responses. However, the first two of these types, the Primary and Secondary Fronts, were found to account for approximately 90% of storm activity along the northern Gulf of Mexico.

The "cold front cycle" has commonly been used to characterize the sequence of events that accompanies a "typical" extratropical storm passage (e.g. Roberts et al., 1987; Roberts et al., 1989; Armbruster et al., 1995; Chaney, 1999). The initial pre-frontal phase includes strong, warm, moist winds that blow from the southerly quadrant. The ensuing frontal phase is characterized by a sudden drop in air pressure, erratic winds, and short-lived, but occasionally intense, squalls. Finally, a post-frontal phase occurs, during which temperature and humidity drop, air pressure rises, and winds are strong and northeasterly to northwesterly. It should be noted, however, that this sequence, although considered typical, exhibits considerable variability. As subsequent analysis will show, some extratropical storms apparently lack one or more of these phases altogether.

Finally, Chaney (1999) identified three storm subtypes in the northern Gulf of Mexico on the basis of the direction of post-frontal winds. Subtype A included storms that were characterized by northwesterly winds (only), Subtype B storms included northeasterly winds (only), and Subtype C storms included both northeasterly and northwesterly winds. Subtype A storms were only half as common as Subtype B storms, which were in turn, only about 25% as common as Subtype C storms. Despite the fact that Subtype C storms were by far the most common, they tended to be dominated by

northeasterly winds, and as a result the overall ratio of northeasterly to northwesterly winds was approximately 2:1. The importance of this will become apparent in Chapter 7 since this classification system will be used as a partial basis for the conceptual model introduced in this dissertation.

5.2 Analysis of Meteorological Events During the Deployment

Aspects from several of the sources discussed above were used to characterize extratropical storms during the study period. It should be noted again that the study period occurred during ENSO conditions, which are known to influence mid-latitude Rossby waves (Aguado and Burt, 1999). Therefore extratropical storms in the study area may not have been typical of "normal" years, although this is a matter of speculation. Since wind velocity is a critical meteorological variable in coastal systems, the onset of storm conditions was considered to occur when a threshold wind speed was exceeded. The value assigned to this threshold was 7.4 m s^{-1}, which was equal to one standard deviation above the mean speed for the study period. The end of the event was identified as the hour that wind speeds fell, and subsequently remained, below this threshold for six hours or more. Wind direction was also analyzed to identify phases of extratropical storm passages that corresponded to the cold front cycle described in the previous paragraph. Pre-frontal winds were defined as those that blew from a direction between 90 and 270° and appeared, from weather maps, to occur prior to a cold front passage. The post-frontal phase included the period subsequent to the frontal passage when wind direction was between 270 and 90°. All other wind conditions were considered fair weather. Storms were also classified on the basis of several of the classification systems discussed in section 5.1, to provide an initial meteorological assessment of the deployment period.

5.3 Meteorological Summary of the Deployment

Wind speed during the deployment averaged 4.8 m s^{-1} and had a mean direction from the northeast (48°). Hourly wind speed and direction for the deployment period are shown in Figs. 5.1 and 5.2. These figures demonstrate the increases in wind speed characteristic of extratropical storms, as well as the veering of the wind field during their passage. According to the quantitative definition outlined in Section 5.2, nine storms occurred during the 61-day deployment, at a frequency of one every 6.8 days. Mean wind speed and direction were 8.1 m s^{-1} and 354°during storms and 3.8 m s^{-1} and 113° during fair weather. Storms during the period were therefore characterized by strong winds blowing from the north, while the mean wind direction during fair weather was southeasterly. Spectral analysis of wind speed during the deployment showed a statistically significant peak in energy at a frequency of roughly every five days, or approximately the same as that of extratropical storm passages (Fig.5.3). This suggests that extratropical storms were responsible for most of the variability in wind speed, a result consistent with published research for the northern Gulf of Mexico (e.g. Chuang and Wiseman, 1983).

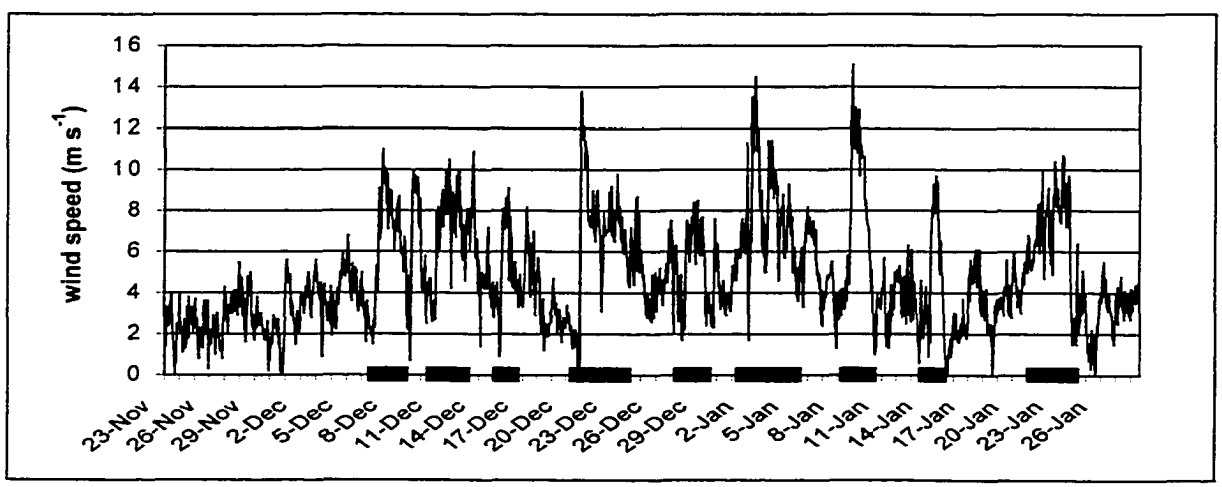

Figure 5.1: Wind speed during the deployment period. The time and duration of extratropical storms are indicated by the black bars along the x-axis.

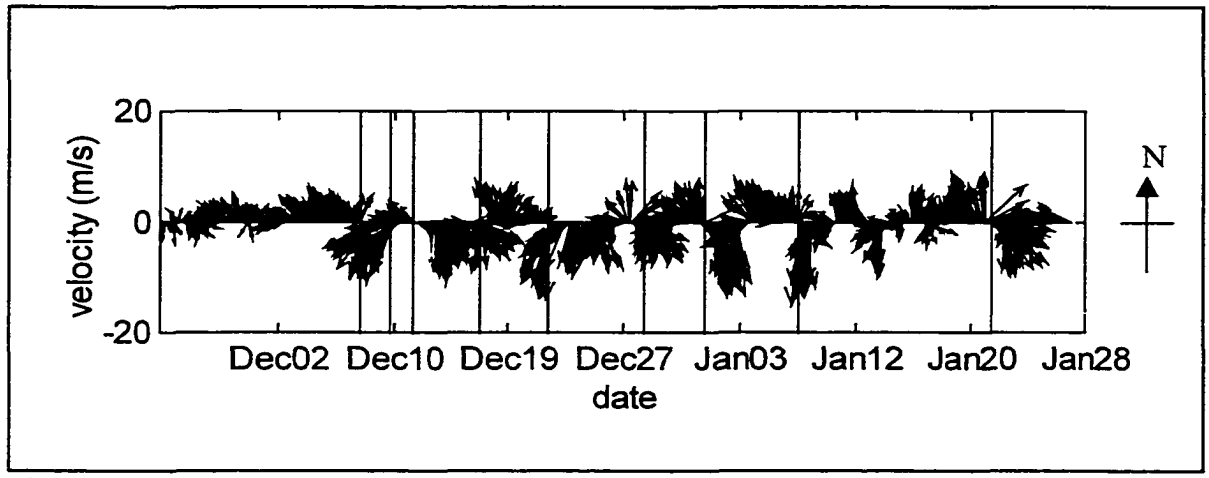

Figure 5.2: Feather plot of hourly wind velocity vectors during the deployment. Storm passages are indicated with vertical lines.

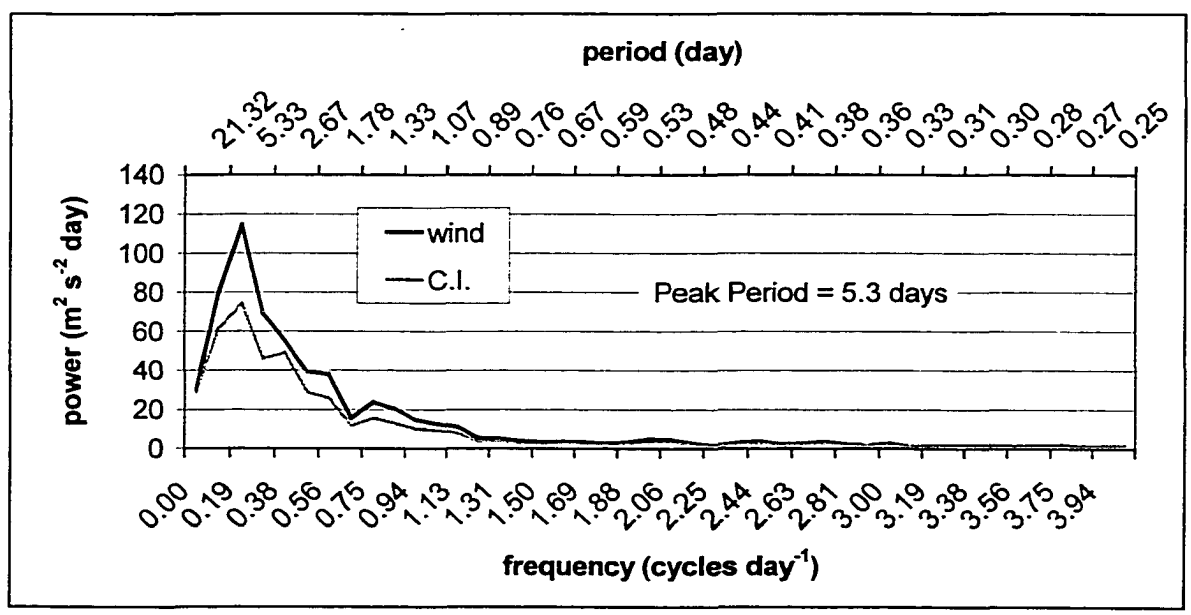

Figure 5.3: Power spectrum of wind speed during the deployment. C.I. represents the 90% confidence interval.

Classification of the storms that occurred during this study, using the models described previously, is shown in Table 5.1. Several results are evident. First, analysis of the synoptic types associated with storms indicates that the majority of cold fronts affecting the coast were aligned obliquely to it (i.e. the migrating cyclone of Roberts et al., 1989). Six of the nine storms were classified as the Primary front type described by Chaney (1999), while an additional two were of the Secondary Front type, and one was a Secondary Gulf Front. Despite the sequence of atmospheric events that "typically" accompany cold front passages, winds above the threshold did not often blow from the south during this study, and as such, only two storms were considered to have a notable pre-frontal phase at all. On the other hand, all storms had a marked post-frontal phase during which strong winds blew from the north.

Table 5.1: Classification of storms during the deployment on the basis of the methods discussed in Section 5.1. In all cases, rank is based on a five-point scale.

Storm	*Month/Day -hour*	*Orientation*	*Max. Velocity (north)*	*Max. Velocity (south)*	*[Sub]Type (Chaney, 1999)*	*V³ (knots³) [Rank]*	*Hsu Rank*	*Dolan & Davis [Rank]*	*Stages*
1	12/8-18	Oblique	5.3	11.0	P[C]	2402 [2]	2	18 [1]	Post
2	12/12-17	Perp.	5.8	10.5	SG[C]	4106 [3]	1	31 [1]	Post
3	12/17-13	Oblique	6.1	9.1	P[C]	774 [1]	1	1 [1]	Post
4	12/22-14	Oblique	8.2	15.3	P[B]	4779 [3]	2	40 [1]	Post
5	12/29-12	Parallel	7.5	8.5	S[C]	1224 [1]	1	3 [1]	Post
6	1/2-22	Perp.	11.5	14.5	S[C]	5712 [4]	2	52 [1]	All
7	1/9-12	Oblique	5.8	15.1	P[C]	3392 [3]	3	27 [1]	Post
8	1/14-20	Oblique	6.3	9.7	P[C]	852 [1]	1	8 [1]	Post
9	1/23-13	Perp.	10.0	10.7	P[A]	3616 [3]	1	178 [3]	All
All	-	-	7.4	11.4	-	2984	-	40	-

Clearly, there was considerable variation in the intensity of storm events, with maximum wind speeds varying almost a factor of two, Power V varying by nearly an order of magnitude, and Dolan and Davis values ranging by more than two orders of magnitude. Storms 3 and 5 were particularly weak, while Storms 2, 4, 7, and 9, and

especially, Storm 6, were energetic. This is an important factor to bear in mind, since it will be demonstrated in later chapters that the relative strength of storms is a key element in determining their influence on the marine environment.

Storms that occurred during this study tended to be weak, according to both the Dolan and Davis and Hsu scales, with each model indicating that only one Rank 3 event took place during the deployment (Table 5.1). There are several reasons for this. The Dolan and Davis scale was based on measured wave height in the Atlantic, which would presumably be much greater than in the Gulf of Mexico as a result of regional oceanographic considerations. The Hsu scale was based on the maximum wind speed calculated from the lowest central pressure of a cyclone in the Gulf of Mexico, whereas this study employs the maximum wind speed at a particular location. Clearly, site-specific wind measurements would be lower unless the cyclone passed directly over the study area.

The Power-V (V-square) rating (Chaney, 1999) was another useful representation of storm intensity employed in this dissertation. Unlike the system used in this study, however, where a value of one standard deviation above the mean was used to define storms, Chaney included all winds that exceeded the mean wind speed for the deployment. As such, the Power-V values reported for storms that occurred during this study are lower than they would be if Chaney's original system had been followed strictly. Bearing these caveats in mind, however, the Power-V classification used here indicated that three storms were weak (Rank 1), five were moderate to significant (Rank 2-3), while only Storm 6 was severe (Rank 4). The reader should note these results, since Power-V classifications will often be referred to during later sections of this dissertation,

and in particular, in Chapter 7, to differentiate between the storms that occurred during the deployment period.

In summary, therefore, extratropical storms were distinguished from fair weather conditions by several characteristics, including wind speed and synoptic-scale patterns. Despite these common features, however, extratropical storms clearly differed from each other in many respects. The implications of both the common, and the somewhat disparate, features of extratropical storms will be a primary topic of subsequent chapters.

CHAPTER 6

HYDRODYNAMICS, BOTTOM BOUNDARY LAYER PARAMETERS AND SEDIMENT TRANSPORT DURING THE ENTIRE DEPLOYMENT PERIOD: TIME- AND FREQUENCY- DOMAIN ANALYSIS AND OVERALL SUMMARY

Long-term measurements in the bottom boundary layer of inner shelves are fairly rare, and published results are often confined to a single storm. Furthermore, as discussed previously, the only research conducted in coastal Louisiana that employed a similar methodology to the present study (i.e. Wright et al., 1997) consisted of two summer deployments devoid of appreciable storm activity. Thus, an important objective of this research is to summarize prevailing winter hydrodynamic, bottom boundary layer, and sediment transport patterns in the region, thereby helping to establish a "climate" from which regularities may be drawn in the future. Furthermore, although it is assumed that meteorological influences, such as extratropical storms and bathymetric features (in this case, Ship Shoal) have important effects on marine processes in the region, the details of these effects are unclear. This chapter will therefore present results of the entire deployment using time-series and spectral (frequency-domain) representations as well as general tabular summaries. In doing so, differences between a variety of weather conditions and between the two locations relative to Ship Shoal will be quantified and the connection between atmospheric forcing mechanisms, bathymetric modification, and marine and sedimentary processes will become evident, preparing the way for more detailed discussions of these linkages in upcoming chapters.

6.1 Initial Considerations: Field Observations

Divers characterized the bed at the field sites as being largely free of bed forms during both the emplacement and retrieval stages of the deployment. While they did report bed

irregularities with an estimated height of 1 cm during the emplacement phase, these were apparently localized, non-periodic, and were thus not likely the result of organized wave or current activity. Unfortunately, it was unrealistic for divers to monitor the bed throughout the duration of the deployment, owing to obvious logistical, financial, and environmental limitations. Video camera surveillance was also impossible as a result of extremely poor visibility. Therefore, the presence of bed forms was neither automatically ruled out nor assumed during this research.

The initial trip to the field sites to retrieve all instrumentation occurred on January 12, 1999. Diver recognizance revealed that all systems, which had initially rested on the bed, were submerged beneath at least 10 cm of sediment, impeding their safe return to the research vessel. Only System 2A, located at the nearshore site and submerged to a lesser extent than the two offshore systems, was retrieved that day. Several subsequent attempts were made to recover the systems at Site 1, and eventually, on February 2, 1999, both were successfully retrieved. The sedimentary material overlying the instrumentation upon recovery was fine sand, similar to typical bed sediment in the study area. Although the cause of the burial of the systems was unclear at the time, two hypotheses were considered for further investigation: 1) overlying deposition of sediment (i.e. bed level increase); or 2) scouring or sinkage of the instruments into the bed (i.e. sensor level decrease).

Recorded data from all systems were used to investigate these hypotheses, but since results were similar in all three cases, only data from System 1B, specifically, bed level (relative to the sonar altimeter) and water depth (to the pressure sensor), will be considered in this section. Time series of these data are shown in Fig. 6.1. One important,

but probably safe, assumption that should be noted was that the instrumentation system moved as a contiguous unit (i.e. it did not warp or bend), and thus, that the location of the sensors relative to each other was constant. The time series of bed level corroborates the field observations, indicating a total increase of approximately 20 cm during the deployment, although large short term-fluctuations, which will be discussed later, are also evident. Unfortunately, this trend is not particularly enlightening in itself since it could be a result of either hypothesized mechanism. Specifically, deposition of sediment would cause the bed to move closer to the (fixed) sensor, whereas downward motion of the entire instrument through sinkage or scour would cause the sensor to move closer to the (fixed) bed.

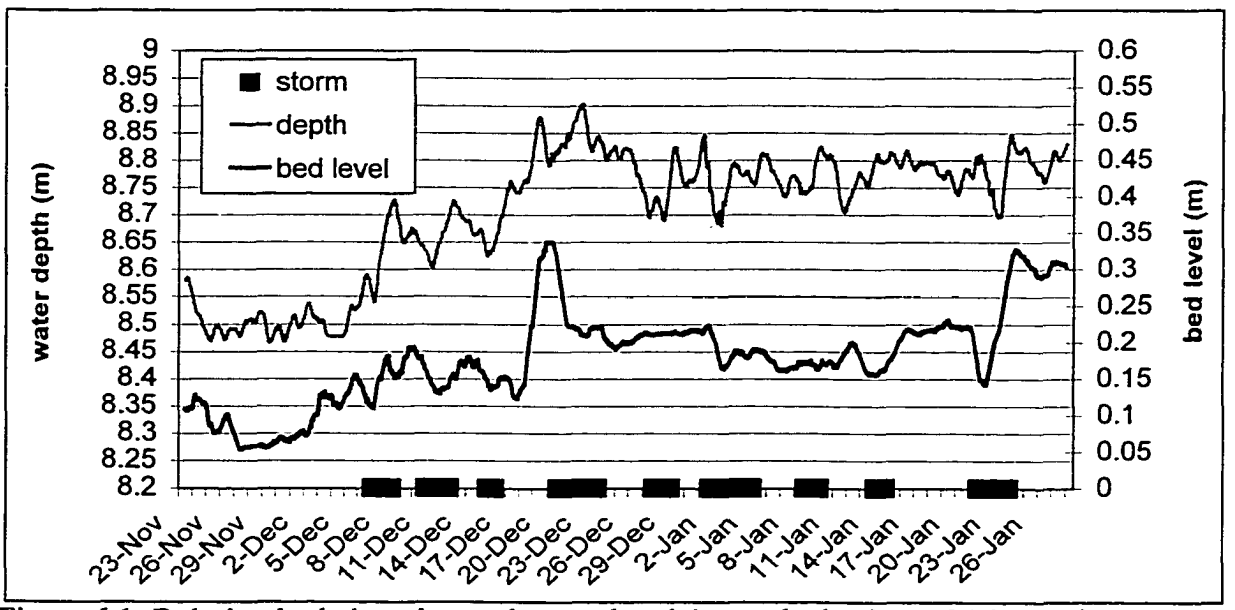

Figure 6.1: Relative bed elevation and water level (smoothed using a 24-h moving average window), as measured by System 1B during the deployment. Storm periods are indicated with black bars, as will be the case in subsequent figures.

However, the pressure gauge also enabled the distance from the system to the sea surface to be quantified. There is no reason to believe that the water level at the site increased over the course of the deployment, beyond obvious short-term fluctuations due

to tides and wind forcing. This is supported by NOAA data from Grand Isle (GDIL1), which indicated little change in water level between the beginning and end of the deployment period of the research. The time series of 24-hour moving average water level at System 1B, however, did indicate a 20-cm water level increase during the period, and more convincingly, these trends in water level were strikingly similar in bed level change. As such, when the sum of the water depth to the sensor and the distance from the sensor to the bed (i.e. the total water depth) was considered, no appreciable long-term trend over the course of the deployment was evident (Fig. 6.2). Thus, it would appear that there was probably no appreciable long-term change in bed level at the sites, but instead, a downward displacement of the instruments relative to it. All calculations of water level or total depth used in this paper were therefore corrected for the influence of deployment-length instrument level change. Figure 6.2: Total water depth (to the bed) measured hourly by System 1B and smoothed using a 24-h moving average window.

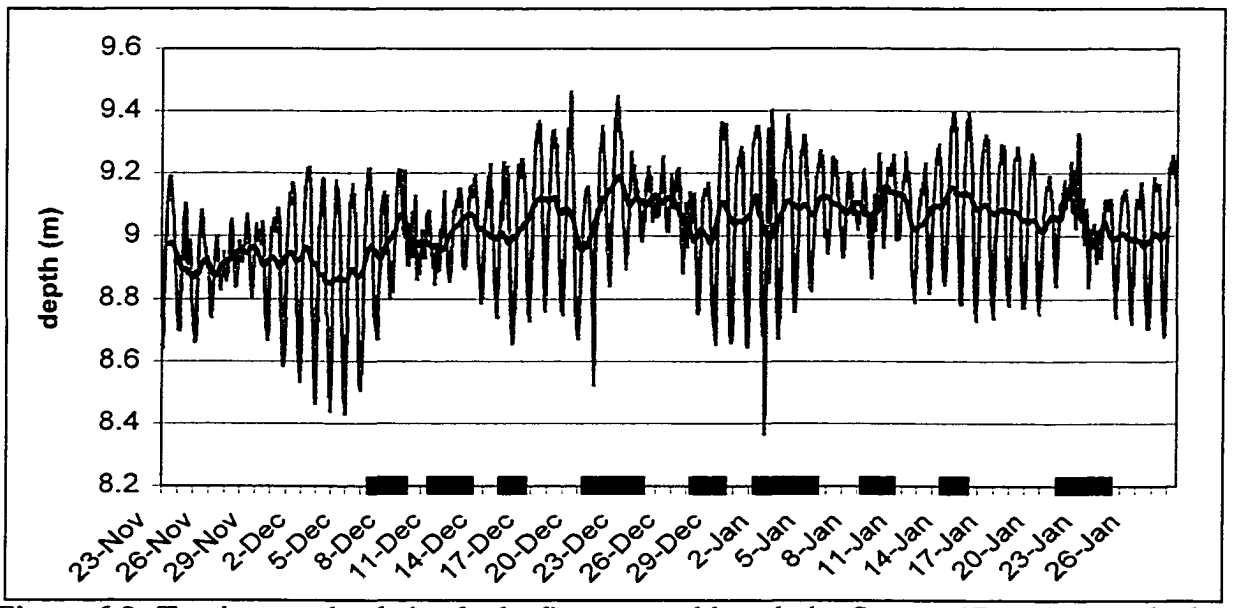

Figure 6.2: Total water depth (to the bed) measured hourly by System 1B and smoothed using a 24-h moving average window.

Two possible causes for the downward displacement of the instruments were suggested previously: in-place sinkage; and scouring accompanied by re-deposition of sediment around the instruments' bases, likely as a result of energetic wave-orbital currents. The second of these possibilities is far more likely, for two reasons. First, sinkage appears somewhat implausible, since the frames of the systems were wide and stable and the seabed in the study area was flat and sandy. Second, the vertical motion of the instruments was highly episodic, suggesting the importance of forcing mechanisms that vary considerably over time, such as hydrodynamic processes. Sinkage, on the other hand, which is driven essentially by the constant force of gravity, would be expected to be fairly consistent temporally. It appears, therefore, that scour was an important factor around the bases of the instruments. However, it is important to point out that flow modification and scour do not appear (with a few exceptions to be noted) to have influenced the sensors themselves, which were separated by tens of centimeters from the heaviest, most-intrusive, parts of the instrument frames.

As noted previously, short-term upward and downward fluctuations of the bed level appear in the deployment record. Unlike episodic deposition of sediment, which can be interpreted from the data record as either bed or instrument displacement, decreases in bed elevation are less ambiguous to interpret since sediment cannot plausibly accumulate under the base of an instrumentation system. Low rates of episodic bed erosion must have therefore occurred locally beneath the bed sensors. It appears, therefore, that in addition to the movement of the systems themselves, short-term fluctuations in bed level, caused by erosion and accretion, occurred during the deployment, suggesting that sedimentary processes during the winter are quite dynamic at these sites.

6.2 Hydrodynamics

An overall summary of hydrodynamic parameters for the entire deployment is shown in Table 6.1. Important points to note include the total depth, which was 1.5-2 m deeper offshore (Site 1) than nearshore (Site 2), and the depth range, which was slightly more than 1.0 m at both sites. Significant wave height and wave orbital velocity were higher at Site 1 than at Site 2, by 36 and 18 %, respectively, which is consistent with the expectation that waves crossing Ship Shoal are attenuated as a result of depth-limited energy dissipation. Wave period was also higher at the offshore site, which likely reflects the reduced importance of northward-propagating long-period swell waves relative to locally generated sea, also due to attenuation of the former across the shoal.

Table 6.1: Summary of hydrodynamic parameters recorded by the systems throughout the deployment. It should be noted (as discussed previously) that the final recording dates of the instruments were different and that the sensors on System 1A were buried for several hours during the deployment.

Location		*Site 1 (Offshore)*		*Site 2 (Nearshore)*
System	*Statistic*	*1A (ADV)*	*1B (WADMAS)*	*2A (ADV)*
Total Depth (m)	Mean	8.8	9.0	7.3
	Minimum	8.2	8.4	6.7
	Maximum	9.2	9.5	7.8
Hs (m)	Mean	n/a	0.61	0.45
	Minimum	n/a	0.07	0.10
	Maximum	n/a	2.80	1.53
Tp (s)	Mean	n/a	5.3	5.0
	Minimum	n/a	3.6	3.6
	Maximum	n/a	9.1	9.1
Orbital Velocity ($cm\ s^{-1}$)	Mean	11.7	10.6	9.9
	Minimum	2.6	0.8	0.0
	Maximum	35.9	53.1	36.5
Current Speed ($cm\ s^{-1}$) (~0.5m above bed)	Mean	5.8	4.6	6.3
	Minimum	0.1	0.1	0.0
	Maximum	44.8	34.2	47.6
Current Speed ($cm\ s^{-1}$) (~1m above bed)	Mean	12.4	8.0	13.9
	Minimum	0.1	0.1	0.0
	Maximum	72.4	53.2	62.3
Current Direction	Mean	245	240	292

In contrast to the somewhat predictable differences in wave parameters between sites, differences in current velocity, while equally evident, were less expected, and in some senses, less explicable. Interestingly, for example, unlike wave energy, mean current speed was approximately 10% higher at Site 2 (nearshore) than Site 1 (offshore). Current direction had a strong westerly component at both sites, which is consistent with general trends suggested in previous research (Crout and Hamiter, 1981; Jaffe, 1997). More notably, however, the across-shelf component was seaward at the offshore site and landward at the nearshore site (Fig 6.3). Since the two sites are separated by only a few kilometers and are thus influenced by nearly equivalent atmospheric and tidal forcing mechanisms, this was apparently the result of flow modulation by the bathymetry associated with Ship Shoal. The reasons for this are not entirely clear, although one likely possibility is that along-shelf currents were steered downslope by gravity when they encountered the shallow shoal, thus resulting in an onshore flow to the north and an offshore flow to the south. Unfortunately, it is difficult to verify this from the available data set. Preliminary results from a more recent deployment that included an instrument located in the center of the shoal, however, suggest that this interpretation is correct. It is clear, therefore, that Ship Shoal exerts a measurable influence on mean current flow, although the details of resultant flow patterns require further quantification. More generally, it is apparent that the shoal has an important effect on regional hydrodynamics, a phenomenon that is presumably also significant on any inner shelf that includes submerged sand bodies or other prominent bathymetric features. This has important implications for bottom boundary layer dynamics and sediment transport on the south-central Louisiana inner shelf, a point that will be discussed further subsequently.

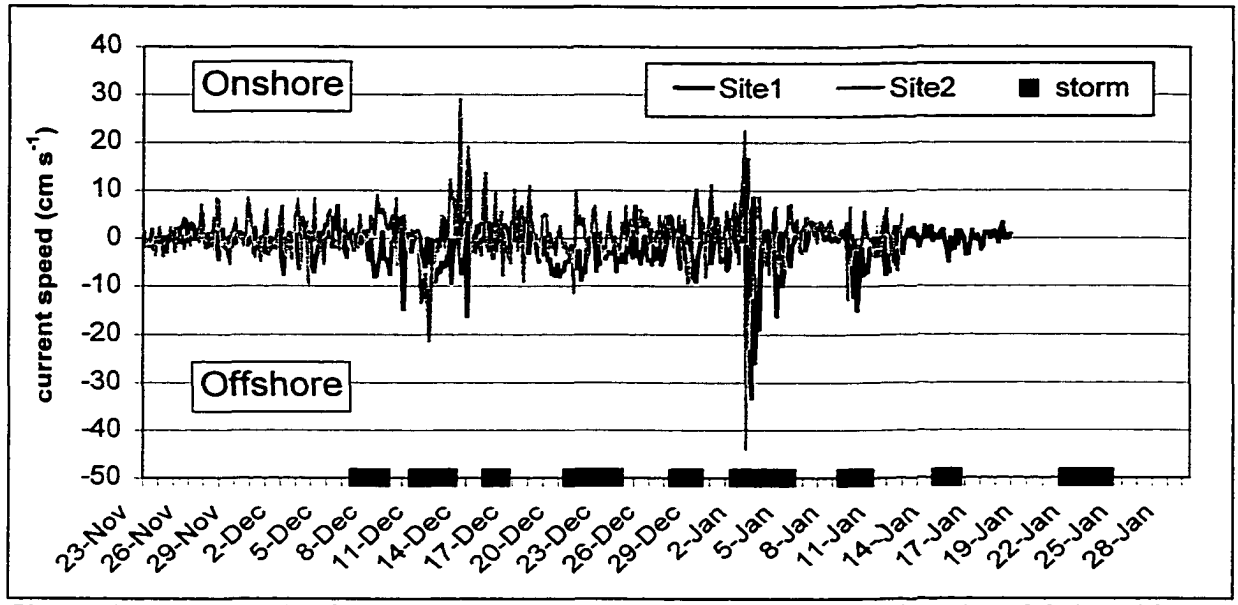

Figure 6.3: Across-shelf current flow during the deployment at Sites 1 and 2 (at ~20 cm above the bed) as measured by Systems 1A and 2A.

Time-series plots clearly illustrate the importance of storms in generating episodic increases in hydrodynamic energy, as well as the differences in hydrodynamic response between the study sites. Figures 6.4 And 6.5 show significant wave height and peak wave period, respectively, at the offshore and nearshore sites, highlighting not only the differences between storms and fair weather, but also the changes in wave characteristics caused by Ship Shoal. Three peaks in wave height are particularly evident, two associated with Storms 6 and 9, respectively, and the other occurring during the interval of fair weather between Storms 3 and 4. The fact that the third of these peaks occurred during a period of fair weather (meteorologically) is particularly noteworthy, and will be considered in detail later in this dissertation. For convenience, this "wave event", which lasted roughly from December 18 at 20:00 UTC to December 20 at 21:00 UTC, will hereafter be referred to as Event W. However, the wave event will be included amongst the fair weather conditions discussed later in this dissertation, since it did occur during "fair weather" as defined on the basis of meteorological parameters. Aside from Event

W, however, significant wave height during storms was several times the mean fair weather value and, as stated previously, was clearly higher at Site 1 (offshore) than at Site 2 (nearshore). Trends in peak wave period (Fig. 6.5) were not especially clear from the time series, although peak period appears to have fluctuated in a temporally similar manner at the two sites. As such, it will be considered in greater detail in later chapters.

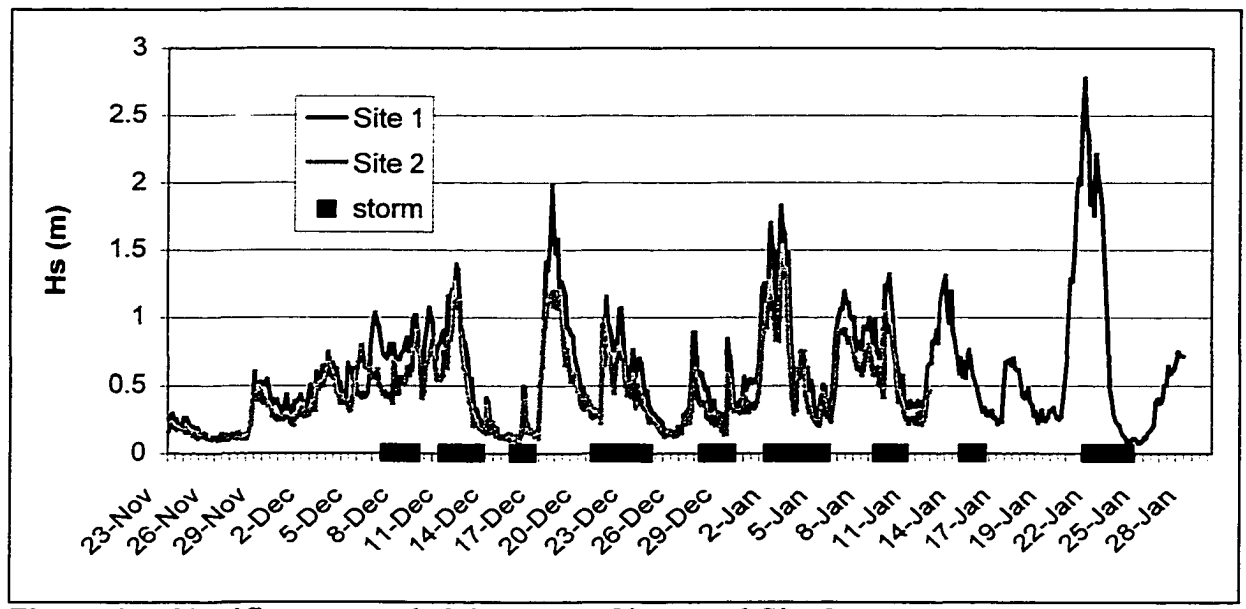

Figure 6.4: Significant wave height (Hs) at Site 1 and Site 2.

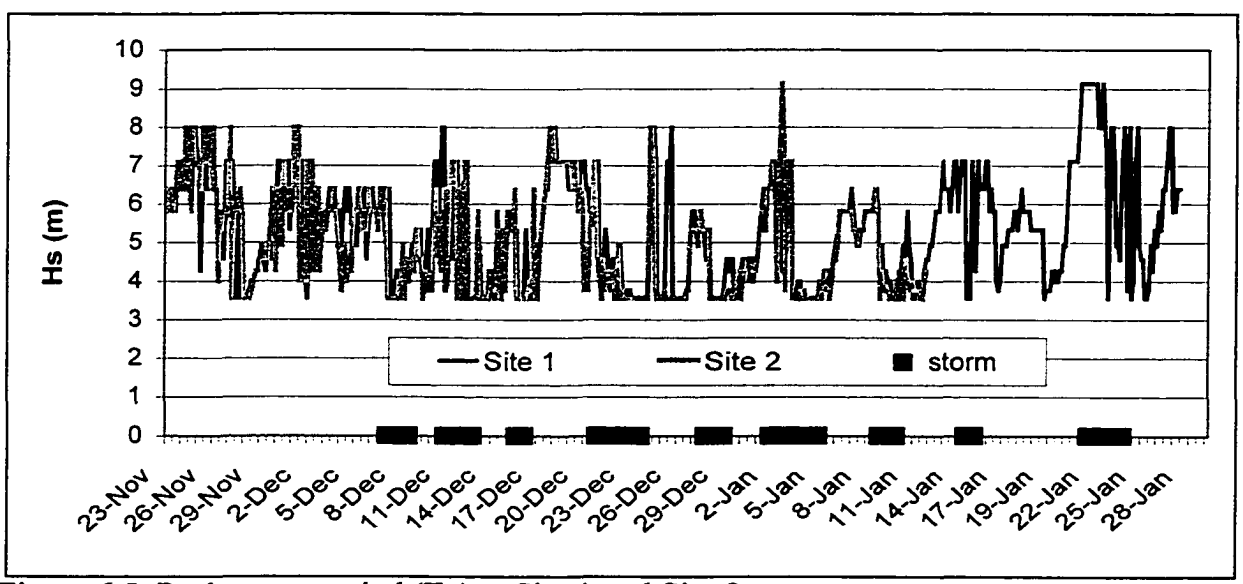

Figure 6.5: Peak wave period (Tp) at Site 1 and Site 2.

Figures 6.6 and 6.7 illustrate mean current and wave orbital speed at Sites 1 and 2, respectively, revealing several regularities. First, dramatic increases in both mean and wave-driven flow tended to accompany storms, particularly Storms 6 and 9 and Event W. Second, although mean and orbital current speeds were similar overall, each attained a relatively higher level at different times during the deployment, apparently as a result of differing meteorological forcing mechanisms. For example, while wave orbital flows were dominant at both sites during Storm 7, comparatively stronger mean currents accompanied Storm 6, particularly at the nearshore site. The situation therefore contrasts both with surf zones, where orbital flows are nearly always dominant, and outer continental shelves, where mean currents are expected to be more important. The near parity between the magnitude of these hydrodynamic mechanisms has clear implications for sediment suspension, which is thought to be closely related to wave orbital flow, and suspended sediment transport, which is strongly influenced by the presence of a mean current (Green et al., 1995). This highlights the uncertainty inherent in the study of sediment transport on the inner continental shelf, since either mean or fluctuating flow mechanisms may dominate, depending on a complex interaction of a variety of geographical and oceanographic factors.

Hydrodynamic variables for all storm and fair weather conditions for Sites 1 and 2 are quantified in Tables 6.2 and 6.3, respectively. As outlined previously, three atmospheric/hydrodynamic situations became evident from an analysis of the time series data: fair weather, extratropical storms (Storms 1-9), and a wave event (Event W). At both sites, hydrodynamic conditions during an average extratropical storm and during the wave event clearly differed from those that occurred during fair weather. As expected,

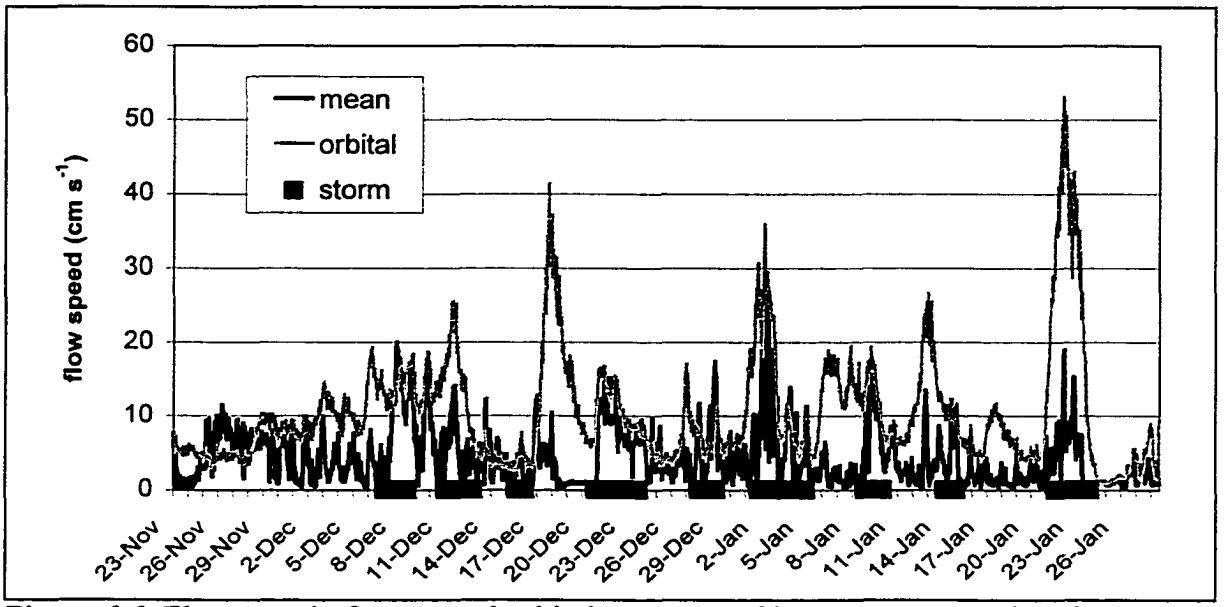

Figure 6.6: Flow speed of mean and orbital currents at Site 1 (as measured by System 1B at ~0.2 m above the bed).

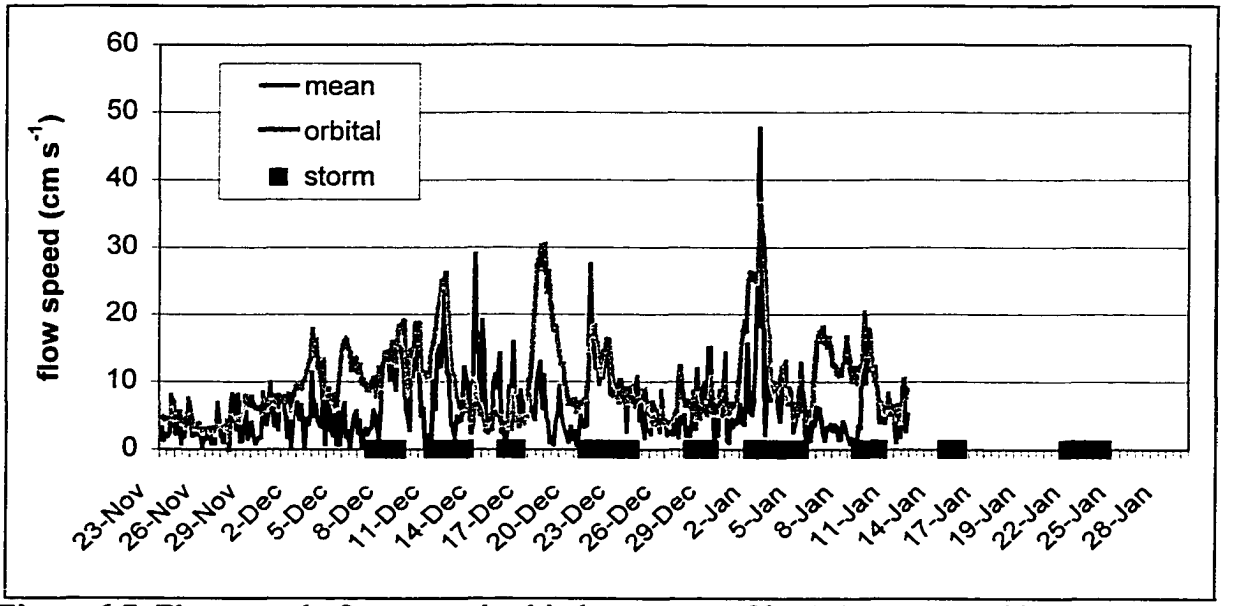

Figure 6.7: Flow speed of mean and orbital currents at Site 2 (as measured by System 2A at ~0.2 m above the bed).

significant wave height and orbital velocity generally increased during extratropical storms, while peak wave period decreased, presumably as a result of sea-like conditions that were generated by sudden increases in wind speed. During the wave event, significant wave height, peak period, and orbital velocity increased dramatically at both sites as well, to levels well in excess of an average extratropical storm. Mean current speed was much higher during extratropical storms than during either fair weather or the wave event, when values were fairly comparable. Current direction at both sites was southwesterly during extratropical storms, and thus had an offshore component, although this was most pronounced at Site 1. Fair-weather current direction was very close to westerly at the offshore site, while it was north-northwesterly at the nearshore site (Site 2), indicating a strong onshore component. Current direction during the wave event was to the northeast at both sites, although it had a much stronger northerly (onshore) component at Site 1 and a stronger easterly component at Site 2.

Although extratropical storms in general were characterized by more energetic hydrodynamic responses than fair weather, with indices measured during some storms many times in excess of average fair weather conditions, there was still considerable variability between storms. In the case of meteorologically-weak events, such as Storm 3, and to some extent, Storm 5, waves and currents were actually less energetic than during typical fair weather conditions. Another notable point is that, even during powerful storms, waves and currents were not necessarily proportionately high—in other words, high waves and strong mean flows were not always concurrent. For example, while waves at the offshore site during Storm 9 were more than twice as high as they were during Storm 1, mean current speed was measurably weaker. It is clear therefore, that

while storms were usually responsible for generating comparatively high-energy hydrodynamic conditions, there was considerable variation between storms.

Table 6.2: Summary of hydrodynamic measurements during extratropical (E.T.) storms, fair weather conditions, and the wave event (Event W) at Site 1 using System 1B (WADMAS). Hs is significant wave height, Tp is peak wave period, and Ub is orbital velocity, while Top, Mid, and Bot refer to current velocity at sensor heights of 100, 60 and 20 cm above the bed, respectively.

	Waves			*Currents*			
Meteorology	*Hs (m)*	*Tp (s)*	*Ub(cm s^{-1})*	*Top (cm s^{-1})*	*Mid (cm s^{-1})*	*Bot (cm s^{-1})*	*Direction*
Storm 1	0.73	4.4	13.5	17.0	15.5	11.1	237
Storm 2	0.69	4.89	12.4	11.7	10.0	5.4	132
Storm 3	0.29	3.77	5.3	4.8	4.2	2.7	346
Storm 4	0.76	3.93	11.7	16.8	15.9	8.8	231
Storm 5	0.33	2.87	6.0	12.1	11.1	7.6	219
Storm 6	0.84	4.81	14.0	13.8	13.1	8.5	167
Storm 7	0.98	4.07	14.4	16.4	15.0	10.0	214
Storm 8	0.67	5.25	10.6	7.5	7.0	4.5	205
Storm 9	1.81	8.91	34.1	14.1	11.9	6.6	49
E.T. Storms	**0.87**	4.99	**15.1**	13.7	**12.5**	7.7	**210**
Fair Weather	**0.52**	5.46	**9.1**	6.2	**5.3**	3.6	**260**
Wave event	**1.26**	6.96	**23.8**	8.7	**7.3**	5.0	**7**

Table 6.3: Summary of storm and fair weather hydrodynamic measurements taken at Site 2 using System 2A.

	Waves			*Currents*	
Conditions	*Hs (m)*	*Tp (s)*	*Ub (cm s^{-1})*	*U (cm s^{-1})*	*Direction*
Storm 1	0.53	3.85	12.3	9.9	288
Storm 2	0.73	5.56	15.8	9.4	146
Storm 3	0.24	3.66	5.6	7.4	301
Storm 4	0.59	3.87	12.2	11.2	274
Storm 5	0.23	3.95	6.3	8.7	191
Storm 6	0.62	4.70	13.2	10.6	173
Storm 7	0.73	5.75	14.0	12.8	262
E.T. Storms	**0.57**	4.27	**12.3**	10.3	**250**
Fair Weather	**0.42**	5.25	**9.2**	5.1	**335**
Wave event	**0.94**	6.99	**21.9**	6.0	**85**

Frequency-domain analysis shows the important time-scales over which across-shelf mean currents fluctuated. Figure 6.8 is a spectral plot of current speed during the deployment. Several statistically significant peaks are evident. The highest (i.e. most energetic) peak is at a period of 5.3-10.7 days, which reflects the importance of quasi-periodic extratropical storm passages in generating currents in the area. The next-highest peak occurred at a period of approximately 24 hours, illustrating the influence of diurnal tides and inertial currents, a phenomenon that will be discussed in more detail in subsequent sections. A minor peak is also evident at 12 hours, equivalent to that of the semi-diurnal tide, which is much less important than the diurnal tide at the study site.

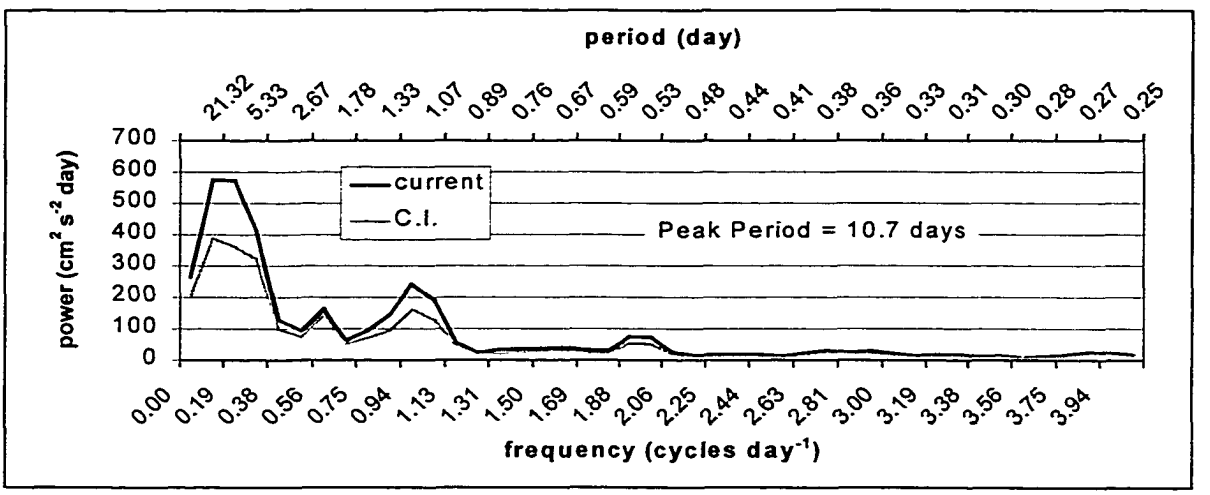

Figure 6.8: Power spectrum of current speed at Site 1. C.I is the 90% confidence interval.

Figure 6.9 is a vector plot of near-bed current velocity at Site 1. It indicates that currents rotated during the deployment on the expected time-scales of 5-10 days, reflecting the influence of extratropical storms, and 24 hours, suggesting the presence of either tidal or inertial currents, although the time-scales themselves may be somewhat difficult to visualize on the figure. Detailed inspection of Figs. 5.2 and 6.9 suggests that wind and near-bottom current generally moved in the same direction, presumably as a result of direct wind stress on the water column. This assessment is supported by cross-

spectral analysis. Figure 6.10 shows that a statistically-significant positive peak between across-shelf winds and currents was present at periods of 5-10 days (the extratropical storm band) while the phase spectrum indicates that there was little or no phase difference between these variables (Fig. 6.11). In other words, southerly winds were coincident with northerly currents, and northerly winds were coincident with southerly currents, with extratropical storms apparently providing the major energy input. The same relationship appears to be true of along-shelf winds and along-shelf currents, although the cross-spectrum was not statistically significant over most frequencies. Cross-spectra of winds and currents orthogonal to each other did suggest possible Ekman effects at storm frequencies farther out on the shelf, but these results were also not statistically significant and are therefore not presented.

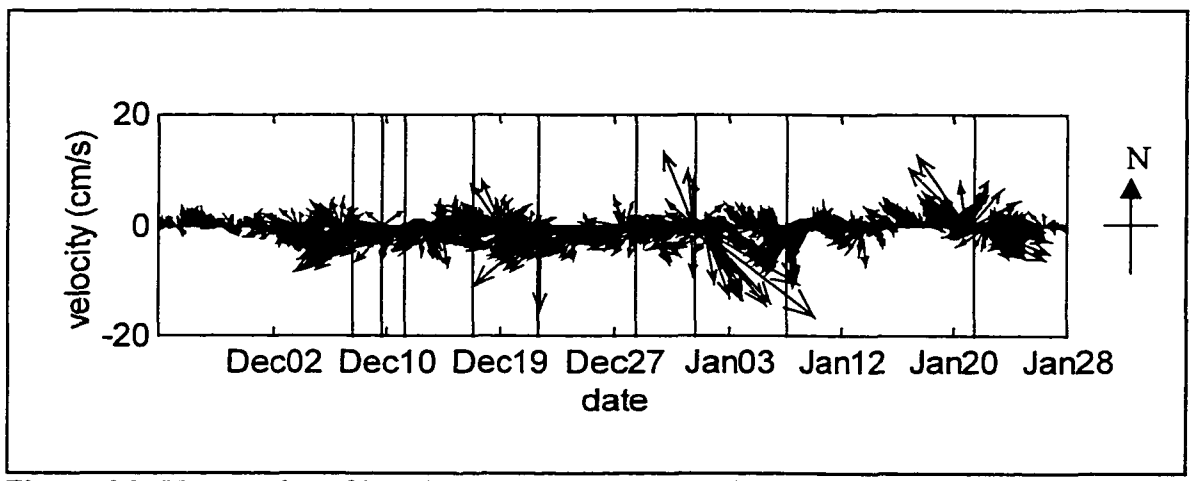

Figure 6.9: Vector plot of hourly current velocity at Site 1 during the deployment. Storm peaks are indicated by vertical lines.

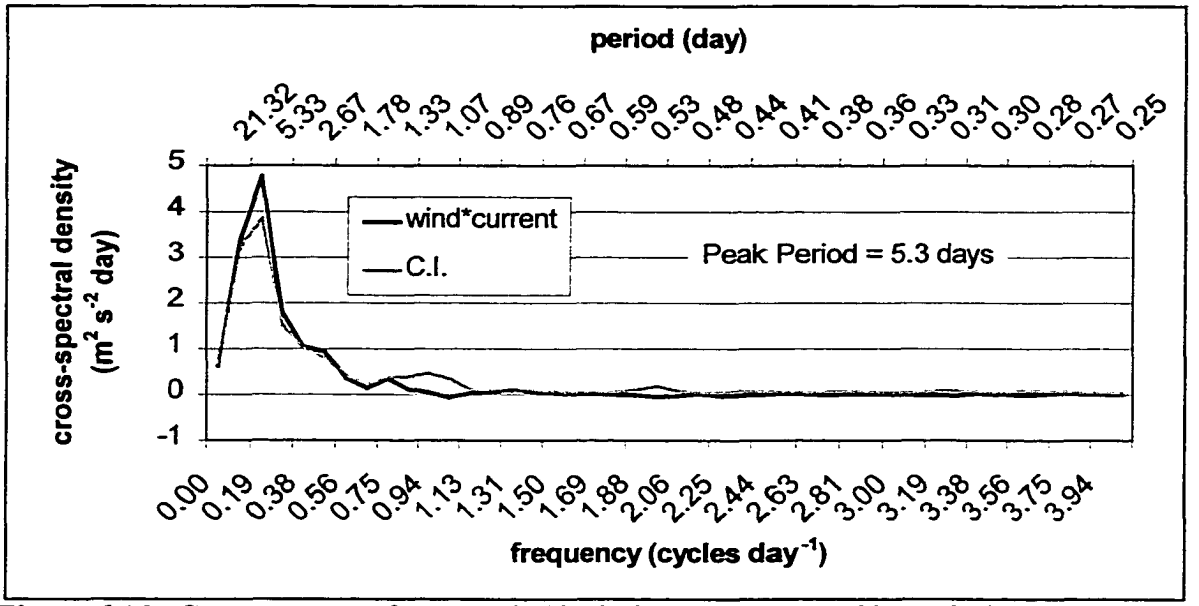

Figure 6.10: Co-spectrum of across-shelf wind and current at Site 1 during the deployment.

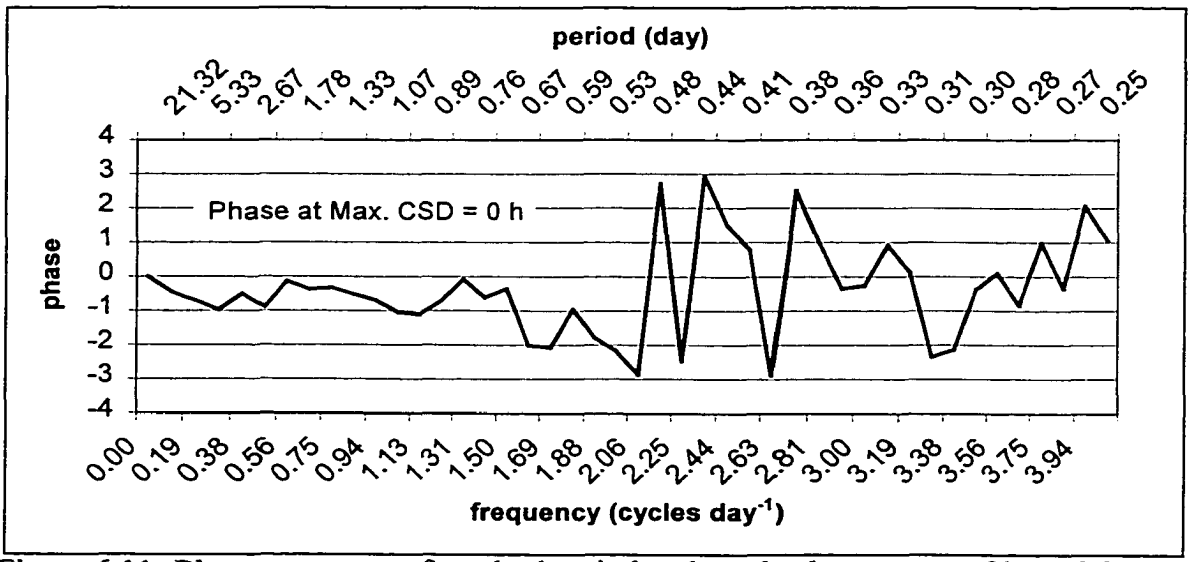

Figure 6.11: Phase spectrum of northerly wind and northerly current at Site 1. Max. CSD refers to the maximum cross-spectral density of across-shelf winds and currents.

The results regarding wind-driven flow are somewhat puzzling since most research, as discussed in Chapter 1, indicates that onshore storm winds normally generate coastal set-up, which causes downwelling (offshore) mean flows near the bed, while the reverse is true for offshore winds. Clearly, on the basis of mass conservation and an impenetrable coastal boundary, either return bottom flow or spatially-variable along-shelf flow is necessary if across-shelf currents are to flow in the same direction for an extended period of time. Inertial currents, which can result when a wind blowing steadily in one direction ceases (Pond and Pickard, 1983), are a possible explanation for the observed behavior. Inertial currents are essentially "remnant" currents that continue to flow despite removal of the forcing mechanism, with their direction and intensity modified by the Coriolis force and friction.

Daddio (1977) discussed the influence of inertial currents at a study site in south-central Louisiana. He stated that the location was sufficiently far from the coast (25 km) for the effect of sea surface slope (i.e. set up) to be negligible. Instead, Coriolis-driven inertial currents, which rotated clockwise with a period of approximately 24 h, accompanied frontal passages. This effect was enhanced when sudden removal of onshore wind forcing released sea surface set-up. It is possible that the near-bottom currents measured during the present study were at least partially the result of this effect, and not exclusively a product of direct wind forcing. Unfortunately, the lack of on-site wind data preclude a more detailed analysis of causal mechanisms. Despite this, the sequence of mean flow patterns that accompanied extratropical storm passages was distinctive, and has clear implications for inner-shelf sediment transport, which will be discussed in later sections.

6.3 Bottom Boundary Layer Parameters

As outlined in Chapter 4, several methods were used to calculate bottom boundary layer parameters, depending at least partially on the instrumentation used. In this section, results from the Reynolds Stress (RS) method are shown for Systems 1A and 2A, while results from the logarithmic profile method are given for System 1B. Although the values computed using the RS method are probably higher than those derived using other means outlined in the literature, relative magnitudes during storm and fair weather conditions, and between the two sites, are useful for comparative purposes.

Hydrodynamic differences between storms and fair weather obviously lead to differences in the bottom boundary layer regime, and these were evident at the deployment sites. Not surprisingly, episodic increases in current- and wave-current shear velocity were associated with storm activity (Figs. 6.12 and 6.13). Shear velocity was particularly high during the period of strong wave-orbital flow accompanying Event W, as well as during Storm 6, when mean flows were particularly strong. The interval of very high shear velocity that occurred during Storm 8 is somewhat difficult to explain, however, given that neither mean nor orbital currents were especially energetic. As discussed previously, however, shear velocity is a complex parameter that is related not only to the flow, but also to non-linear wave and current interaction, physical bottom roughness and sediment transport. In light of these considerations, it is notable that Storm 8 was characterized by a particularly high apparent bottom roughness value, potentially as a result of physical roughness elements, such as ripples, which could account for the anomalously high shear velocity.

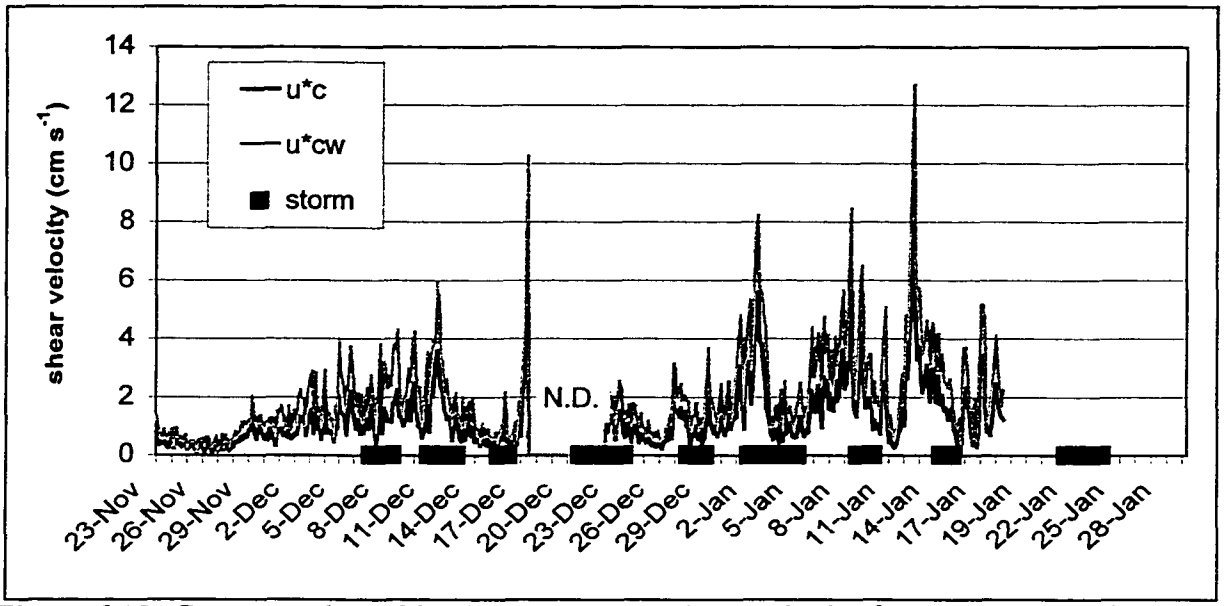

Figure 6.12: Current and combined wave-current shear velocity from Site 1, based on data from System 1A. N.D. = no data.

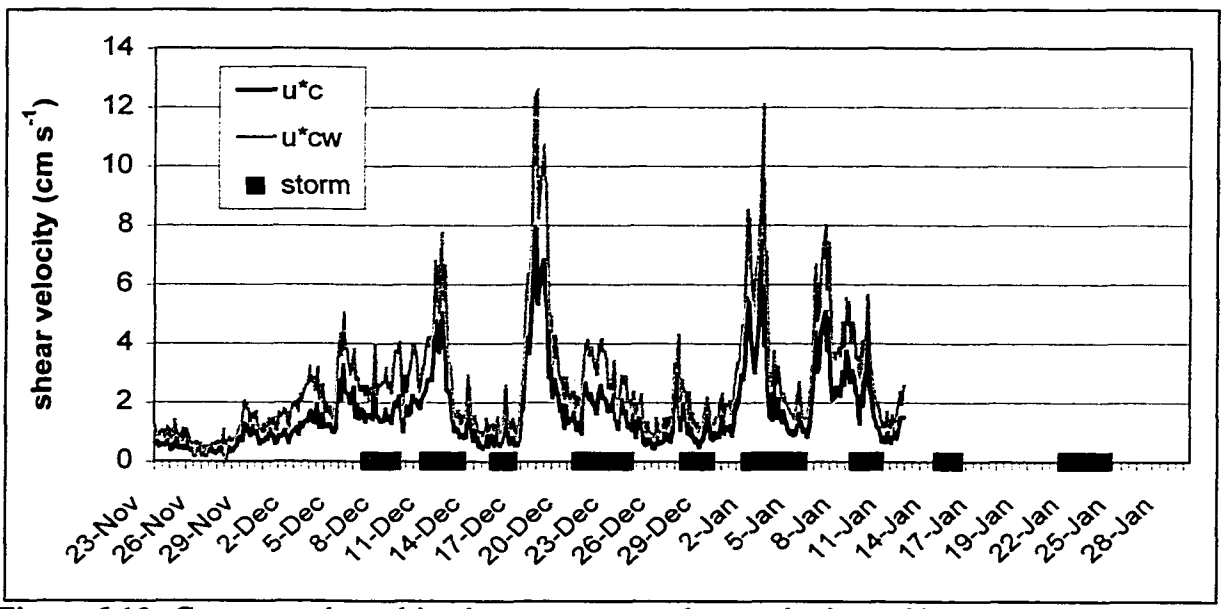

Figure 6.13: Current and combined wave-current shear velocity at Site 2.

Tables 6.4-6.6 summarize bottom boundary layer parameters for different conditions during the deployment. As indicated previously by the time series, current- and wave-current shear velocity were appreciably higher during storms than during fair weather, suggesting an increased potential for sediment entrainment and transport during high-energy events. However, there was also considerable variation between individual storms, largely as a result of their meteorological and hydrodynamic intensity. Not surprisingly, the more powerful storms, such as Storms 2, 4, 6 and 7, were characterized by high shear velocity values. Current shear velocity was in excess of 1.5 cm s^{-1}, and combined wave-current shear velocity exceeded 3.0 cm s^{-1}, during these events as calculated using the Reynolds Stress (RS) method. On the other hand, the shear velocities during Storm 3 and Storm 5 were weaker than during fair weather at two of the systems. Shear velocity during Event W was roughly equivalent to that of an extratropical storm according to data from System 1B, however, it was much higher than any extratropical storm as calculated using the RS method at Site 2.

Table 6.4: Summary of bottom boundary layer parameters (current, and wave-current, shear velocity, apparent bottom roughness, R-squared, wave friction factor, 100-cm drag coefficient, and wave boundary layer thickness) at Site 1, calculated based on System 1B (WADMAS) data for extratropical storms, fair weather, and the wave event.

	*u*c (cm s^{-1})*	*u*cw (cm s^{-1})*	*Zo (cm)*	*r2*	*fw*	*CD100*	*WBL (cm)*
Storm 1	1.50	2.63	2.21	0.972	0.037	0.0114	1.41
Storm 2	1.61	2.42	5.73	0.954	0.040	0.0143	1.62
Storm 3	0.41	0.67	1.25	0.968	0.022	0.0057	0.31
Storm 4	1.54	2.62	1.36	0.939	0.045	0.0063	1.34
Storm 5	1.02	1.62	2.02	0.930	0.056	0.0135	0.81
Storm 6	1.36	2.31	2.89	0.847	0.033	0.0139	1.55
Storm 7	1.42	2.27	1.69	0.910	0.031	0.0072	1.15
Storm 8	0.85	1.38	3.72	0.796	0.023	0.0170	0.86
Storm 9	1.64	3.06	3.84	0.970	0.016	0.0106	3.25
All Storms	**1.41**	**2.37**	**3.00**	**0.923**	**0.035**	**0.0116**	**1.60**
Fair Weather	**0.64**	**1.09**	**3.23**	**0.848**	**0.028**	**0.0217**	**0.76**
Wave event	**1.40**	**2.29**	**7.52**	**0.895**	**0.013**	**0.0204**	**2.06**

Table 6.5: Summary of bottom boundary layer parameters (current, and wave-current, shear velocity, apparent bottom roughness, wave friction factor, 100-cm drag coefficient, and wave boundary layer thickness) at Site 1, calculated based on data from System 1A for extratropical storms, fair weather, and the wave event. ** It should be noted that a full data set was not available for Event W, owing to burial of the instrumentation.

	$u*c$ (cm s^{-1})	$u*cw$ (cm s^{-1})	Zo (cm)	f_w	$CD100$	WBL (cm)
Storm 1	1.20	2.16	2.19	0.0326	0.0094	1.16
Storm 2	1.89	3.08	3.11	0.0298	0.0094	1.96
Storm 3	0.45	0.78	5.91	0.0360	0.0463	0.36
Storm 4	1.06	1.54	0.69	0.0261	0.0048	0.70
Storm 5	0.89	1.56	0.97	0.0318	0.0074	0.77
Storm 6	2.03	3.21	1.52	0.0284	0.0052	2.00
Storm 7	2.43	3.66	1.05	0.0378	0.0031	1.88
Storm 8	2.28	3.61	3.25	0.0388	0.0061	2.54
All Storms	**1.66**	2.67	**2.11**	0.0326	**0.0090**	1.58
Fair Weather	**1.12**	1.87	**3.22**	0.0311	**0.0182**	1.35
Wave Event**	**1.00**	1.61	**4.28**	0.0294	**0.0249**	1.24

Table 6.6: Summary of bottom boundary layer parameters (current, and wave-current, shear velocity, apparent bottom roughness, wave friction factor, 100-cm drag coefficient, and wave boundary layer thickness) at Site 2,calculated based on System 2A data for storms, fair weather, and the wave event

Conditions	$u*c$ (cm s^{-1})	$u*cw$ (cm s^{-1})	Z_0 (cm)	f_W	$CD100$	WBL (cm)
Storm 1	1.58	2.70	3.42	0.0462	0.0079	1.53
Storm 2	3.03	4.40	6.75	0.0383	0.0085	3.16
Storm 3	1.04	1.45	2.15	0.0540	0.0116	0.66
Storm 4	1.97	3.12	2.23	0.0557	0.0057	1.65
Storm 5	0.86	1.38	0.72	0.0457	0.0063	0.71
Storm 6	2.46	3.88	3.15	0.0472	0.0065	2.80
Storm 7	2.34	3.46	1.56	0.0490	0.0041	1.66
All Storms	**2.08**	3.22	**3.10**	0.0481	**0.0068**	1.95
Fair Weather	**1.58**	2.50	**5.76**	0.0447	**0.0168**	1.76
Event W	**4.91**	7.59	**8.02**	0.0198	**0.0056**	6.85

Coefficient of determination (r^2) estimates, obtained by applying log-linear regression to the stacked current meter data from System 1B, were used to evaluate the degree to which flows were characterized by a well-organized logarithmic structure. Values were generally higher during storms than during fair weather, as has been reported previously for extratropical storm passages (Pepper et al., 1998; Pepper et al., 1999). An increase in the statistical significance of logarithmic flow profiles did not

always accompany strong currents, however, as illustrated by Storm 6, which was characterized by r^2 values similar to those during fair weather (~0.85). This was caused by a few extremely low r^2 values that occurred during the waning phases of the storm, when apparent bottom roughness (z_{0c}) was very high (10-15cm). However, the reason for these large z_{0c} values during the final hours of the storm is unknown.

Apparent bottom roughness (z_{0c}), in most cases, decreased during storm activity, when values were generally less than 3.0 cm, as compared with mean fair weather values of 3.0-6.0 cm. Increased values were also observed, however, during some high-energy events, such as Storm 2, and especially during Event W. Drag coefficients at 100 cm above the bed (C_{D100}) usually decreased during storms, when mean values were near 0.01, roughly half the mean fair-weather value, likely as a result of the decreased bottom roughness. The response of these factors to storm activity is thought to be a function of bed form changes during the deployment, as described previously by several authors (e.g., Amos et al, 1999). It is possible that during prolonged fair weather periods, wave ripples eventually formed, increasing the physical roughness of the bed, while high-energy conditions caused bed forms to be washed out. Unfortunately, the limited observations made of the bed during this study neither confirm nor disprove this, and as such, further investigation of this question is necessary.

The wave friction factor (f_w), was higher during storms than during fair weather, although interestingly, it was high during one of the weakest events (Storm 3) and low during one of the strongest (Storm 9). In addition, it was very low during the wave event. It is somewhat unclear why this was the case, although it should be noted that wave friction factor was calculated numerically, based on a very complex set of interactions

between bottom boundary layer variables, and thus generalizations based on meteorological conditions may not be entirely appropriate. Wave boundary layer (WBL) thickness, on the other hand, is strongly a function of combined wave-current shear velocity ($u_{*_{cw}}$), as shown in Equation. 4.21, and thus responded much more predictably, occasionally reaching values during strong extratropical storms, and during the wave event, that were more than twice that of mean fair weather conditions. As was the case with nearly all bottom boundary layer parameters, however, deviations from general patterns were sometimes apparent. Not surprisingly, this variability was also present in the sediment transport data, which will be discussed in the next section.

6.4 Sediment Suspension and Transport

Sedimentary variables, including suspended sediment concentration and sediment transport rate, were characterized by more dramatic and punctuated fluctuations than hydrodynamic or bottom boundary layer parameters. The reasons for this are twofold: first, sediment suspension is subject to a threshold value, below which concentration and transport are zero; and second, sediment transport rate is ultimately subject to a power law, such that increases in flow velocity lead to exponential increases in transport.

6.4.1 Sediment Suspension

Suspended sediment concentration at each site is shown in Fig. 6.14. Sediment suspension increased greatly during storms—at Site 1, Storms 4 and 6, and Event W had the highest concentrations, while at Site 2, the maximum concentration occurred during Storm 6. Concentration was higher at Site 1 than at Site 2, likely as a result of the higher wave energy that occurred offshore during the majority of the deployment.

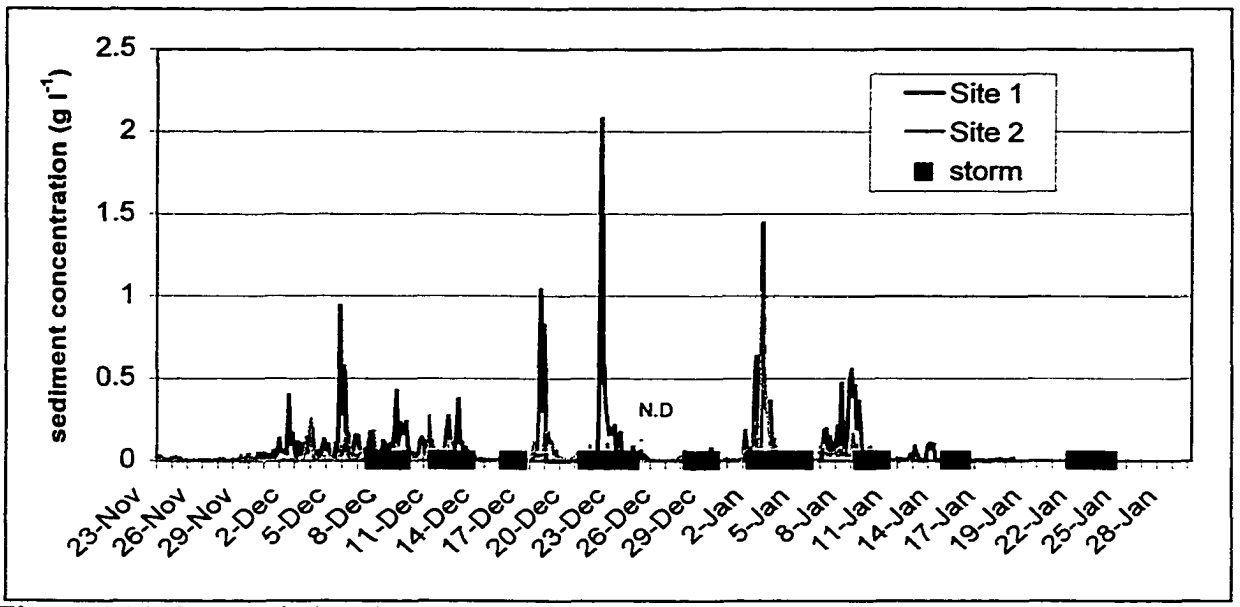

Figure 6.14: Suspended sediment concentration at the deployment sites as measured by Systems 1A and 2A. N.D.= No data for Site 1.

6.4.2 Sediment Transport Predicted using the GMR and MPM Models

Sediment transport was episodic and storm-driven at the two locations in both the across- and along-shelf directions according to the modeled and cospectral estimates. As noted in earlier chapters, the absolute values of the sediment transport predictions varied widely, and as such, they should be used chiefly as relative indices for the purposes of comparison; specifically, sediment transport rate tended to be highest with the GMR method, followed by the MPM, and SCP methods, respectively. Nonetheless, trends tended to be quite similar regardless of the method used.

Figures 6.15-6.18 illustrate, and Tables 6.7 and 6.8 quantitatively summarize, directional sediment transport rates as predicted using the Grant-Madsen-Rouse (GMR) method for suspended load and the Meyer-Peter and Muller (MPM) method for bed load. Generally speaking, the highest rates of along- and across-shelf sediment transport were associated with storms, most notably (extratropical) Storms 2, 6 and 7 as well as with the wave event (Event W), at Site 2 where a full data set was available. As shown in Tables

6.7 and 6.8, sediment transport during certain storms was several times higher than fair-weather values, while the transport rate at Site 2 during Event W exceeded the mean fair-weather rate by nearly an order of magnitude. Unfortunately, however, significant gaps in the data for Site 1 precluded a representative assessment of sediment transport at this location during Event W.

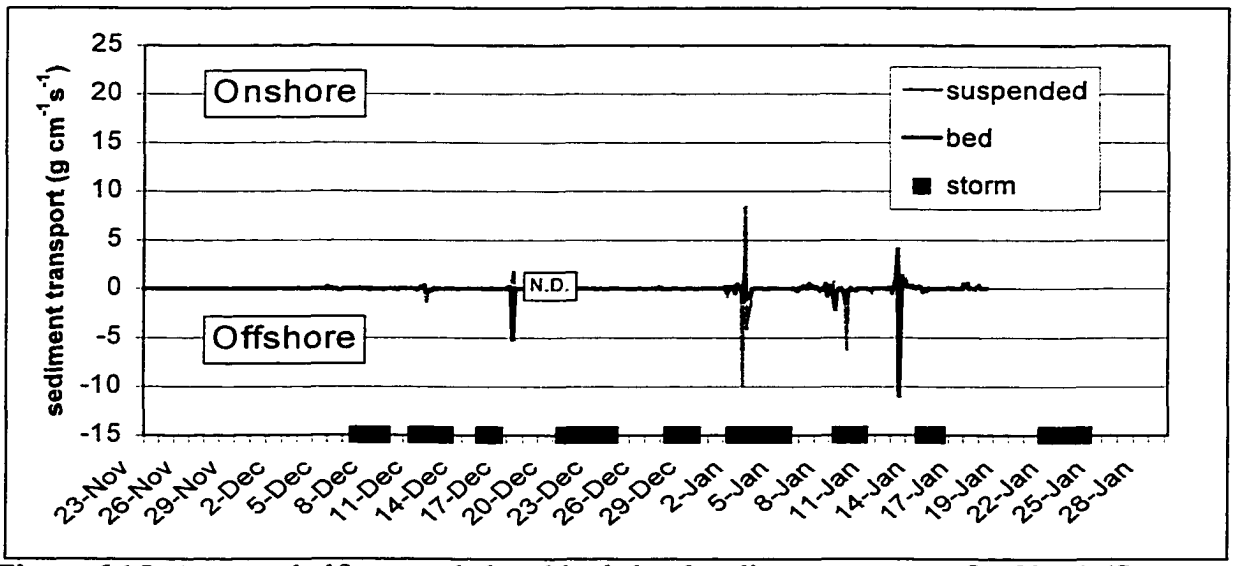

Figure 6.15: Across-shelf suspended and bed -load sediment transport for Site 1 (System 1A) as predicted using the GMR and MPM methods. N.D.= No data.

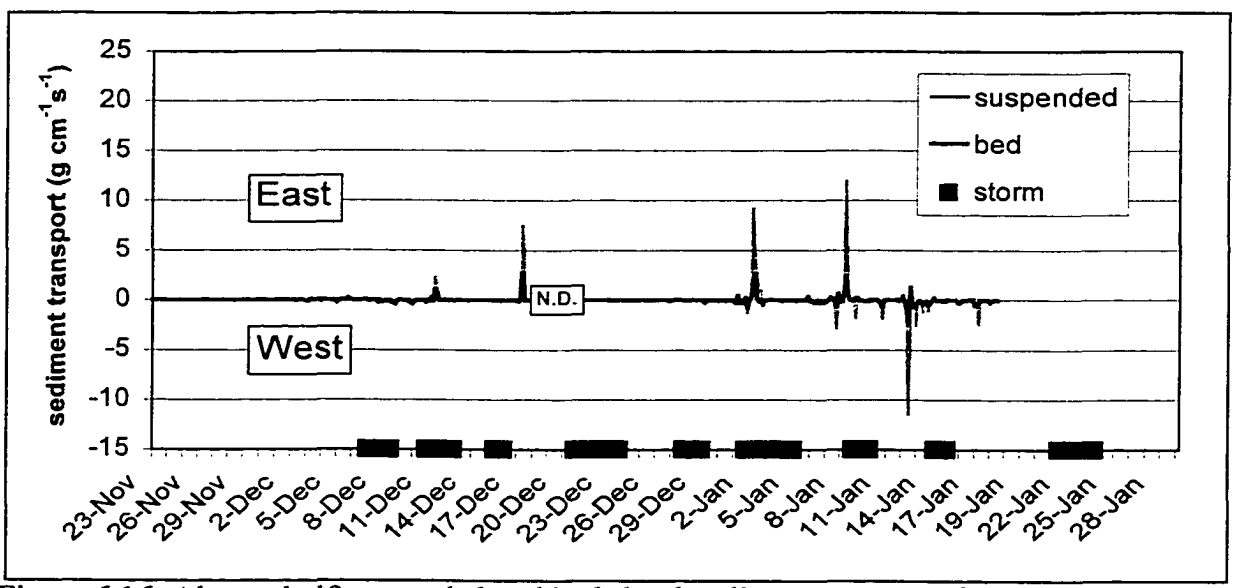

Figure 6.16: Along-shelf suspended and bed -load sediment transport for Site 1 (System 1A) as predicted using the GMR and MPM methods (respectively). N.D.= No data.

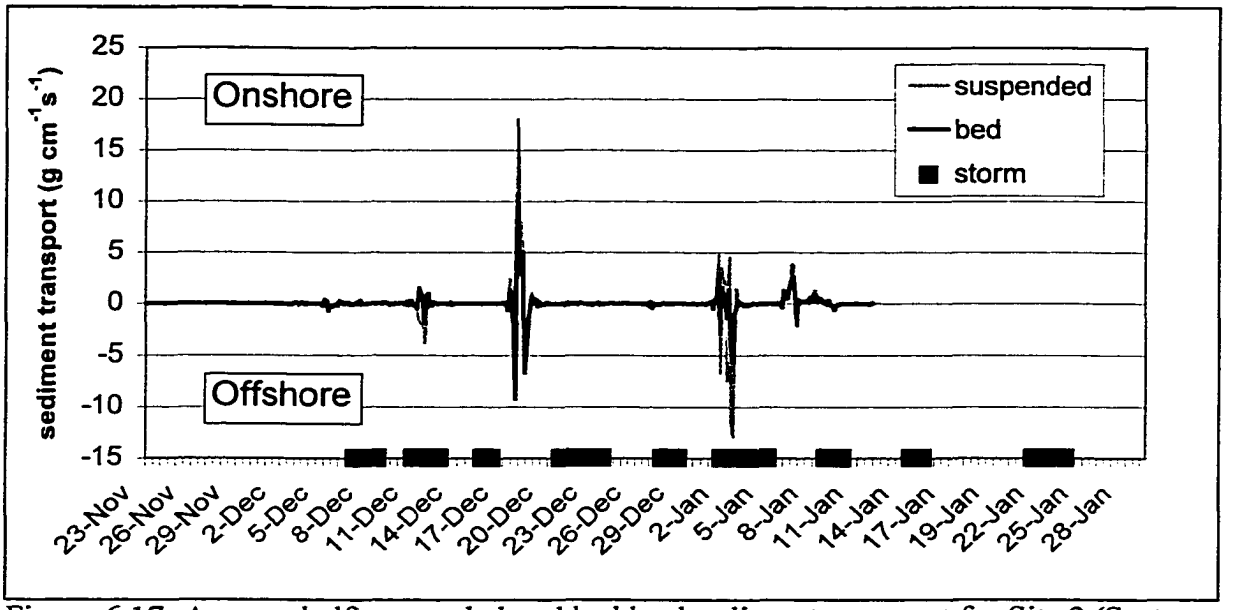

Figure 6.17: Across-shelf suspended and bed load sediment transport for Site 2 (System 2A) as predicted using the GMR and MPM methods (respectively).

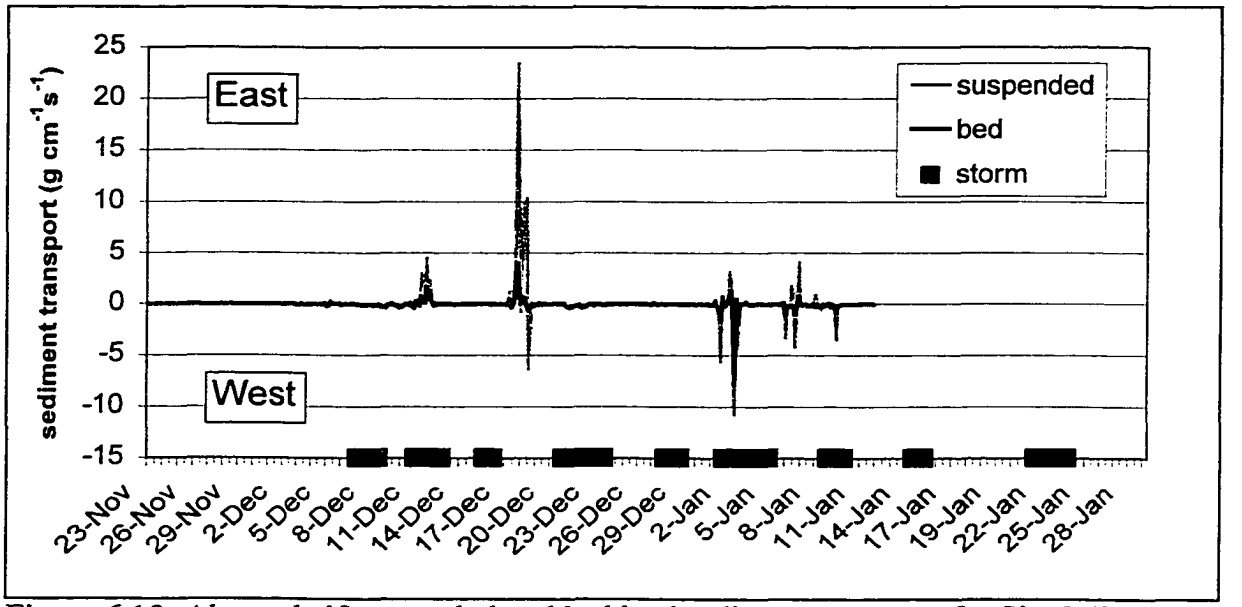

Figure 6.18: Along-shelf suspended and bed load sediment transport for Site 2 (System 2A) as predicted using the GMR and MPM methods (respectively).

Table 6.7: Predicted sediment transport for Site 1 based on data from System 1A analyzed using the GMR and MPM models. **It should be noted that a full data set was not available for Storms 4 or W, owing to burial of the instrumentation.

	GMR		*MPM*	
	Q (mg cm^{-1}s^{-1})	*Direction*	*Q (mg cm^{-1}s^{-1})*	*Direction*
Storm 1	25.8	251	56.6	245
Storm 2	213.3	109	82.1	113
Storm 3	0.0	348	0.3	338
Storm 4**	0.7	297	5.5	203
Storm 5	0.6	203	8.1	196
Storm 6	1425.1	120	159.0	120
Storm 7	1157.8	135	355.2	166
Storm 8	284.1	269	115.9	260
All Storms	**549.1**	139	**97.8**	145
Fair Weather	**138.7**	298	**85.6**	253
Wave event**	**44.2**	68	**79.8**	135

Table 6.8: Predicted sediment transport for Site 2 based on data from the GMR and MPM models.

	GMR		*MPM*	
	Q (mg cm^{-1}s^{-1})	*Direction*	*Q (mg cm^{-1}s^{-1})*	*Direction*
Storm 1	20.2	295	101.2	296
Storm 2	1356.3	129	674.6	95
Storm 3	4.8	276	20.8	309
Storm 4	112.5	291	175.1	261
Storm 5	0.7	309	12.0	324
Storm 6	2223.3	197	965.8	258
Storm 7	544.8	268	267.7	287
All Storms	**810.7**	182	**412.9**	256
Fair Weather	**584.8**	50	**325.0**	47
Wave event	**7087.4**	73	**3330.6**	47

Despite the higher values of sediment transport rate during storms that occurred overall, there was considerable variation between storms. Storms 3 and 5 resulted in little or no sediment transport, while strong storms, as discussed above, caused highly elevated sediment transport rates. It is apparent, therefore, that overall sediment transport was dominated by larger storms, including the wave event. It is also interesting that the mean sediment transport rate during fair weather was not zero as calculated by these techniques, indicating that sediment transport may occur at Ship Shoal during winter fair

weather conditions. This contrasts with conclusions from previous research, which have suggested that fair-weather resuspension and transport of bottom sediment is unlikely for much of the Louisiana continental shelf (e.g. Adams et al., 1987; Wright et al., 1997).

Sediment transport direction was, in general, highly variable, not only as a result of the occurrence of different types of weather conditions, but also between storms, over the course of individual storms, and in some instances, between the two sites. Predicted fair weather transport was westerly at Site 1, and easterly at Site 2, with the across-shelf vector tending to be onshore at both sites. Mean extratropical storm transport was offshore at both sites, with an easterly component at Site 1 and a westerly component at Site 2. Strong offshore components were most pronounced during energetic storms, which, as noted previously, generally dominated overall transport. Landward transport was sometimes evident, however, during weaker events, such as Storm 3. This was particularly notable at the nearshore site (Site 2), where roughly half of the storms transported sediment onshore, although generally at lower rates than the seaward transport that occurred at this site during stronger storms. One exception to this was Storm 4, which was fairly energetic, but appeared to have a slight landward component (at Site 2), owing to the presence of mean west-northwesterly flowing currents. During the wave event (Event W), transport was easterly, and by 3 out of 4 indices, onshore.

Within storms, transport direction fluctuated by 180° on a very short time scale (i.e. several times per storm) as is particularly evident in Figs. 6.15 and 6.17. This may have been related to diurnal fluctuations resulting from either tidal or inertial current flow, or to other variations in relative wave and current energy and direction. In regards to this, it should again be noted that according to the Grant-Madsen model, small

modifications in the relative strength or direction of waves and currents often cause dramatic shifts in sediment transport direction. The cause of these rapid directional shifts will be considered in more detail in subsequent chapters

6.4.2 Sediment Transport Predicted using Cross-Spectral Methods

Although an outline of cross-spectral methods employed in this study was provided in Chapter 4, a discussion of the specific causes of sediment transport over different frequency ranges, in the context of the field data, is warranted. Mean transport is simply the product of the mean current and mean suspended sediment concentration present at the measurement location during the entire burst interval. On the other hand, sediment transport over a particular frequency range implies oscillatory flow, whereby net transport will occur because more sediment is present in the water column during one phase of flow than the other (e.g. during the onshore, as opposed to the offshore stroke of a wind wave). Directional sediment transport in the frequency domain is therefore a function of the flow and suspended sediment concentration spectra, and the coherence and phase relationships between the two. During this deployment, the maximum value of the flow spectrum nearly always coincided with the peak wave period; however, this was not necessarily the case for the concentration spectrum, which often had no significant peaks at all, indicating weak coherence between oscillatory flow and sediment suspension. Phase relationships between flow and concentration varied considerably as well, causing large fluctuations in directional sediment transport estimates.

The implications of these spectral differences will be discussed in terms of two "end-member" cases that have been selected from Storm 6. Only across-shelf sediment fluxes will be considered during the following discussion since the most important shifts

in wind and wave direction associated with extratropical storms in the region are in this direction. The first instance (Case 1) occurred 3 hours prior to the passage of the cold front and involved low rates of low-frequency and wind-wave transport against the direction of wave propagation, which was northeasterly. The second (Case 2), which occurred 6 hours subsequent to the frontal passage, involved moderate and very high respective rates of low-frequency and wind-wave transport in the direction of wave propagation, which was also northeasterly. During both of these bursts, waves were considerably higher than the mean of 0.45 m for the study period—for Case 1, significant wave height was 0.83 m, while for Case 2, it was 1.31 m. Similarly, suspended sediment concentration was elevated for the two cases, which had mean concentrations of 0.57 and 0.37 mg l^{-1}, respectively.

Figure 6.19 shows the suspended sediment concentration spectra for the two time periods. The spectrum for Case 1 had no notable peaks, and thus, sediment concentration during this time was likely well-represented by the mean burst-averaged concentration. On the other hand, in Case 2, there was a very pronounced peak in suspended sediment concentration at wind-wave frequencies, suggesting that oscillatory flows had an important influence on sediment suspension at this time. The coherence spectrum of these two variables, shown in Fig. 6.20, also provides an indication of the relative importance of wind waves in the two situations. Clearly, there was a high, statistically significant peak at wind-wave frequencies in Case 2, while in Case 1, the only significantly coherent peak was at low frequencies, in a region where, in any case, little energy was present in the concentration spectrum. The phase spectrum (Fig. 6.21) shows that for Case 1, suspended sediment concentration was always approximately 180° out of phase with the

oscillatory flow, which is perhaps not highly significant, given the low levels of coherence between the two variables. In contrast, the phase of flow and concentration for Case 2 was between 45-90° for the range of the spectrum from periods of 5.3 to 12.8 s. Therefore, the highest suspended sediment concentrations were associated with the forward motion of wave flow, and transport at low- and wind-wave frequencies was in the direction of wave propagation. It should be noted, however, that although the example provided involved transport in the directions of the propagating waves, other instances were evident when high oscillatory sediment transport against the peak direction of propagating waves occurred.

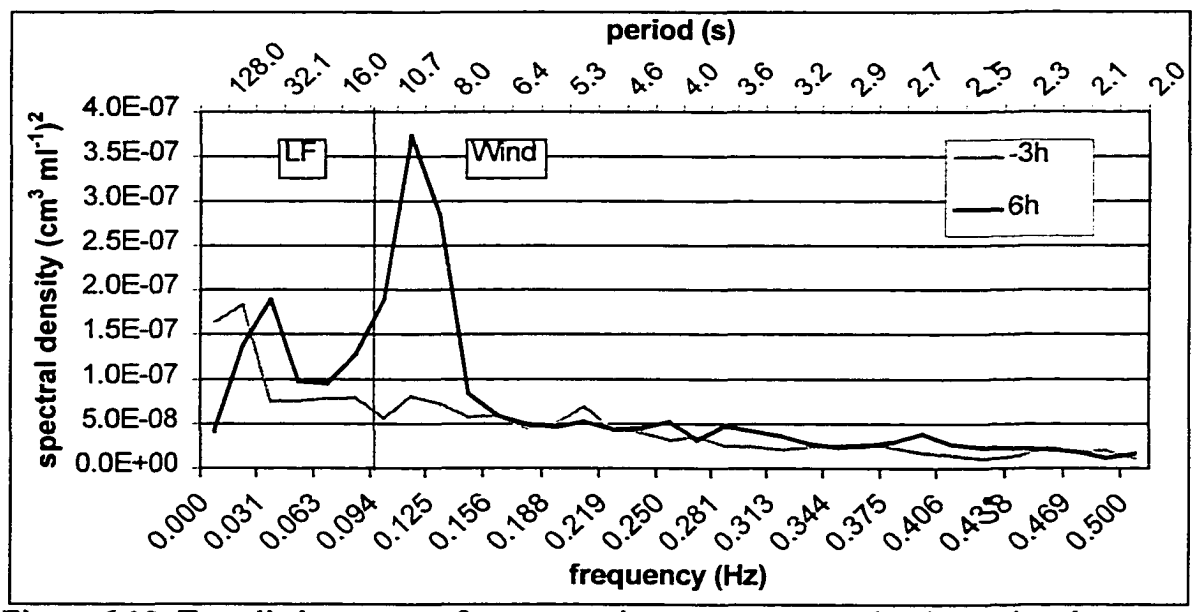

Figure 6.19: Two distinct types of concentration spectra, wave-dominated and non-wave dominated, observed 3 hours prior and 6 hours subsequent to the frontal passage at Site 2 during the deployment. LF = low frequency, Wind = wind-wave frequency.

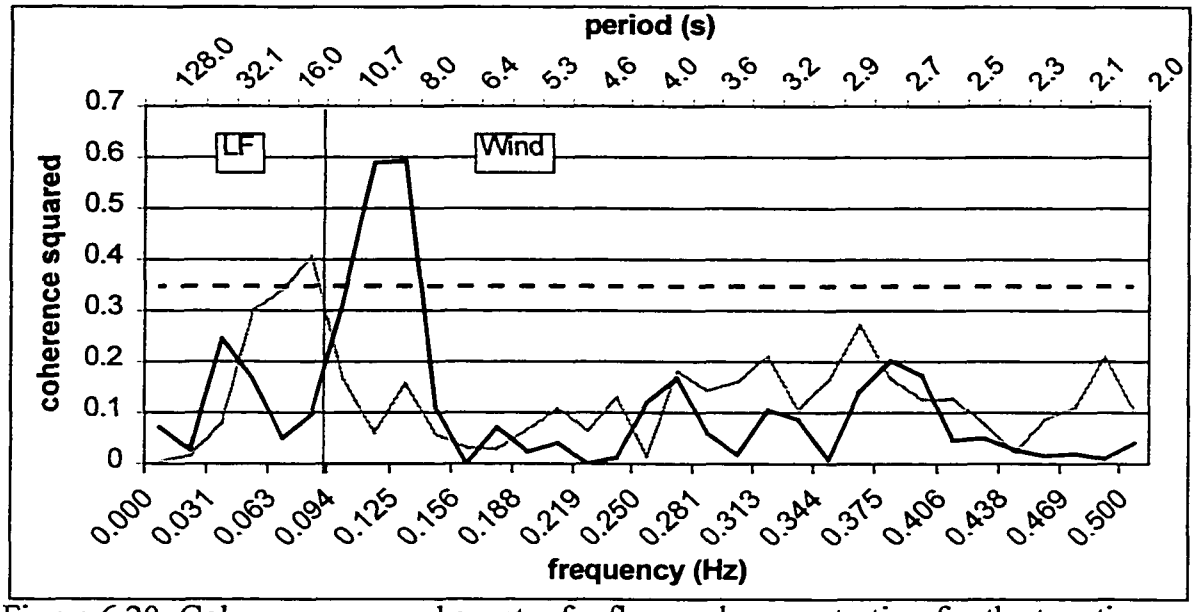

Figure 6.20: Coherence squared spectra for flow and concentration for the two time periods shown in Fig. 6.19. The dashed line indicates the 95% confidence interval. LF = low frequency, Wind = wind-wave frequency.

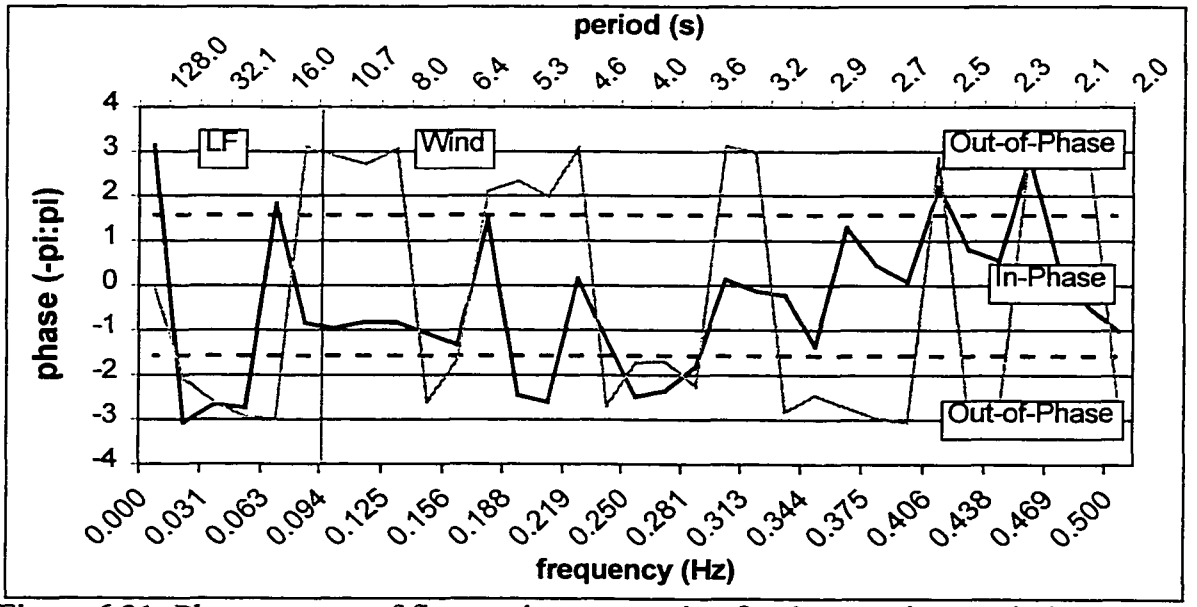

Figure 6.21: Phase spectra of flow and concentration for the two time periods shown in Fig. 6.19. LF = low frequency, Wind = wind-wave frequency.

It is clear that during certain conditions at the study site, such as in Case 2, discussed above, a strong peak in suspended sediment concentration, which was coherent with oscillatory flow, was generated at wind-wave frequencies, resulting in high suspended sediment transport in that range of the spectrum. However, wave characteristics alone were insufficient to account completely for this phenomenon, since similar wave conditions occurred throughout much of Storm 6, and yet directional wind-wave flux varied widely. A number of additional factors, including the distance of the sensor from the bed, the presence and morphology of bed forms, and the formation of secondary flow structures, such as wave vortices, may have been important (Hanes and Huntley, 1986; Green et al., 1990; Osborne and Greenwood, 1993; Vincent and Downing, 1994). The nature and possible causes of this will be discussed further in Chapters 7 and 8.

Tables 6.9 and 6.10 summarize suspended sediment transport predicted using cross-spectral methods at Sites 1 and 2. The first point to note is that sediment transport rate and direction at each site varied considerably according to frequency, as well as between weather conditions and individual extratropical storms, with transport directed toward all four directional quadrants at various times. As a result, total net (vector) transport was often substantially lower than would be expected on the basis of the gross (scalar) sum of the individual components. This was most important at Site 1, where high but widely-varying sediment-transport components during extratropical storms resulted in a total mean storm transport that was lower than during either fair weather or the wave event. In particular, mean flux during storms tended to be southerly, while oscillatory flux was predominantly northward.

Table 6.9: Cospectral estimates of suspended sediment transport (mg $cm^{-1}s^{-1}$) at System 1A (~20 cm above the bed). Periods are: Mean: averaged over 81 s (1.3 minutes); Low frequency: =>10.25s;Wind Wave: 2.15s-10.24s. **It should be noted that a full data set was not available for Storms 4 or W, owing to burial of the instrumentation.

	Mean Flux		*Low-frequency Flux*		*Wind-Wave Flux*		*Total Flux*	
	mg $cm^{-1}s^{-1}$	*Direction*	*mg $cm^{-1}s^{-1}$*	*Direction*	*mg $cm^{-1}s^{-1}$*	*Direction*	*mg $cm^{-1}s^{-1}$*	*Direction*
Storm 1	14.1	252	4.0	76	2.6	75	7.6	251
Storm 2	8.6	146	2.3	349	9.6	1	7.6	46
Storm 3	0.0	57	0.1	167	0.1	232	0.1	187
Storm 4**	15.9	253	4.9	29	14.8	177	18.5	215
Storm 5	1.1	249	0.3	59	0.9	81	0.6	334
Storm 6	47.8	141	8.2	338	22.1	351	20.9	89
Storm 7	2.8	171	2.2	157	12.1	237	13.8	218
Storm 8	0.2	278	0.3	39	0.2	76	0.3	25
All Storms	**11.4**	166	**2.9**	7	**3.4**	345	**3.6**	145
Fair Weather	**2.2**	250	**2.5**	316	**10.5**	312	**14.7**	306
Wave event**	**5.6**	29	**11.8**	185	**20.6**	195	**28.3**	188

Table 6.10: Cospectral estimates of suspended sediment transport (mg $cm^{-1}s^{-1}$) at System 2A (~20 cm above the bed). Periods are: Mean: averaged over 512 s (8.5 minutes); Low frequency:=>10.25s;Wind Wave: 2.15s-10.24s.

	Mean Flux		*Low-Frequency Flux*		*Wind-Wave Flux*		*Total Flux*	
	mg $cm^{-1}s^{-1}$	*Direction*	*mg $cm^{-1}s^{-1}$*	*Direction*	*mg $cm^{-1}s^{-1}$*	*Direction*	*mg $cm^{-1}s^{-1}$*	*Direction*
Storm 1	21.6	294	1.3	116	1.5	167	19.4	291
Storm 2	30.6	141	1.7	321	1.2	359	27.4	140
Storm 3	0.8	279	0.0	103	0.0	103	0.8	279
Storm 4	31.7	287	1.7	94	1.1	106	28.6	288
Storm 5	0.1	353	0.0	167	0.0	179	0.1	353
Storm 6	151.1	140	2.4	314	12.3	71	152.9	136
Storm 7	49.2	266	2.3	79	2.4	107	44.0	265
All Storms	**36.7**	155	**0.7**	7	**3.7**	74	**36.7**	148
Fair Weather	**2.6**	334	**0.3**	257	**1.5**	358	**4.0**	338
Wave event	**21.5**	47	**4.8**	224	**9.3**	20	**24.5**	38

Bearing in mind the observations discussed in the previous paragraph, transport rates were generally higher during individual energetic extratropical storms, such as Storms 4, 6, and 7, than during fair weather conditions, as was the case with the modeled results. Sediment transport rates at the "mean" frequency were usually dominant, followed by wind-wave frequencies (i.e. periods of 2.15 s-10.24 s), with low-frequency

transport commonly playing lesser role. In particular, it is notable that mean flux had a much higher relative importance at Site 2 (nearshore) than at Site 1. This result is important to the validity of this analysis, given the uncertainties involved in predicting oscillatory flux, as introduced in preceding paragraphs and to be discussed subsequently. Predicted sediment transport rates during the wave event were high relative to not only fair weather, but also most extratropical storms. At Site 1, these increased rates were due predominantly to contributions at low- and wind-wave frequencies, while at Site 2, increased mean flux accounted for the largest portion of the total. Calculated sediment transport rate for various frequency components during fair weather conditions at both sites tended to be fairly low, but by no means insignificant, in comparison with the wave event and strong extratropical storms. Fair-weather transport at wind-wave frequencies was most important at Site 1, with mean transport predominating at Site 2. This is not surprising, since it was observed that the spectral concentration peaks at the two sites differed—at Site 1, the peak in the spectrum of suspended sediment concentration occurred at wind-wave frequencies during 31% of the deployment, while this occurred only 12% of the time at Site 2. The results presented above appear to largely reflect the fact that wave energy was much lower, while currents were somewhat stronger, on the landward side of Ship Shoal.

As was the case with predicted sediment transport rate, transport direction calculated using spectral methods varied between sites, weather conditions, individual extratropical storms, and frequency components. Fair weather conditions were characterized by the most uniform trends in sediment flux direction, with northwesterly transport occurring at nearly all frequencies, and in total, at both sites. During

extratropical storms, total transport was southeasterly, largely as a result of offshore mean fluxes that occurred during strong events, particularly during Storm 6, when the along-shelf vector was easterly. Transport at low frequencies, which tended to be low in any case, was onshore, although the along-shelf component varied from storm to storm. Wind-wave transport during extratropical storms varied widely, with strong onshore, offshore, easterly and westerly transport occurring during different events. The net result was onshore transport, although this was northwesterly at Site 1 and northeasterly at Site 2. Transport at both sites during the wave event was northeasterly at mean frequencies and southwesterly at low frequencies; however, wind-wave flux was southwesterly at Site 1 and northeasterly at Site 2. This, and the difference in the relative dominance of mean and wind-wave transport, resulted in an overall south-southwesterly transport at Site 1 and northwesterly transport at Site 2 during this event. It appears, therefore, that the influence of Ship Shoal on hydrodynamic parameters ultimately modifies suspended sediment transport patterns in the area as well.

At Site 2, suspended sediment concentration was in phase with the "forward" oscillatory motion of wind waves during 56% of the deployment (in the across-shelf direction), or stated differently, across-shelf transport at wind-wave frequencies was in the same direction as the waves 56% of the time (Fig. 6.22). This resulted in a net wind-wave transport in the direction of wave propagation. Across-shelf transport at low frequencies was in the direction of wave propagation 49% of the time, and the overall direction of sediment transport opposed that of wave propagation. Thus, wave activity appears to have been responsible for both onshore and offshore transport, which is consistent with the results of Wright et al. (1991) for the mid-Atlantic bight. Interestingly,

across-shelf transport at low and wind-wave frequencies was in the same direction 63 % of the time. Also, despite the fact that high-frequency wave activity (>0.2 Hz) was associated with the post-frontal phases of extratropical storms, sediment suspension was never at a maximum at these frequencies. On the other hand, sediment suspension was sometimes maximized at lower wind-wave frequencies (0.2-0.1 Hz) during intervals of longer period waves, such as during fair weather and pre-frontal conditions. These phenomena will be discussed in greater detail in terms of specific storm events in Chapters 7 and 8.

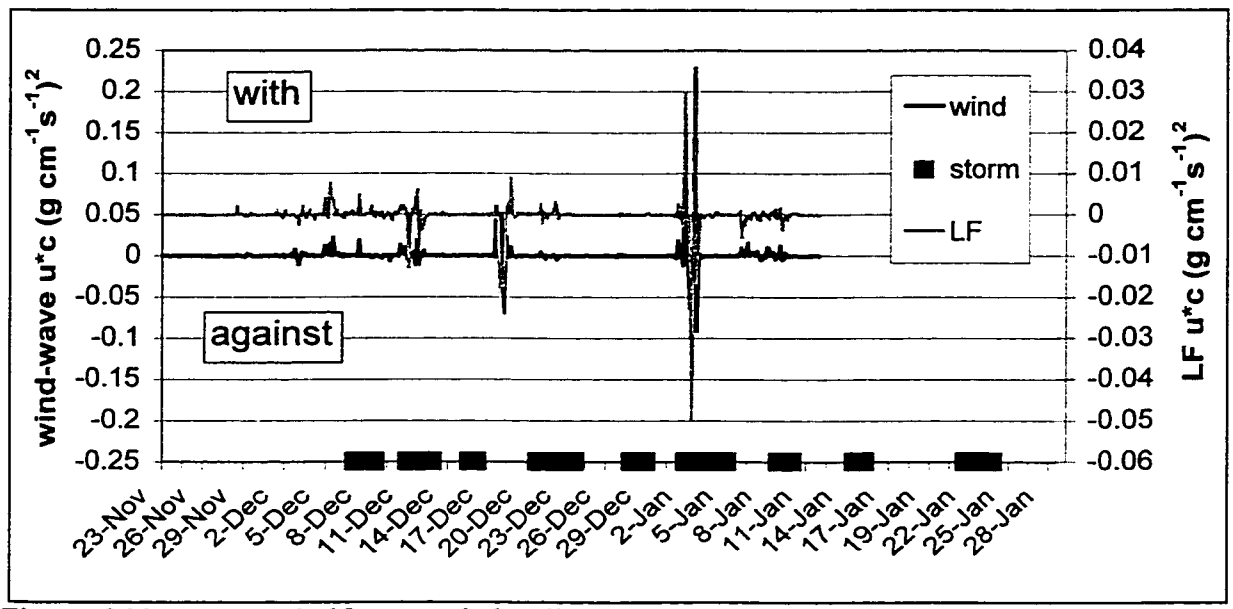

Figure 6.22: Across-shelf suspended sediment transport at wind-wave (wind) and low-frequencies (LF), relative to the across-shelf component of wave propagation at Site 2.

6.5 Summary

This chapter has demonstrated several concepts. First, Ship Shoal apparently has an important effect on marine processes in the study area, reducing wave energy, modulating current flow, and influencing bottom boundary layer parameters and directional sediment transport. Second, winter hydrodynamic, bottom boundary layer and sedimentary

responses on the inner shelf of Louisiana are episodic, and are most often associated with extratropical storm passages. Third, the passage of occasional "wave events" during fair weather conditions (meteorologically) may cause large increases in hydrodynamic and bottom boundary layer energy, resulting in increased sediment transport. Fourth, hydrodynamic and sedimentary responses are highly dependent upon the characteristics of a particular storm; some storms may actually be associated with less energetic conditions in the marine environment than occur during fair weather. Finally, the responses discussed above are variable over the course of individual storms, with overall, and frequency-dependent sediment transport being particularly sensitive to the phase of the storm. In particular, transport at low- and wind-wave frequencies varies considerably in both magnitude and direction over short time-scales, likely as a result of changes to the bed and in sensor position relative to it. These points, and in particular, the final two, will be discussed in much greater detail in subsequent chapters in the context of individual events and on the basis of an extratropical storm model for the Louisiana inner shelf that will be introduced.

CHAPTER 7

A METEOROLOGICAL AND HYDRODYNAMIC CLASSIFICATION SYSTEM FOR LOCAL EXTRATROPICAL STORMS ON THE LOUISIANA INNER SHELF

Clearly, all extratropical storms are unique—even basic characteristics such as duration, synoptic-scale structure, and wind velocity, differ from storm to storm. Non-linear air-sea-sediment interactions on a variety of scales further complicate these differences, causing complex and varied inner-shelf responses. In particular, rates and directions of sediment transport associated with storms are difficult to estimate owing to their dependence on, and sensitivity to, a large number of interrelated processes. It is to be expected, therefore, that numerous meteorological classification systems for coastal environments, many of which were discussed in Chapters 1 and 5, appear in the literature. All of these systems are designed to be applicable for certain purposes and as such, tend to focus on specific combinations of variables. Obviously, therefore, no single storm classification scheme can completely account for all coastal phenomena.

Nevertheless, as Chapters 5 and 6 demonstrated, there are significant hydrodynamic, bottom boundary layer, and sedimentary, as well as meteorological, differences between extratropical storms and fair weather in the northern Gulf of Mexico. These chapters also made it apparent, however, that there was considerable variation among extratropical storms, suggesting that a two-tiered storm/non-storm classification system may not be adequate to categorize inner-shelf processes in coastal Louisiana. The purpose of this chapter is thus to outline a classification system for extratropical storms in the Northern Gulf of Mexico based on their synoptic characteristics and wind patterns, as well as their typical hydrodynamic, bottom boundary layer and sedimentary responses.

The proposed classification system draws heavily upon Chaney's (1999) storm subtypes and Power V classification, as discussed in Chapter 5, with modifications deemed appropriate for the Louisiana inner shelf. Given the wide range of factors considered, it is only semi-quantitative, and a certain amount of subjectivity has been introduced both in assigning a level of importance to different variables, and in identifying spatial and temporal patterns in the data. Furthermore, the system is not intended to be exhaustive, in that it is quite plausible that extratropical storms do occur that are not well-represented by any of the storm types proposed—indeed, the first two storm types that will be discussed are probably most accurately considered to be end-members on a continuum of storms. Finally, and perhaps most importantly, it should be noted that only nine storms were incorporated in this study, and therefore caution must be used when interpreting how representative these may be. Despite these limitations, however, the system is potentially a useful means by which the interaction of a wide range of important variables may be summarized for the Louisiana inner shelf.

Although all parameters are interconnected, and all were originally used to some degree to establish the classification system itself, material in this chapter will be presented in the same fashion as in Chapters 4 and 6. Section 7.1 is intended to present the general premises of the classification system from a meteorological standpoint, including the synoptic-scale characteristics of the storm types and typical sequences of wind velocity. Section 7.2 will focus on hydrodynamic parameters, including wave characteristics and current velocity. Section 7.3 will discuss bottom boundary layer parameters and sediment transport. Finally, Section 7.4 will serve as a summary and conclusion. A wide variety of means will be used to illustrate points being made,

including diagrams, tables, and various types of time- and frequency-domain graphs. These may represent either conceptualizations or specific examples, and may be non-, semi-, or completely quantitative. Distinctions will be made, however, to clarify the source and intent of all figures and tables.

7.1 Meteorological Characteristics of the Storm Types

Three extratropical storm classes, Type 1, or Southwest, storms, Type 2, or Southeast, storms and Type 3, or Weak, storms, were delineated on the basis of two criteria: 1) overall wind intensity; and 2) mean wind direction. Following Chaney (1999), overall wind intensity was based on the Power-V ranking; Types 1 and 2 storms had a Power-V index exceeding 2000, and comprised two end members on a continuum of possible storms. Type 3 storms had a Power-V index less than this, and were thus considered weak. The reason for this distinction, as was initially demonstrated in Chapter 6, is that weak storms appeared to exert only a minimal impact on inner-shelf hydrodynamics and sediment transport. In contrast, Types 1 and 2 storms exerted a strong influence, and were classified on the basis of the average direction of their prevailing winds, which influenced other inner-shelf processes. These two storm types closely follow the storm subtypes of Chaney (1999), as discussed in Chapter 5, except that Chaney's Subtype C, in which winds blew toward both the northeasterly and northwesterly quadrants, was eliminated by considering only the vector mean wind direction. Other models introduced in Chapter 5, including Chaney's (1999) seven synoptic subtypes, were not incorporated into the classification system used here.

Of the nine storms that occurred during the deployment, three were Type 1 (Storms 1, 4, and 7), three were Type 2 (Storms 2, 6, and 9), and three were Type 3

(Storms 3, 5, and 8). Idealized representations of Types 1 and 2 storms, including their synoptic characteristics and their associated pre-and post- frontal wind patterns are shown in Figs. 7.1 and 7.2, while Type 3 storms are not shown, since their defining characteristic is intensity, represented fully by the Power-V index. As illustrated in Fig. 7.1, Type 1 storms involve a cold front crossing the coast at an oblique angle, with a strong high-pressure cell following it to the north. Although a low-pressure cell is present in these situations, it is located too far away to exert a strong influence. As a result, during the pre-frontal stages of the storm, only weak winds blow from the south, veering somewhat as the front migrates to the east. Following the passage of the front, strong winds blow from the north—these may be northerly, or northeasterly at first, but are predominantly northeasterly overall, owing to the clockwise rotation of anticyclonic winds. As noted previously by Chaney (1999), therefore, such storms are dominated by the high-pressure cell that trails the front, rather than by a cyclone.

Type 2 storms (Fig. 7.2) are characterized by a cold front crossing the coast at an roughly perpendicular angle, with a strong low-pressure cell just to the north. Strong winds blow from the south during the pre-frontal phase, as they are "sucked into" this low-pressure cell, and veer west to east as the cell migrates. Following the passage of the front, strong winds blow from the northwest as they rotate around the low-pressure cell. Thus, the most important synoptic difference between the two storm types is the respective dominance of the anticyclone (High) during Type 1 storms and the cyclone (Low) during Type 2 storms, while the primary difference between the local wind velocity of these storms is the smaller relative strength of northerly pre-frontal winds and the larger eastward wind component during the post-frontal phase of Type 1 storms.

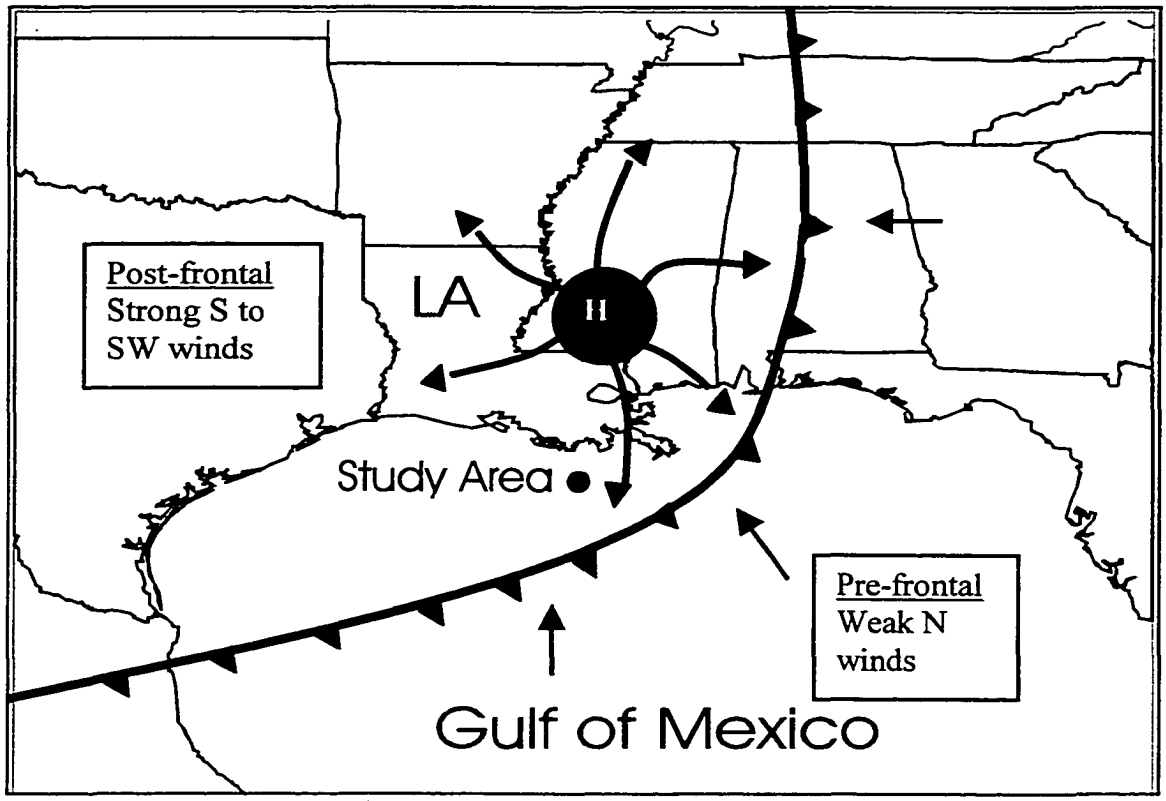

Figure 7.1: Synoptic weather pattern for a Type 1 storm. Arrows show wind direction.

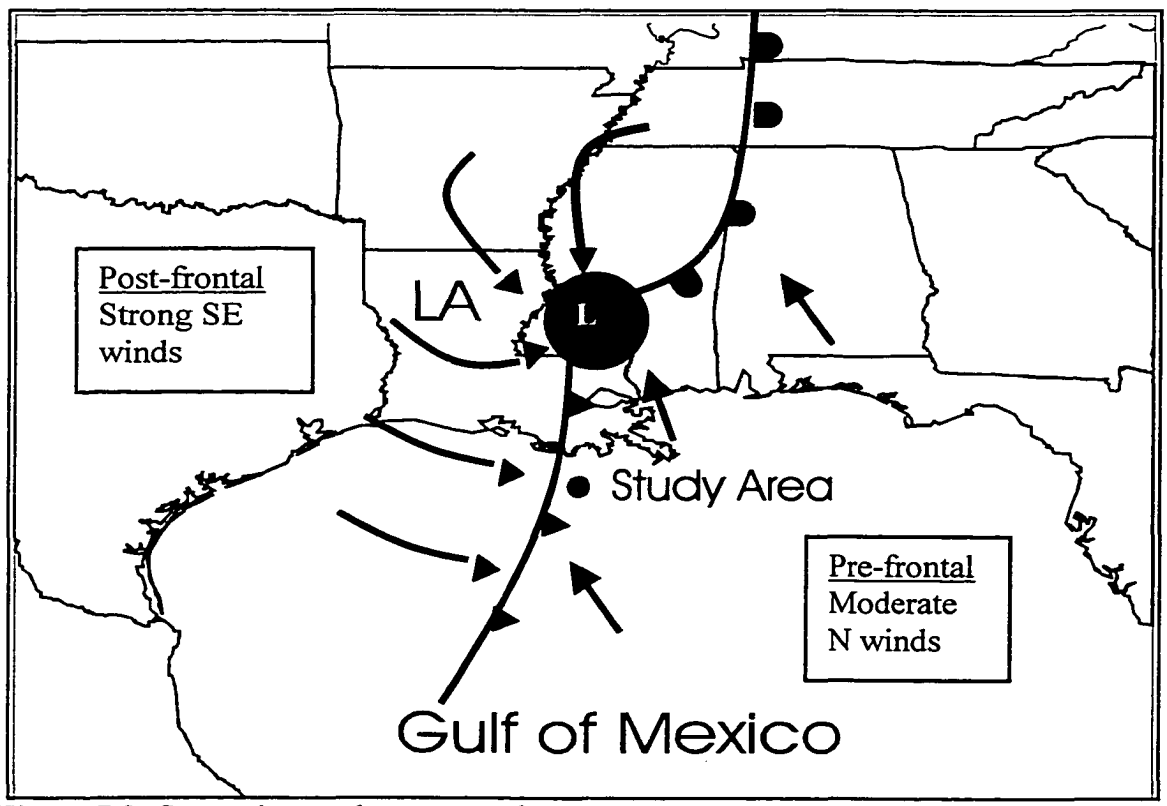

Figure 7.2: Synoptic weather pattern for a Type 2 storm. Arrows show wind direction.

Type 3 is a "catch-all" category for all extratropical storms that are weak, in that they do not exceed a Power V rating of 2000. These storms have been afforded their own category in the proposed classification system since it was demonstrated in Chapter 6 that weak extratropical storms are often associated with inner-shelf responses that are less energetic than those that occur during fair weather. Given this intensity-based classification, Type 3 storms are not generally characterized by any particular synoptic pattern except that their occurrence is not usually associated with the presence of strong high or low-pressure cells in the vicinity of the Louisiana coast. As such, Type 3 storms may have a wide variety of wind-direction patterns, although wind speed is, of course, generally low in comparison with Types 1 and 2 storms. The meteorological characteristics of each storm type outlined above is summarized in Table 7.1.

Table 7.1: Meteorological characteristics of Types 1, 2 and 3 storms that occurred during the deployment.

Characteristic	*Type 1*	*Type 2*	*Type 3*
Storms in Class	1, 4, 7	2, 6, 9	3-5, 8
Power V index [rank]	>2000 [>1]	>2000 [>1]	<2000 [1]
Dominant Pressure Cell	High (Anticyclone)	Low (Cyclone)	variable
Pre-Frontal Wind Speed	low	moderate	low
Pre-Frontal Wind Direction	southerly	southeasterly	variable
Post-Frontal Wind Speed	high	high	moderate
Post-Frontal Wind Direction	north/northeasterly	north/northwesterly	variable

Examples of the wind velocity that accompanied the three storm types during this deployment are shown in Figs. 7.3-7.5, which depict Storms 7, 6, and 5, respectively. While some variation from the storm type characteristics outlined previously are evident in these records, the general trends are clear. During the Type 1 storm (Storm 7 is depicted in Fig. 7.3), fairly weak winds blew predominantly from the south prior to the passage of the front, following which, the wind velocity became strong and north- to

northeasterly. These winds persisted until approximately 48 hours subsequent to the cold-front passage, when the wind again became southerly. Figure 7.4 shows wind velocity vectors for Storm 6, a Type 2 storm. Moderately strong southeasterly winds blew during the pre-frontal phase of this event, followed by a shift to strong northwesterly winds, which, as was the case with Storm 7, became southerly 2-3 days subsequent to the frontal passage. Although there is some variability in the wind velocity associated with Type 3 storms, Storm 5 (Fig. 7.5) appears to have been a typical example of this class. In this case, successive low- and high-pressure cells appear to have passed to the north of the study area as part of a frontal system aligned nearly parallel to the coastline. As such, southerly pre-frontal and northerly post-frontal winds veered until approximately 32 hours subsequent to the frontal passage.

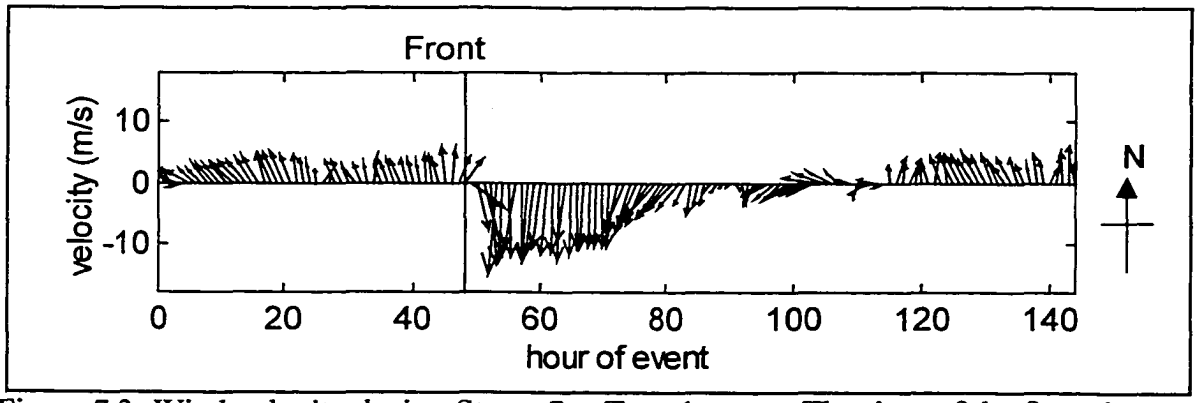

Figure 7.3: Wind velocity during Storm 7, a Type 1 storm. The time of the frontal passage is indicated by the line at hour 48.

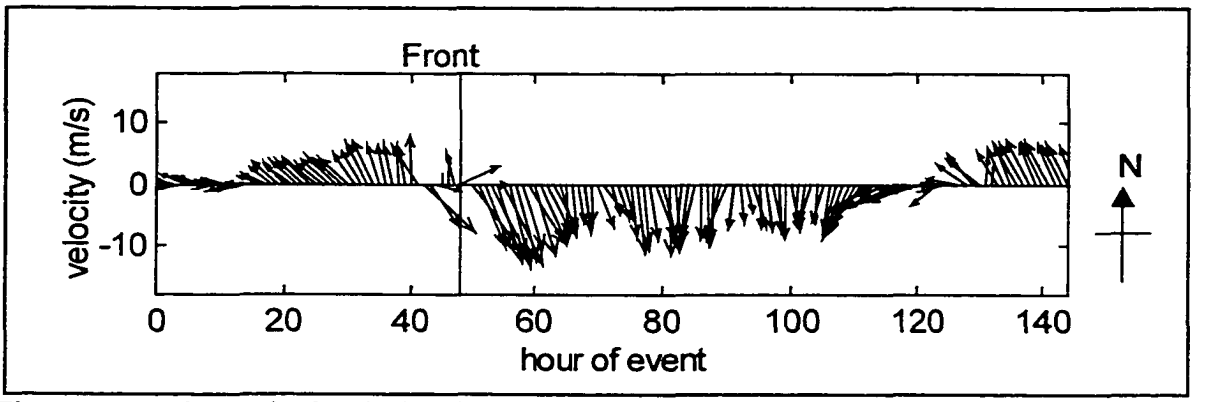

Figure 7.4: Wind velocity during Storm 6, a Type 2 storm. The time of the frontal passage is indicated by the line at hour 48.

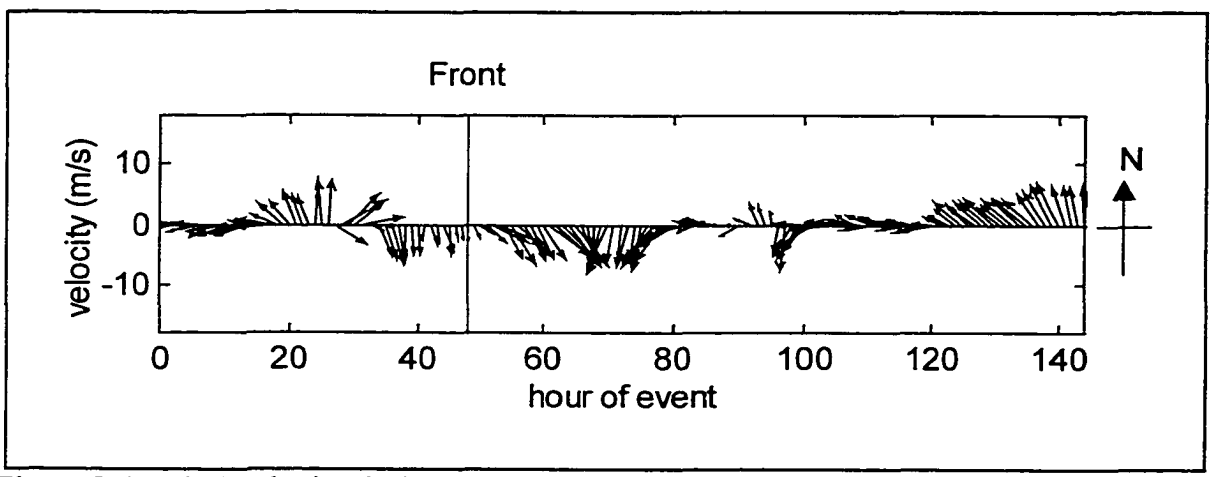

Figure 7.5: Wind velocity during Storm 5, a Type 3 storm. The time of the frontal passage is indicated by the line at hour 48

It should be noted prior to the presentation of tabular data that throughout the chapter, the term "Storm" will refer to all time periods when storm conditions, according to the criteria outlined in Chapter 5, occurred, while "Pre-" and "Post-frontal" phases refer consistently to the 24-hour period prior to, and following, the frontal passage, respectively. As such, the values given for "Storm" conditions are not merely the mean of

the "Pre-" and "Post-frontal" values. This system, although potentially confusing at first glance, was chosen so as to account for the influence of the well-documented pre- and post-frontal phases of extratropical storms (Roberts et al. 1987; Roberts et al. 1989; Armbruster et al., 1995; Chaney and Stone, 1996; Chaney, 1999).

Table 7.2 outlines the mean meteorological parameters for the three storm types as measured during the deployment. These are expected, since they directly and indirectly provided the initial basis for the classification system. The most important points to note include the fact that Type 1 storms tended to be shorter in duration than Type 2 storms, although their mean wind speed was higher. Type 3 storms, on the other hand, were characterized by both shorter duration and lower wind speed than the other storm types. The mean wind speed during the pre-frontal stage was considerably higher during the pre-frontal stage of Type 2 storms than it was during Type 1 storms, for the reasons outlined previously, while pre-frontal values for Type 3 storms fell between the two, possibly because the category incorporated storms of various synoptic types. Overall, mean wind direction was northeasterly in the case of Type 1 storms, and northwesterly in the cases of Type 2 and Type 3 storms. This closely reflects the direction of post-frontal winds, rather than the comparatively insignificant pre-frontal winds, which, as indicated previously, seldom reached storm status, except in the case of Type 2 storms.

Table 7.2: Mean and standard deviation of meteorological parameters for the storm types. Standard deviation is shown in brackets.

Storm		All Storms		Pre-frontal		Post-frontal	
Type	Duration (h)	Speed ($m.s^{-1}$)	Direction	Speed ($m.s^{-1}$)	Direction	Speed ($m.s^{-1}$)	Direction
1	44 (22.0)	8.7 (0.08)	20	2.9 (0.75)	116	9.6 (0.42)	16
2	64 (10.0)	8.1 (0.3)	332	6.9 (0.74)	124	8.6 (0.84)	316
3	19 (8.0)	6.7 (0.7)	343	4.0 (1.04)	327	6.1 (0.26)	356
All	**43**	8.1	**354**	4.2	**161**	8.1	**350**

7.2 Hydrodynamic Characteristics Associated with the Storm Types

7.2.1. Wave Characteristics

Table 7.3 shows wave characteristics at both sites for each of the storm types. Wave energy, as indicated both by wave height and near-bed orbital velocity, was highest at each site during Type 2 storms, followed by Type 1 storms, while values for Type 3 storms were actually lower than those for fair weather. Wave period was considerably higher for Type 2 storms than for the other two storm types at both sites. It appears, therefore, that Type 2 storms were most important in terms of wave generation, with Type 1 storms also playing a potentially important role, and Type 3 storms being insignificant. As such, only Types 1 and 2 storms will be considered further.

Table 7.3: Mean wave characteristics for the three storm types as measured at Sites 1 and 2, respectively.

	Site 1			*Site 2*		
Storm Type	*Hs (m)*	*Tp (s)*	*Ub (cm s^{-1})*	*Hs (m)*	*Tp (s)*	*Ub (cm s^{-1})*
1	0.80	4.51	12.7	0.60	3.8	12.58
2	1.06	5.82	19.1	0.66	5.0	14.29
3	0.42	4.26	7.2	0.28	3.8	6.04
All Storms	**0.87**	**4.99**	**15.1**	**0.57**	**4.3**	**12.28**

Time series of significant wave height and peak wave period for representative Types 1 and 2 storms (Storms 6 and 7) are shown in Figs. 7.6 and 7.7. Type 1 storms (Fig. 7.6) were characterized by a dramatic increase in significant wave height and an accompanying decrease in peak wave period associated with the onset of northerly post-frontal winds. On the other hand, wave response to Type 2 storms, as illustrated by data from Storm 6 (Fig. 7.7), was more complex. The time series of significant wave height had two peaks, the lower of which occurred immediately prior to the frontal passage, while the higher occurred just subsequent to it. Maximum hourly significant wave height (Hs) during this event was 1.83 m and Hs exceeded 1.5 m for 10 consecutive hours

around the peak of the storm. Peak wave period increased gradually to approximately 8 s prior to the frontal passage, following which, it suddenly decreased to 3.76 s. It then fluctuated between the high- and low-frequency values for 24 hours, at which point it leveled off at approximately 4 s.

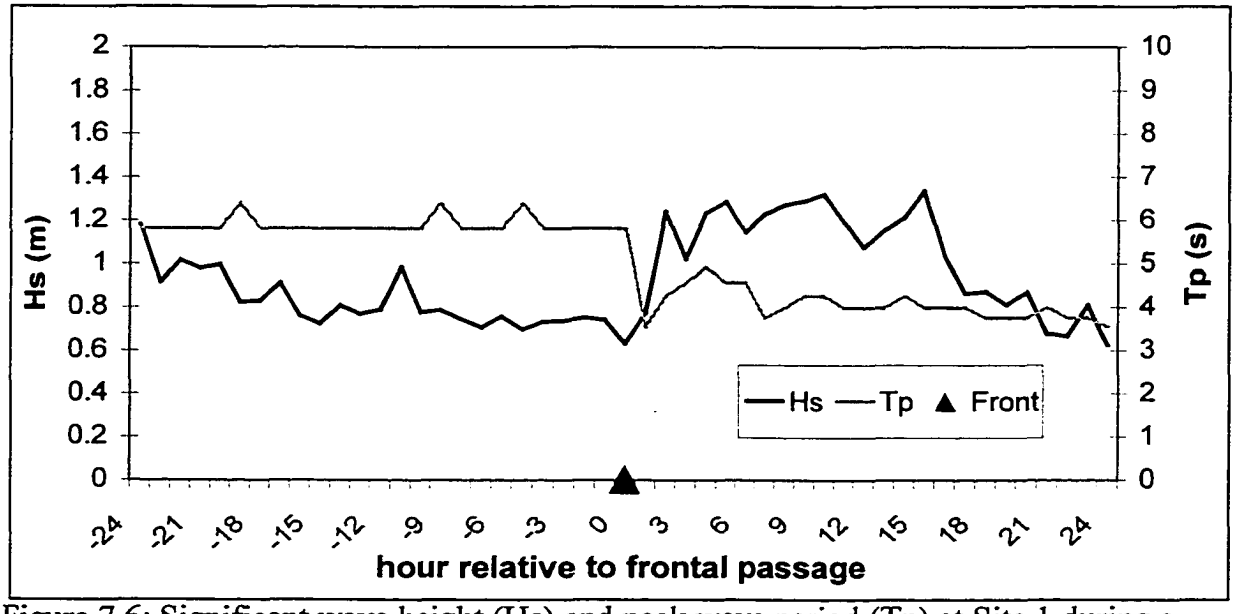

Figure 7.6: Significant wave height (Hs) and peak wave period (Tp) at Site 1 during a Type 1 storm (Storm 7).

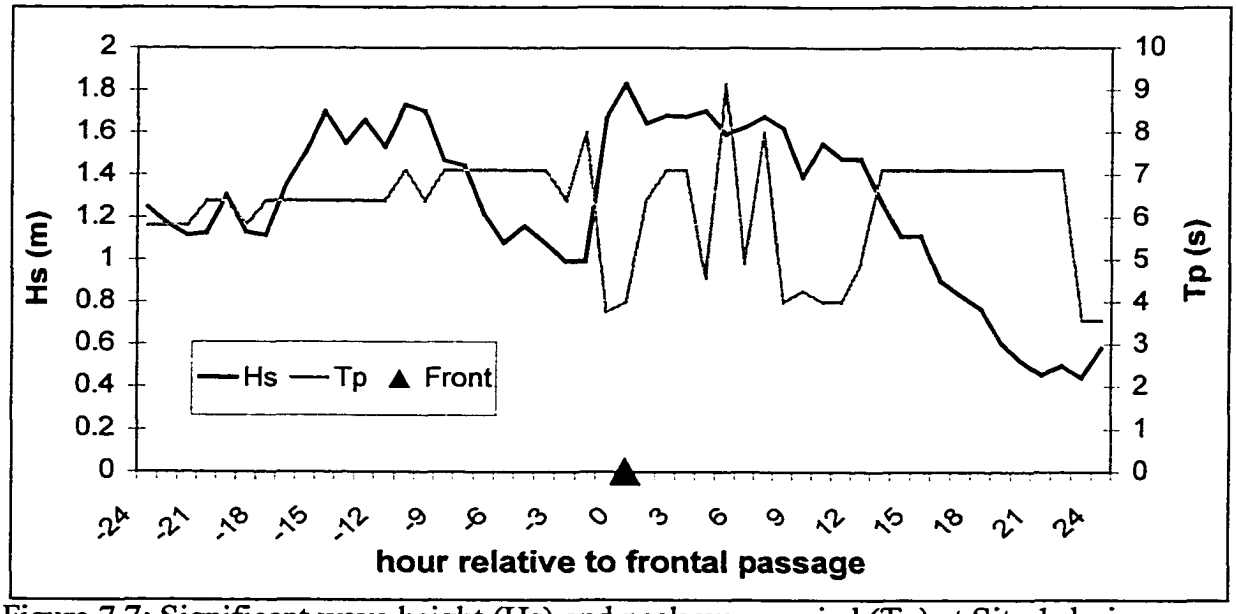

Figure 7.7: Significant wave height (Hs) and peak wave period (Tp) at Site 1 during a Type 2 storm (Storm 6).

Changes in wave parameters during Types 1 and 2 storms are further elucidated by Figs. 7.8-7.9, which are color-coded time series plots of hourly frequency spectra. A fairly narrow band of wave energy at periods above 5 s occurred during the pre-frontal phase of both Types 1 and 2 storms, although wave energy and period during this phase were higher during the Type 2 storm. Both storm types also had a conspicuous interval of reduced wave energy nearly coincident with the frontal passage. Following the passage of the front, however, the wave field differed considerably between the storm types. The Type 1 storm had a unimodal spectrum, with wave energy concentrated around a period of 4 s, while the Type 2 storm had a bimodal spectrum, with peaks occurring at approximately 8 and 4 s periods. It appears, therefore, that longer-period (swell) waves are more prevalent during the pre- and post- frontal phases of Type 2 storms than they are during Type 1 storms, when post-frontal storm waves dominate.

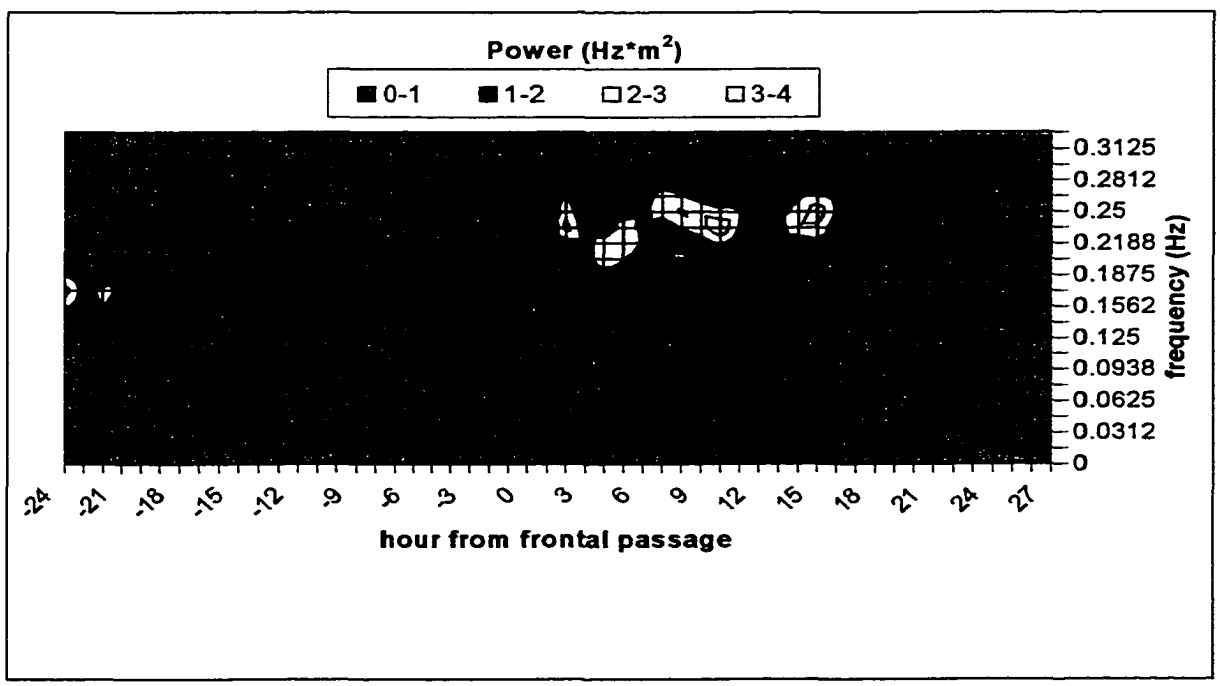

Figure 7.8: Color-coded time series plots of hourly frequency spectra for Storm 7, a Type 1 storm. Note that peak frequency increases (period decreases) upward.

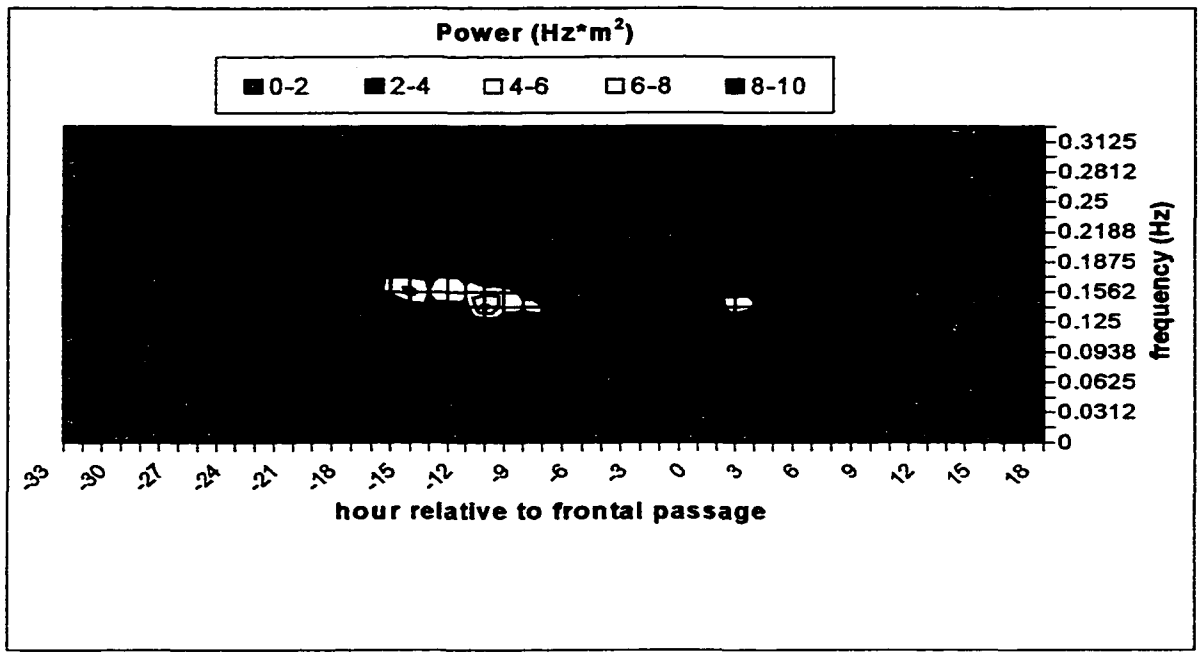

Figure 7.9: Color-coded time series plots of hourly frequency spectra for Storm 6, a Type 2 storm. Note that peak frequency increases (period decreases) upward.

The directional characteristics of waves associated with various phases of the two storm types provide additional information regarding their dynamics and generating mechanism. Figs. 7.10 and 7.11 are vector plots of non-dimensional wave direction during a Types 1 and 2 storms, respectively. In both cases, wave direction was uniformly toward the northwest during the pre-frontal stage. Immediately following the passage of the front, however, wave direction differed between storm types—in the case of the Type 1 storm, there was an immediate shift to southerly waves, while wave direction during the Type 2 storm vacillated between northeasterly and southeasterly before ultimately aligning with the (northerly) wind direction approximately 24 h later. It should be noted that this does not reflect sudden (i.e. hourly) shifts in wave direction, but instead, minor changes in the relative energy level, and thus, the dominance, of the longer- and shorter-period wave bands. This is clearly indicative of the continued importance of longer-period waves throughout the duration of Type 2 storms.

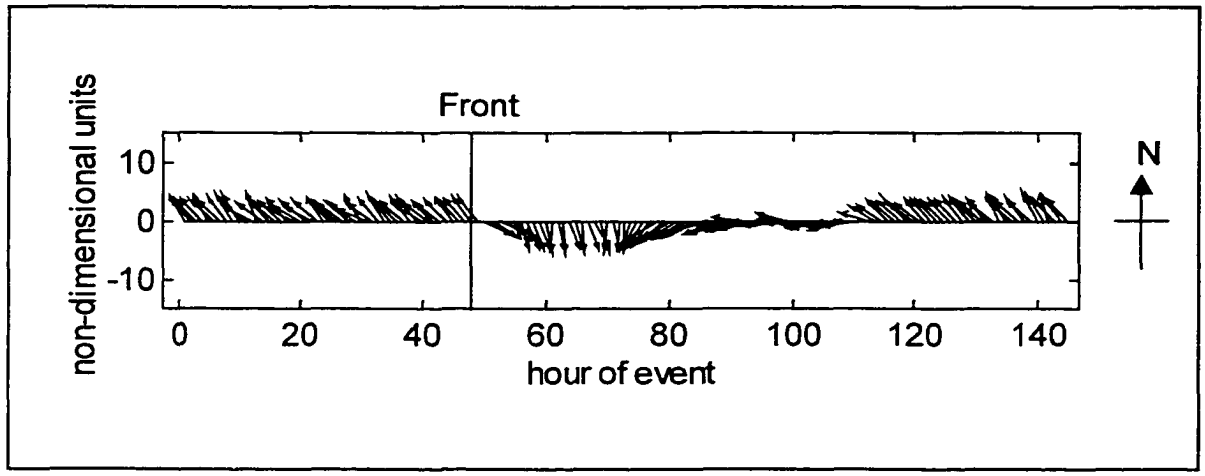

Figure 7.10: Non-dimensional wave direction during Storm 7, a Type 1 storm. The time of the frontal passage is indicated by the line at hour 48.

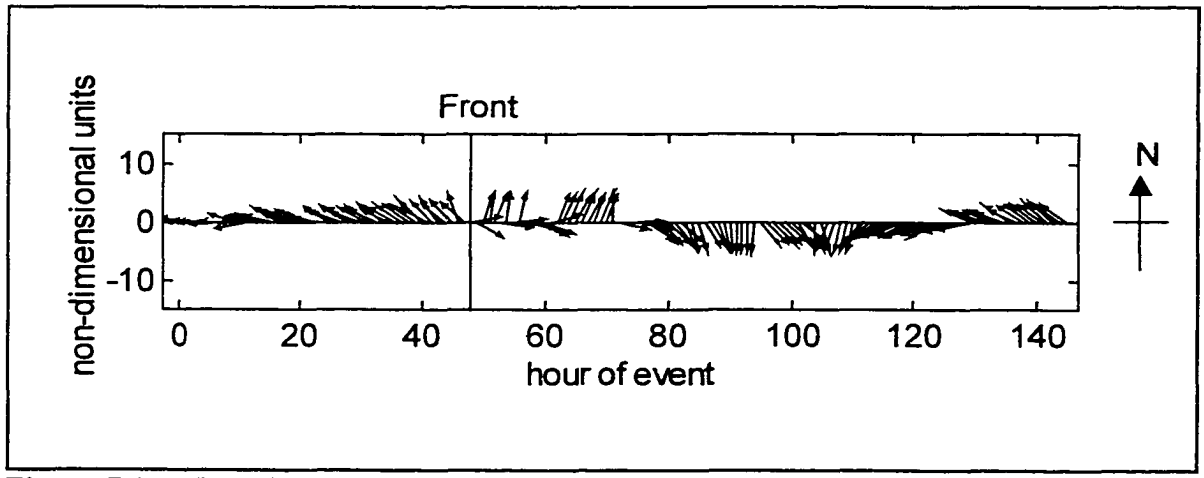

Figure 7.11: Non-dimensional wave direction during Storm 6, a Type 2 storm. The time of the frontal passage is indicated by the line at hour 48.

Figures 7.12-7.16 show the hourly directional wave spectra during various phases of Types 1 and 2 storms, thereby providing more detailed representations of the evolution of the directional wave field. Directional spectra during the Type 1 storm were generally unimodal for both the pre- and post-frontal phases, with waves propagating northwesterly 11 h prior to the frontal passage (Fig. 7.12) and southerly 10 h subsequent to it (Fig. 7.13). This is consistent with the interpretation that Type 1 storms are characterized by a complete shift from pre-frontal onshore swell waves to offshore post-frontal storm waves.

On the other hand, the Type 2 storm was characterized by a three-stage evolution of the directional wave field. As shown in Fig.7.14, the single peak associated with swell-dominated waves that occurred 10 h prior to the frontal passage had a direction of 307°. Figure 7.15 shows the directions associated with the two-frequency peaks evident in the spectrum 8 h subsequent to the frontal passage. Apparently, the longer period swell continued to propagate roughly from north to south during this time, while a short-period sea component built up in an easterly direction. Thirty hours after the frontal passage, the swell-dominated peak had subsided and high-frequency waves with a direction of 140°, roughly the same as that of the wind, were dominant (Fig. 7.16). It thus appears that two wave fields were present during the majority of the post-frontal phase of Storm 6, with the lower-frequency (longer-period) wave band gradually being supplanted by higher-frequency waves. This is illustrated graphically in Fig. 7.17, which depicts the differing trends in wave direction associated with the 8s and 4s wave bands. It indicates the persistence of northerly, and particularly northwesterly, waves in the longer period band and a gradual clockwise rotation of the 4s wave band toward the south as post-frontal storm winds became important.

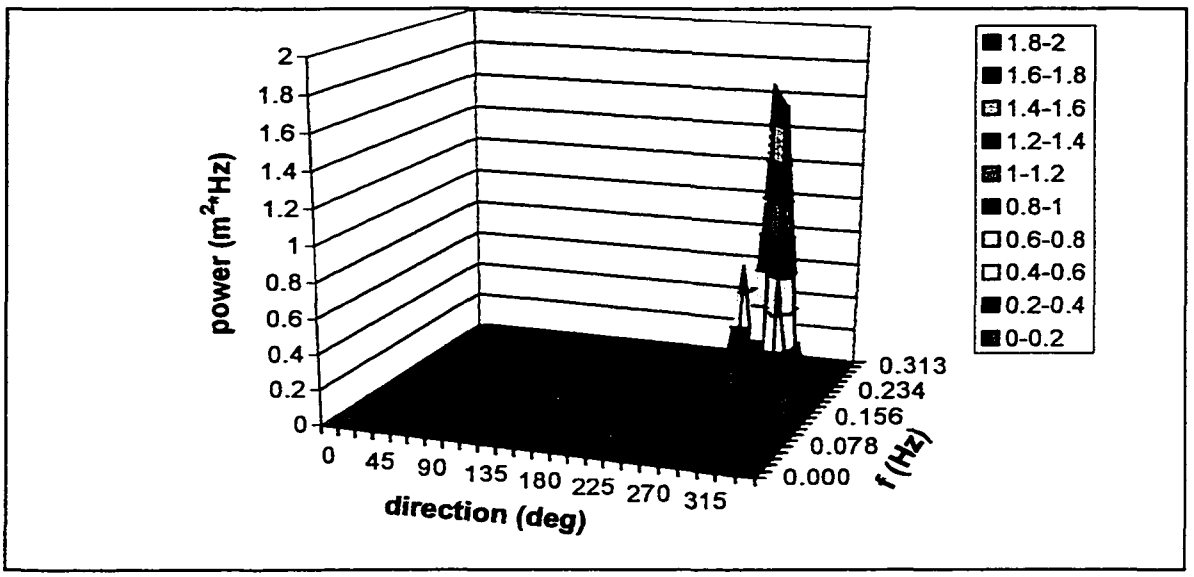

Figure 7.12: Directional wave spectrum for Site 1, 11 hours prior to the passage of the cold front during a Type 1 storm (Storm 7 at 1:00 UTC, Jan 9, 1999).

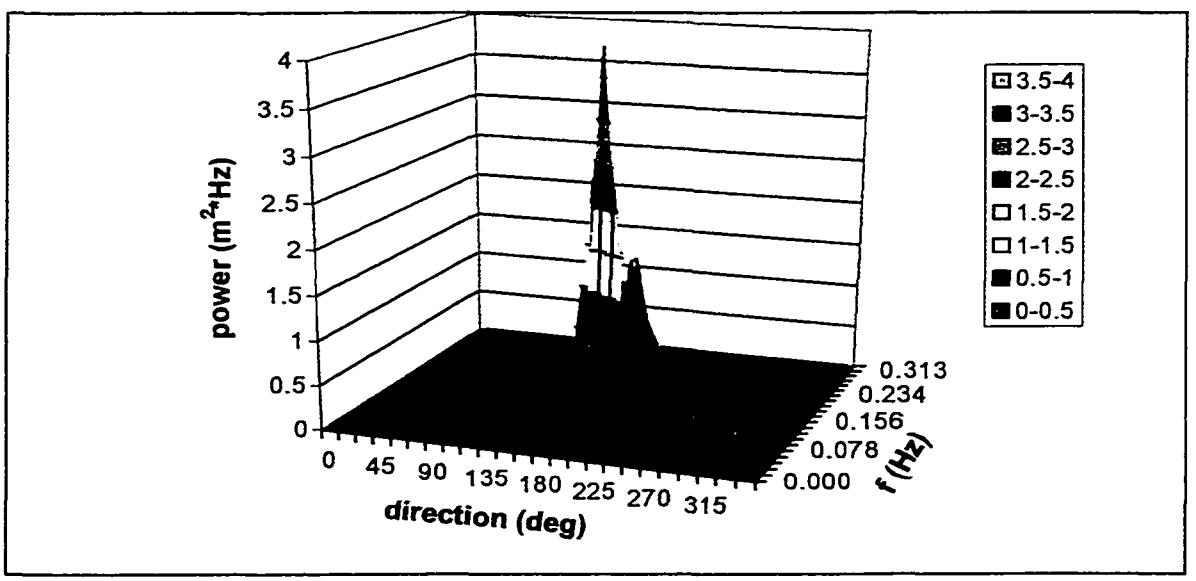

Figure 7.13: Directional wave spectrum for Site 1, 10 hours subsequent to the passage of the cold front during a Type 1 storm (Storm 7 at 22:00 UTC, Jan 9, 1999).

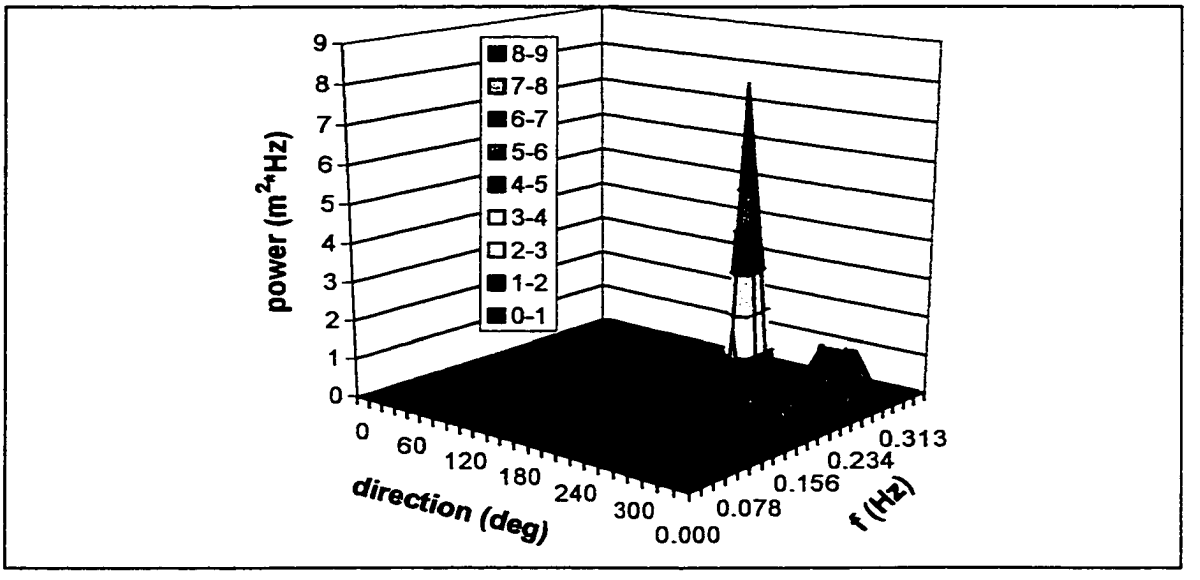

Figure 7.14: Directional wave spectrum for Site 1, 10 hours prior to the passage of the cold front (11:00 UTC, Jan 2, 1999).

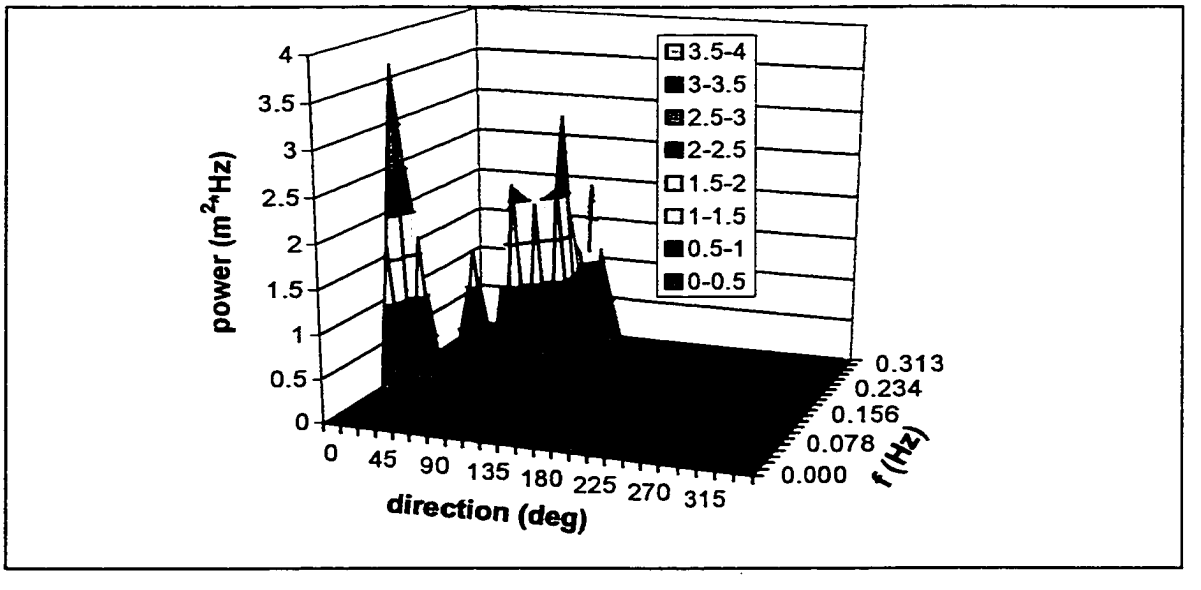

Figure 7.15: Directional wave spectrum for Site 1, 8 hours subsequent to the passage of the cold front (05:00 UTC, Jan 3, 1999).

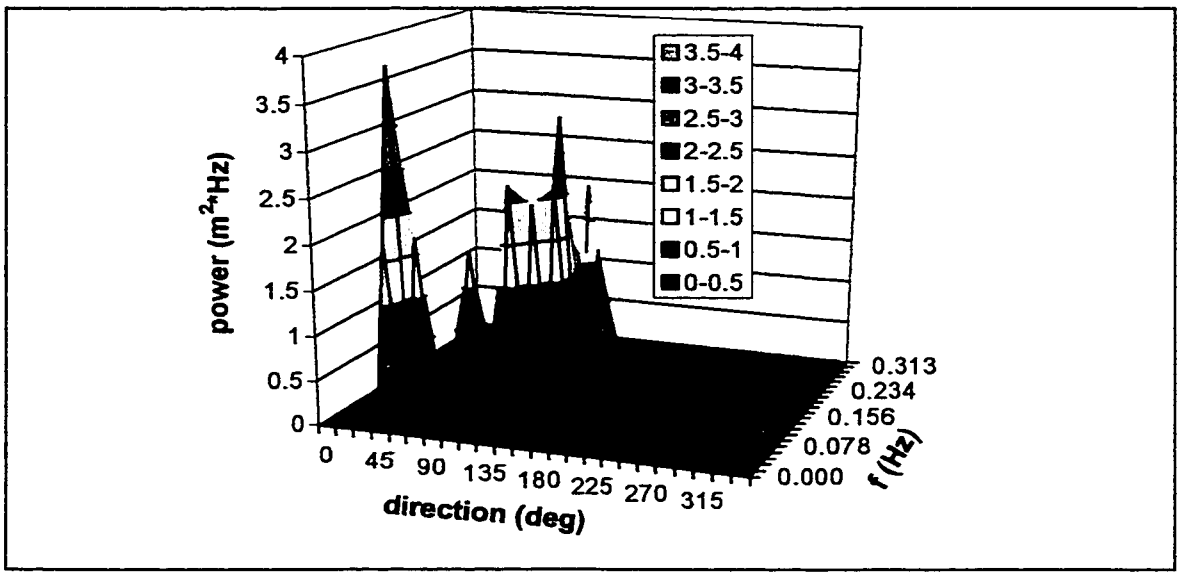

Figure 7.16: Directional wave spectrum for Site 1, 30 hours subsequent to the passage of the cold front (08:00 UTC, Jan 4, 1999).

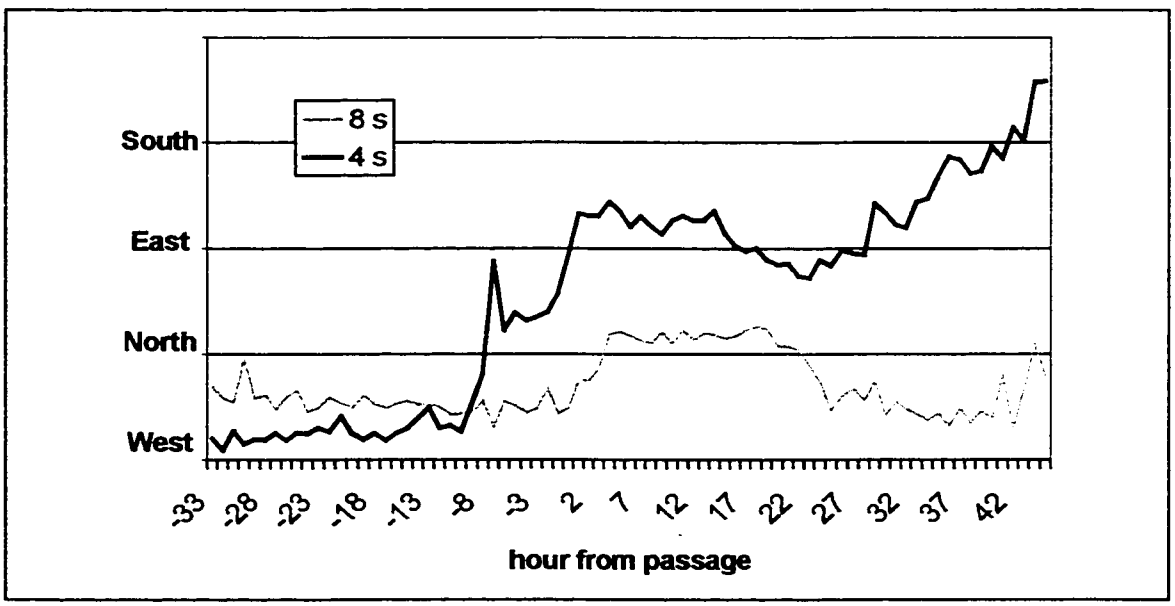

Figure 7.17: Time series of the direction of 4 s waves (sea) and 8 s waves (swell) during the storm passage.

Clearly, the storm types differed in terms of their associated wave characteristics. Type 2 storms appear to have had the most energetic wave field overall, particularly during the pre-frontal phase. Significant contributions to the energy spectrum resulted from both long-period northerly swell waves, and short-period, southerly storm waves, both of which were present during the majority of the post-frontal phase. Type 1 storms, on the other hand, were dominated by short-period southerly waves subsequent to the frontal passage. Unlike Type 2 storms, which were often characterized by complex, bimodal spectra, wave spectra during Type 1 storms tended to be fairly unimodal. These trends appear to be the result of the relative influence of northerly and southerly winds during different storm types. As outlined previously, Type 1 storms were characterized by weak southerly pre-frontal winds and energetic northerly pre-frontal winds, thus resulting in higher southerly post-frontal storm waves. In contrast, the strong southerly pre-frontal winds that accompanied Type 2 storms acted over a larger fetch than was present during periods of northerly winds, resulting in the generation of northerly long-period waves that were energetic enough to persist throughout much of the storm. This also explains the relative reduction in significant wave height and peak wave period at Site 2 during Type 2 storms, since northerly, and not southerly, waves are primarily influenced by attenuation across Ship Shoal. Finally, as noted earlier, wave energy during Type 3 storms was generally no higher than during fair weather.

7.2.2. Current Characteristics

Mean current velocity was already shown to be directly related to wind velocity at the study sites. Specifically, a stronger wind leads to a stronger wind-driven current, and the current direction tends to follow that of the wind, with important modifications occurring

as a result of tidal and inertial effects. These modifications predominantly consist of a clockwise rotation over time at a period of approximately 24 hours. It is not surprising, therefore, that aside from these observed rotational patterns, the trends in current velocity associated with the three storm types were similar to that of wind. Figure 7.18 is a vector plot of current velocity for Storm 7, a Type 1 storm. It indicates that currents were fairly weak and variable during the low-energy conditions prior to the frontal passage, while during the subsequent 48 hours, currents became strong, steady, and southwesterly. Figure 7.19 shows the current velocity during Storm 6, a Type 2 storm. Unlike the previous example, a brief period of strong northerly currents, which reached a maximum speed of 41.3 cm s^{-1}, occurred during the pre-frontal phase of the storm. These currents strengthened further and became southeasterly during the storm's post-frontal phase, reaching a maximum speed of 53.2 cm s^{-1}. The current direction then began to veer with a period of approximately 24 hours. Nonetheless, southerly and southeasterly currents during this time were clearly the strongest, and as a result, southeasterly currents were dominant overall during the post-frontal phase of Type 2 storms. Figure 7.20 shows the current pattern that accompanied Storm 5, a Type 3 storm. It bears some qualitative resemblance to both previous examples. Like the Type 1 storm, pre-frontal currents were fairly weak and variable, and southwesterly currents appear to have predominated during the post-frontal phase. On the other hand, current veering was evident following the frontal passage, as occurred during Storm 6. Current speed, however, was much lower during this weak storm than during either the Type 1 or 2 storms. Once again, this is the result of the fact that Type 3 storms are characterized by their intensity, rather than by their synoptic-scale structure.

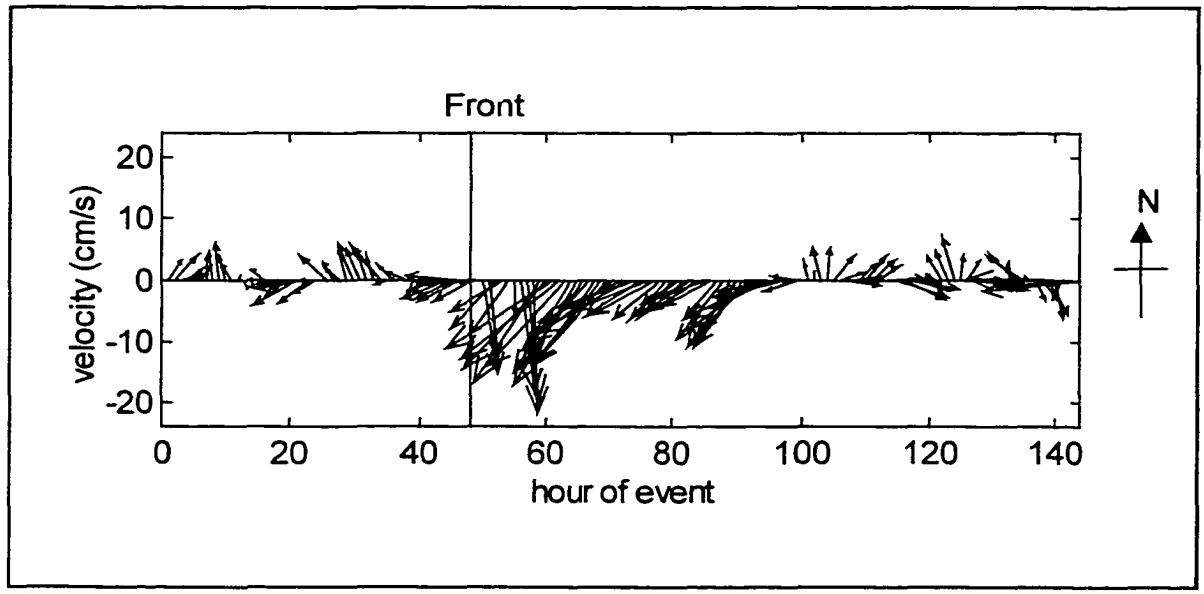

Figure 7.18: Current velocity at Site 1 (~100 cm above the bed) during Storm 7, a Type 1 storm. The time of the frontal passage is indicated by the line at hour 48.

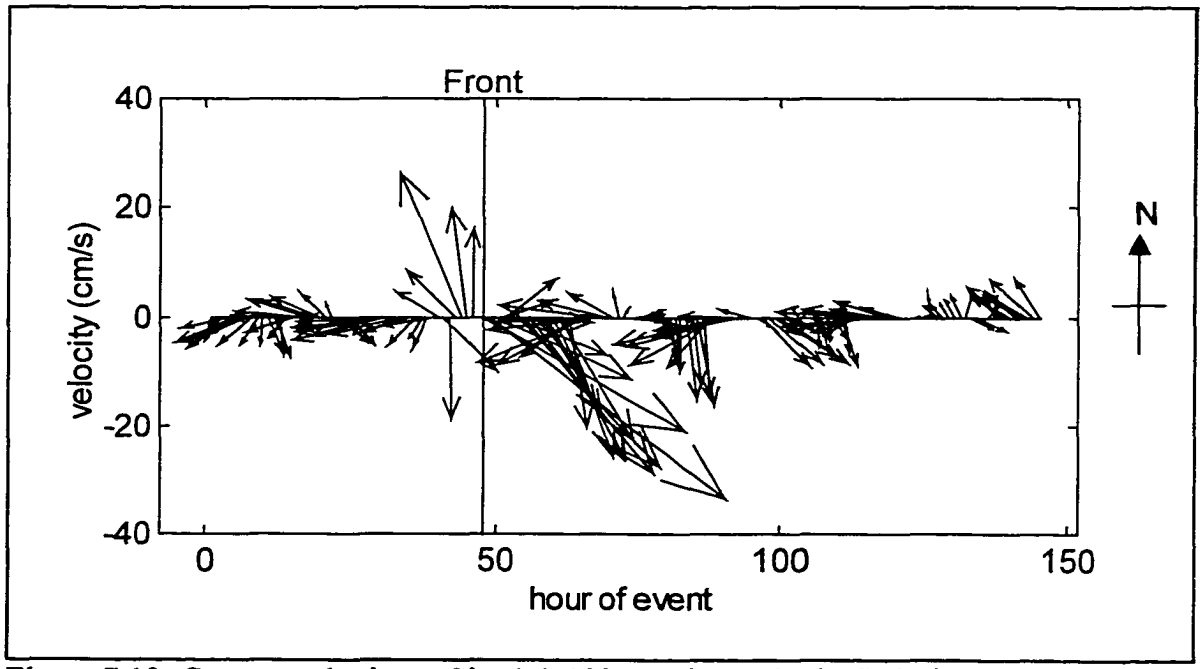

Figure 7.19: Current velocity at Site 1 (~100 cm above the bed) during Storm 6, a Type 2 storm. The time of the frontal passage is indicated by the line at hour 48.

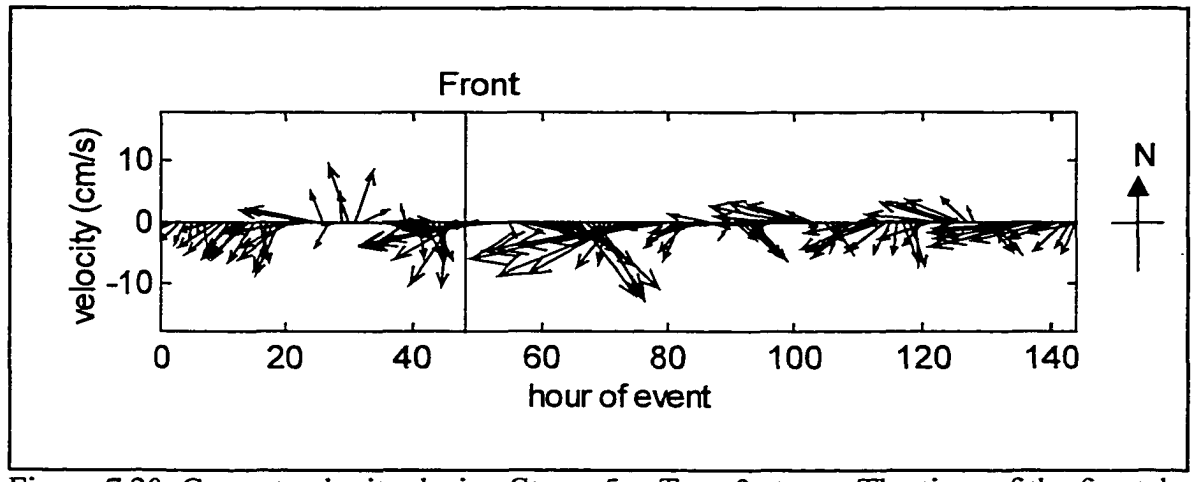

Figure 7.20: Current velocity during Storm 5, a Type 3 storm. The time of the frontal passage is indicated by the line at hour 48.

The reasons for these patterns have been discussed to some extent previously; however, some points require elaboration. Obviously, the absence of strong currents prior to the frontal passage, except during Storm 6, was the likely result of the fairly weak winds that predominated during the pre-frontal phase of Types 1 and 3 storms. Similarly, the powerful southeasterly or southwesterly post-frontal currents observed immediately following the frontal passage were probably the result of strong, direct wind stress during the post-frontal phase. The veering of currents that occurred during the post-frontal phase of Types 2 and 3 storms was probably caused by inertial oscillations, as explained in Chapter 6; however, the apparent absence of this phenomenon during Storm 7 is notable. It is possible that storms that have a strong pre-frontal phase, particularly Type 2 storms, cause water level set-up along the adjacent coast, which when released, enhances inertial effects (Daddio, 1977). Such set-up is unlikely to occur in situations where there are only weak winds and currents prior to the frontal passage, as appears to be the case for Type 1 storms. Unfortunately, this problem cannot be completely addressed with the present data

set, since the measured water level at the study site, which is a considerable distance offshore, is not expected to have a predictable effect on currents.

Table 7.4 provides quantitative hydrodynamic information for the three storm types based on the field deployment data. Points to note include the fact that overall and post-frontal current speeds were highest during Type 1 storms and weakest during Type 3 storms. During the pre-frontal phase of Type 2 storms, however, current speed was nearly twice as high as it was during the pre-frontal phase of Type 1 storms. Mean current direction during this phase was northwesterly for Types 1 and 2 storms, and southwesterly for Type 3 storms. More importantly, however, mean post-frontal current was southwesterly during Types 1 and 3 storms, and southeasterly during Type 2 storms, which is closely reflected in the overall current direction for these events.

Table 7.4: Mean current parameters for the three storm types as measured at approximately 1 m above the bed by System 1B at Site 1.

	Storms		*Pre-frontal*		*Post-Frontal*	
Storm Type	*Speed (cm s^{-1})*	*Direction*	*Speed (cm s^{-1})*	*Direction*	*Speed (cm s^{-1})*	*Direction*
1	16.5	229	5.8	316	17.4	228
2	13.2	141	11.7	287	17.2	123
3	9.1	224	6.1	262	7.5	225
All Storms	**13.7**	210	**7.8**	284	**14.0**	190

7.3 Bottom Boundary Layer Parameters

Standard bottom boundary layer parameters for Site 1, calculated by applying the logarithmic profile (LOG) method to current data from System 1B, are presented in Table 7.5. The results obtained by applying the Reynolds Stress (RS) method to the 3-D current data from Systems 1A and 2A are not presented here, largely owing to the smaller data sets available, and the fact that general trends apparent from these systems were similar. Shear velocity was almost identical overall during Types 1 and 2 storms, and was, as

expected, much lower during Type 3 storms. During the 24 hours prior to the frontal passage, however, shear velocity was much higher for Type 2 storms than for either Types 1 or 3, which had nearly equivalent values. Shear velocity values were higher during the post-frontal than the pre-frontal phase for all types of storms, with Type 2 storms again being characterized by the highest values, and Type 3 storms by the lowest. Apparent bottom roughness was clearly highest during Type 2 storms, and lowest overall during Type 1 storms, particularly during the post-frontal stage. The reasons for this are unclear, although it is possible that high wave activity occurring during the pre-frontal phase of Type 2 storms created physical bed roughness elements such as wave ripples. These may have been absent, or at least less prominent, during the other storm types, and additionally, may have been washed out by strong post-frontal currents during Type 1 storms. However, this conclusion is highly speculative.

Table 7.5: Current-induced and combined wave-current shear velocity (u^*_c and u^*_{cw}, respectively), and apparent bottom roughness (z_0) for the three storm types at Site 1, as calculated by applying the logarithmic profile (LOG) method to data from System 1A.

	All Storm Conditions			*Pre-frontal (24h)*			*Post-frontal (24h)*		
Storm Type	u^*_c (cm s^{-1})	u^*_{cw} (cm s^{-1})	z_0 (cm)	u^*_c (cm s^{-1})	u^*_{cw} (cm s^{-1})	z_0 (cm)	u^*_c (cm s^{-1})	u^*_{cw} (cm s^{-1})	z_0 (cm)
1	1.51	2.55	1.66	0.63	1.16	3.37	1.52	2.57	1.69
2	1.52	2.56	4.11	1.23	2.43	4.09	2.01	3.22	4.07
3	0.83	1.34	2.35	0.68	1.07	3.33	0.75	1.21	3.43
All Storms	**1.41**	**2.37**	**3.00**	**0.84**	**1.55**	**3.60**	**1.42**	**2.33**	**3.04**

Figures 7.21 and 7.22 are time series of current- and wave-current shear velocity during Types 1 and 2 storms. In both cases, peaks occurred during the pre- and post-frontal phases of the storms, separated by a period of distinctly lower values concurrent with the frontal passage. During the Type 1 storm, however, post-frontal shear velocities were considerably higher than they were prior to the frontal passage, with peak values of nearly twice the magnitude. On the other hand, the highest shear velocity that occurred

during the Type 2 storm actually preceded the frontal passage, although an extended period of elevated values persisted during the post-frontal phase. It has already been demonstrated that pre-frontal winds, waves and currents tended to be more energetic during Type 2 storms than Type 1 storms, and it appears likely, therefore, that this resulted in higher relative pre-frontal shear velocities. These results have important implications for sediment transport, as will be discussed in the next section.

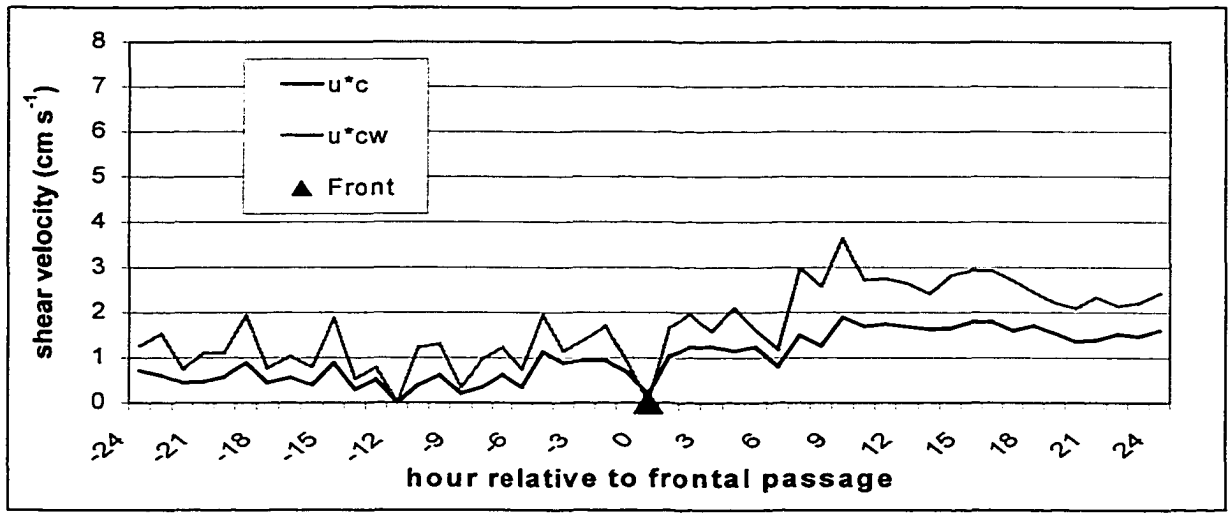

Figure 7.21: Current and wave-current shear velocity (u_{*c} and u_{*cw}, respectively) at Site 1 (System 1B) during a Type 1 storm (Storm 7). Trends were similar at Site 2.

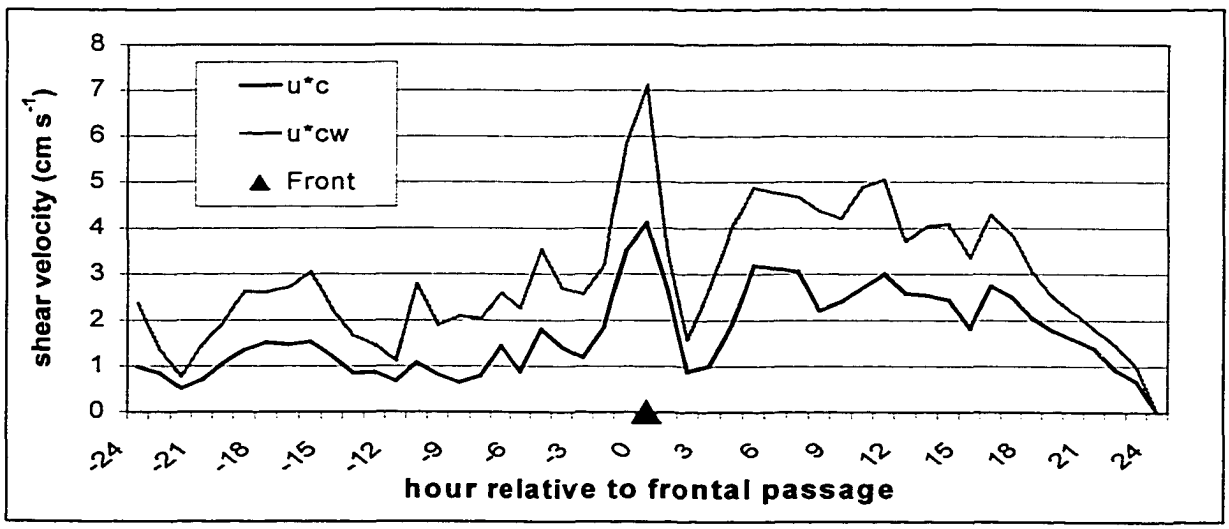

Figure 7.22: Current and wave-current shear velocity (u_{*c} and u_{*cw}, respectively) at Site 1 (System 1B) during a Type 2 storm (Storm 6). Trends were similar at Site 2.

7.4 Sediment Transport

Sediment transport predictions, much like hydrodynamic and bottom boundary layer parameters, vary considerably, although somewhat regularly, based on the type of storm driving the response. This section is intended to highlight these regularities and to suggest possible reasons for them, within the context of the classification system. As has been stressed repeatedly during this dissertation, however, considerable uncertainty exists in estimating sediment transport rates, and as such, specific quantities are presented here chiefly for the purposes of comparison. Despite this limitation, however, it is instructive to present examples from storm Types 1 and 2 to illustrate the temporal variation in across- and along-shelf sediment transport during extratropical storms.

Figures 7.23 and 7.24 illustrate temporal across- and along-shore suspended and bed load sediment transport patterns associated with a Type 1 storm (Storm 7) as calculated for Site 1 using the GMR and MPM methods, respectively. Prior to the cold front passage, sediment transport was near zero in both the across- and along-shelf directions, while 3-9 h subsequently, a pronounced peak in south-southwesterly suspended sediment transport, and southerly bed load transport occurred. The pattern during the Type 2 storm (Storm 6) at Site 1 was slightly more complex, although trends in bed and suspended load transport were remarkably similar (Figs. 7.25 and 7.26). Prior to the frontal passage, and persisting until 6 h subsequent to it, sediment transport was offshore, at which time, a sharp onshore peak occurred. This was followed by a prolonged period of offshore transport. Aside from a short period of westerly transport during the pre-frontal phase, along-shore transport was consistently easterly, with the highest values occurring immediately following the frontal passage.

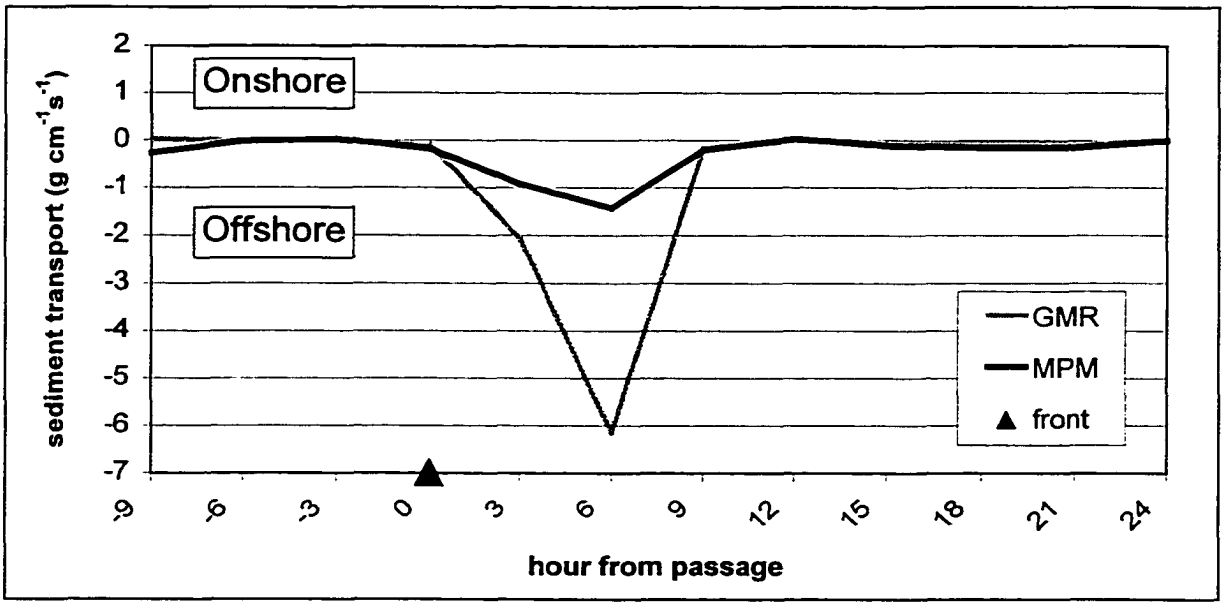

Figure 7.23: Across-shelf sediment transport during Storm 7, at Site 1 (System 1A) as predicted using the Grant-Madsen-Rouse (GMR) and Meyer-Peter and Muller (MPM) methods.

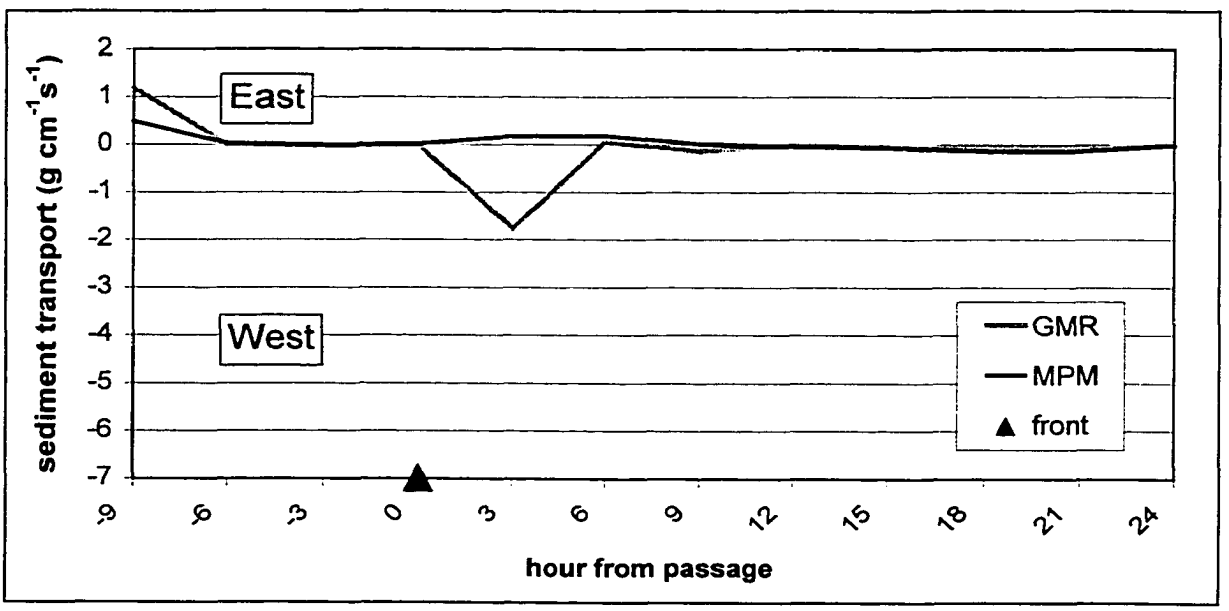

Figure 7.24: Along-shelf sediment transport during Storm 7, at Site 1 (System 1A) as predicted using the Grant-Madsen-Rouse (GMR) and Meyer-Peter and Muller (MPM) methods.

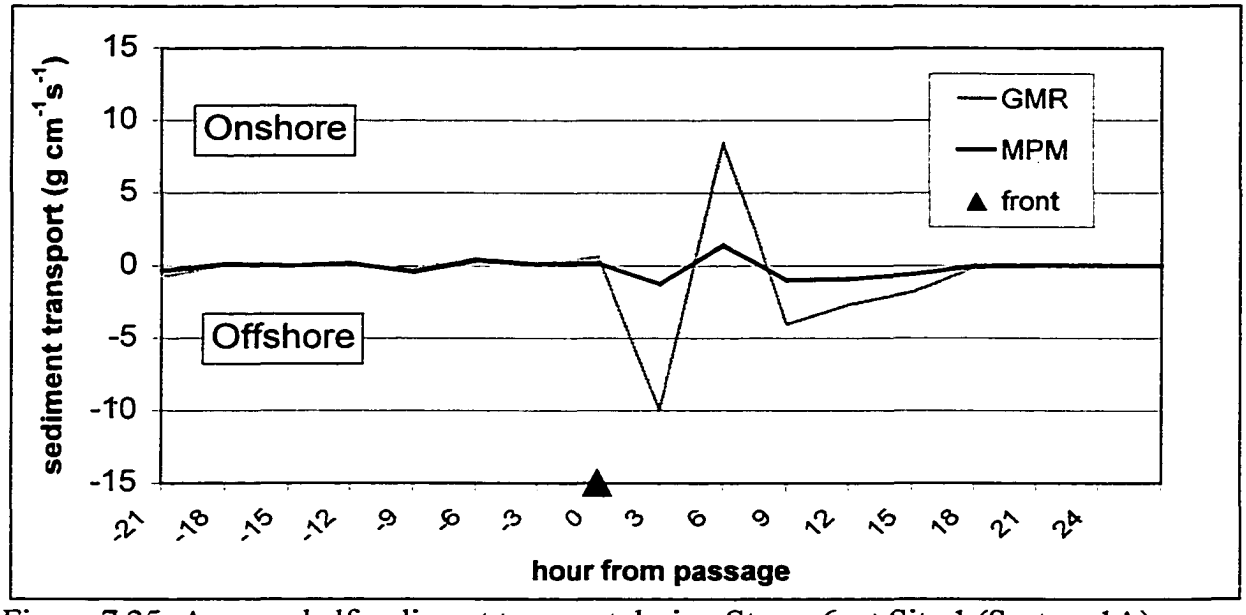

Figure 7.25: Across-shelf sediment transport during Storm 6, at Site 1 (System 1A) as predicted using the Grant-Madsen-Rouse (GMR) and Meyer-Peter and Muller (MPM) methods.

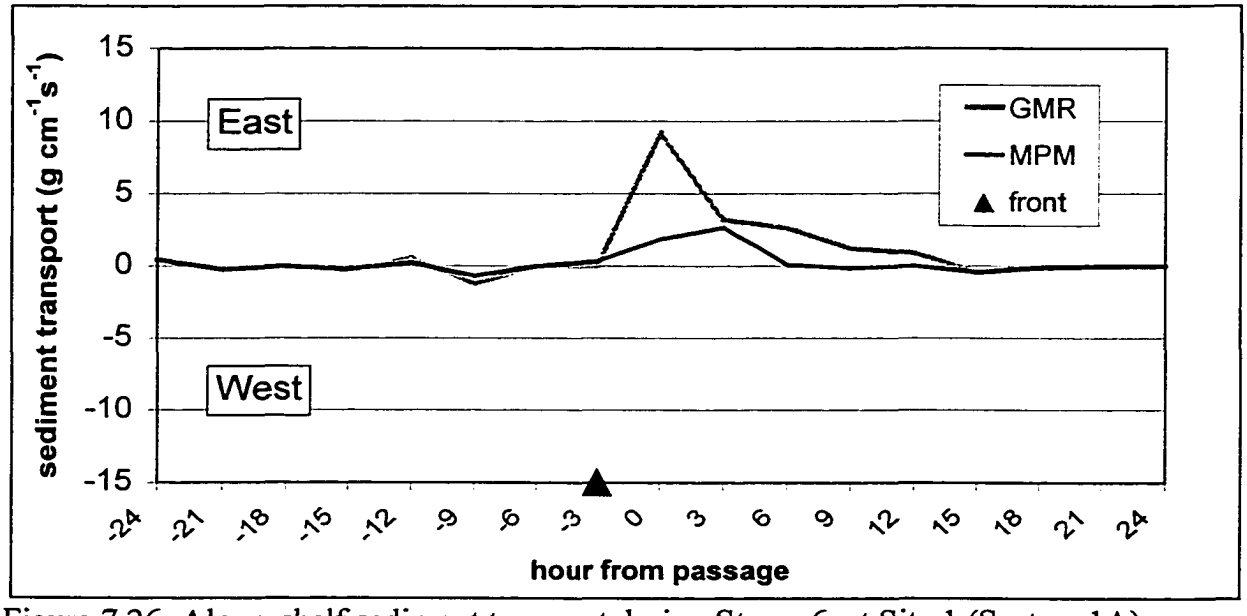

Figure 7.26: Along-shelf sediment transport during Storm 6, at Site 1 (System 1A) as predicted using the Grant-Madsen-Rouse (GMR) and Meyer-Peter and Muller (MPM) methods.

Table 7.6 summarizes the overall suspended and bed load transport estimates for Sites 1 and 2 during the three storm types, as estimated using the Grant-Madsen-Rouse (GMR) and Meyer-Peter and Muller (MPM) methods, respectively. It is immediately evident that at both sites, and according to both methods, Type 2 storms were responsible for the largest rates of sediment transport, followed by Type 1 storms, which had transport rates several times lower. Type 3 storms, as suggested previously, were characterized by sediment transport rates much lower than either Type 1 or 2 storms. Both suspended and bed load sediment transport direction ranged between southerly and westerly during Type 1 storms, depending on the prediction method used and the location. As has been suggested from previous analysis, transport had a stronger offshore component at Site 1, where the overall direction was nearly southerly, than at Site 2, where transport was predominantly westerly. Suspended sediment transport during Type 2 storms was toward the southeast; however, unlike with Type 1 storms, there was a stronger offshore component at Site 2 than at Site 1. Bed load transport during Type 2 storms was southwesterly at Site 1, and southeasterly at Site 2. During Type 3 storms, sediment transport tended to be westerly, with a southerly component at Site 1 and a northerly component at Site 2.

Table 7.6: Sediment transport predicted with the GMR and MPM methods for Systems 1A and 2A using the Reynolds stress technique for calculating shear stress.

Site	1				2			
	GMR		MPM		GMR		MPM	
Storm Type	Q (mg cm^{-1}s^{-1})	Dir.	Q (mg cm^{-1}s^{-1})	Dir.	Q (mg cm^{-1}s^{-1})	Dir.	Q (mg cm^{-1}s^{-1})	Dir.
1	289.2	195	144.7	190	175.8	273	173.9	259
2	1095.6	120	388.1	118	1871.8	174	847.8	205
3	57.0	268	56.3	255	2.2	232	15.2	316
All Storms	459.1	139	178.7	145	810.7	182	412.9	256

Tables 7.7 and 7.8 show the flux of sediment at a variety of frequency ranges predicted for the two sites using the SCP method in conjunction with the ADV data (Systems 1A and 2A). Transport at all frequencies was highest during Type 2 storms, and not surprisingly, extremely low (in fact, almost negligible) during Type 3 storms. In terms of frequency components, mean transport was highest for all storm types at both sites, followed by wind-wave and low-frequency flux. Mean transport was generally westerly during Type 1 and 3 storms, and was distinctly southeasterly during Type 2 storms, as was the case with the results from the GMR method. The direction of low-frequency flux varied widely between storms. During Types 1 and 3 storms, northeasterly flux prevailed at Site 1, while southeasterly flux was evident at Site 2. On the other hand, low-frequency transport was northwesterly at both sites during Type 2 storms.

Table 7.7: Cospectral estimates of suspended sediment transport (mg $cm^{-1}s^{-1}$) at System 1A (~20 cm above the bed) for the three storm types. Periods are-Mean: averaged over 81 s (1.3 minutes); Low-frequency:=>10.25s;Wind-Wave: 2.15s-10.24s.

	Mean Flux		Low-frequency Flux		Wind-Wave Flux		Total Flux	
Storm Type	mg $cm^{-1}s^{-1}$	Direction	mg $cm^{-1}s^{-1}$	Direction	mg $cm^{-1}s^{-1}$	Direction	mg $cm^{-1}s^{-1}$	Direction
1	12.3	250	3.3	49	8.9	186	14.2	220
2	37.6	142	7.0	341	20.9	356	17.8	78
3	0.3	252	0.1	56	0.2	37	0.2	347
All Storms	**11.4**	165	**2.9**	4	**3.4**	345	**3.6**	145

Table 7.8: Cospectral estimates of suspended sediment transport (mg $cm^{-1}s^{-1}$) at System 2A (~20 cm above the bed) for the three storm types. Periods are-Mean: averaged over 512 s (8.5 minutes); Low-frequency:=>10.25s;Wind-Wave: 2.15s-10.24s.

	Mean Flux		Low-frequency Flux		Wind-Wave Flux		Total Flux	
Storm Type	mg $cm^{-1}s^{-1}$	Direction	mg $cm^{-1}s^{-1}$	Direction	mg $cm^{-1}s^{-1}$	Direction	mg $cm^{-1}s^{-1}$	Direction
1	31.9	282	1.7	94	1.3	122	28.7	281
2	121.1	140	2.6	317	8.6	66	120.3	136
3	0.3	287	0.0	111	0.0	124	0.3	286
All Storms	**36.7**	155	**0.7**	7	**3.7**	74	**36.7**	148

Disparate directions of wind-wave flux, depending on the deployment location and the storm type, also occurred. At Site 1, transport at wind-wave frequencies was nearly offshore during Type 1 storms, almost directly onshore during Type 2 storms, and toward the northeast during Type 3 storms. At Site 2, on the other hand, wind-wave flux was southeasterly during storm Types 1 and 3, and northeasterly during Type 2 storms. Net transport direction tended to be similar to the mean flux direction at Site 2, and as a result was southwesterly during Types 1 and 3 storms, and southeasterly during Type 2 storms. However, the importance of the wind-wave component at Site 1 resulted in a net east-northeasterly transport direction during Type 2 storms.

Figures 7.27-7.30 illustrate predicted across- and along-shelf sediment transport over different frequencies at Site 2 during the two storm types. During Storm 7, which is the Type 1 storm shown in Figs. 7.27 and 7.28, mean transport was predominantly onshore prior to the frontal passage as well as during a transport peak immediately following it, while during the majority of the post-frontal phase, it was relatively high and offshore. Mean along-shelf transport was westerly throughout the storm, and was particularly high subsequent to the frontal passage. Transport in the low-frequency and wind-wave bands varied considerably over the course of the storm, often reversing direction during the three-hour intervals separating bursts. Generally speaking, however, low-frequency transport was most commonly northeasterly, particularly subsequent to the frontal passage. Across-shore transport in the wind-wave band, on the other hand, was most commonly onshore prior to the frontal passage, and offshore subsequently. A minor easterly component at wind-wave frequencies also occurred throughout both the pre- and post-frontal phases of the storm.

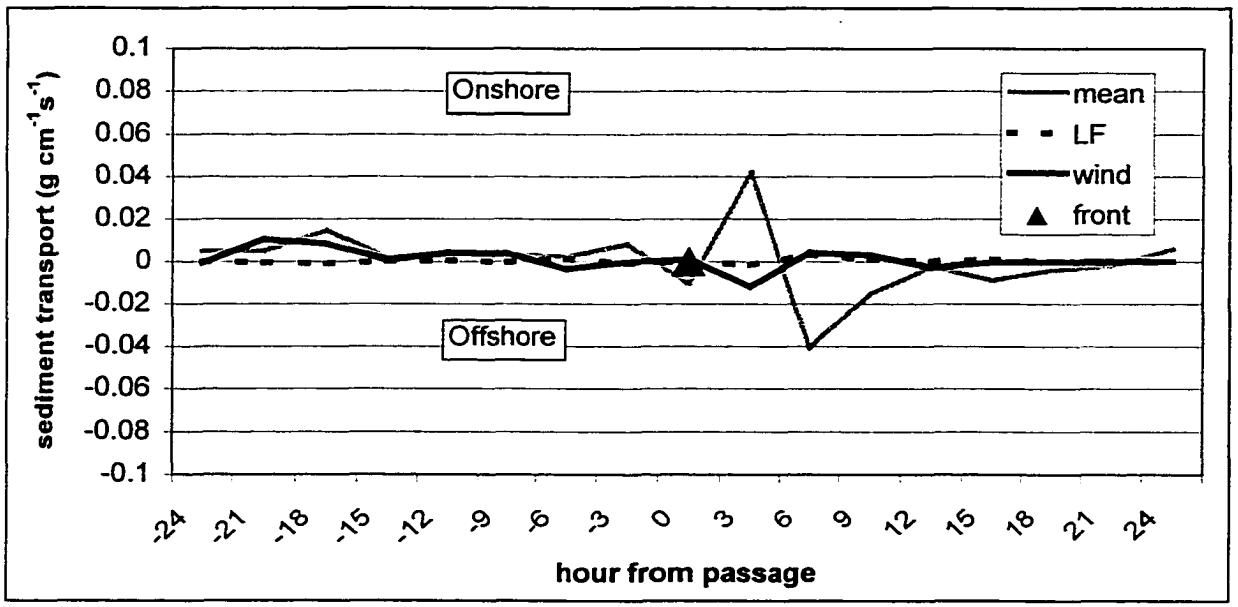

Figure 7.27: Across-shelf suspended sediment transport during a Type 1 storm (Storm 7), at mean, low (LF), and wind-wave frequencies, as predicted for Site 2 on the basis of the cross product of flow and concentration measured by System 2A.

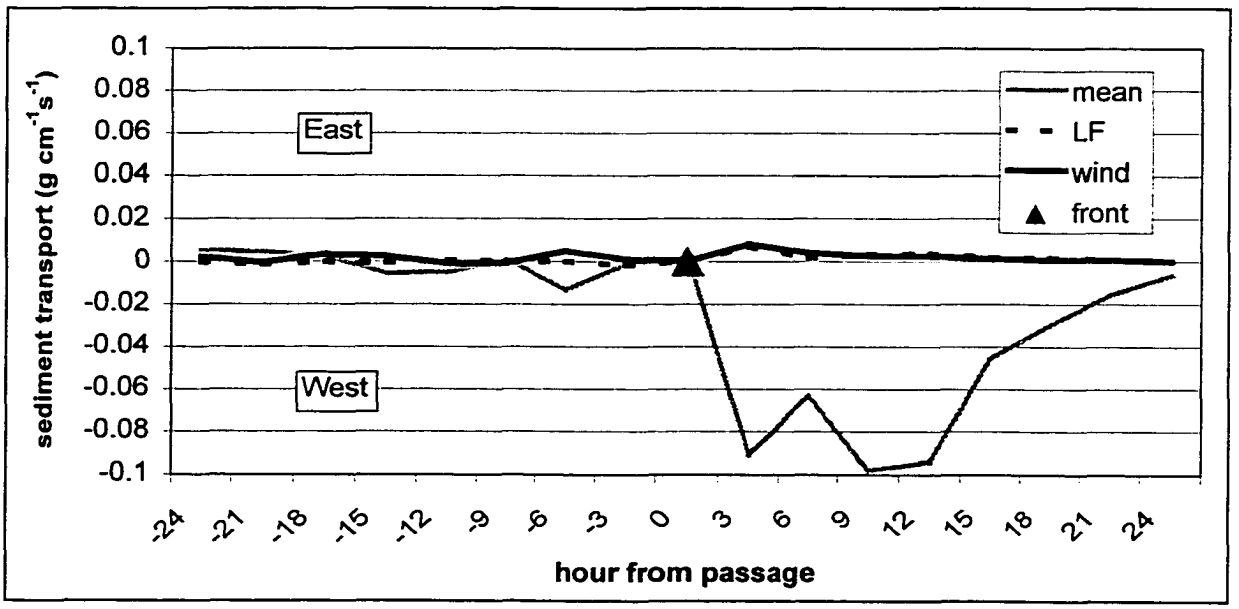

Figure 7.28: Along-shelf suspended sediment transport during a Type 1 storm (Storm 7), at mean, low (LF), and wind-wave frequencies, as predicted for Site 2 on the basis of the cross product of flow and concentration measured by System 2A.

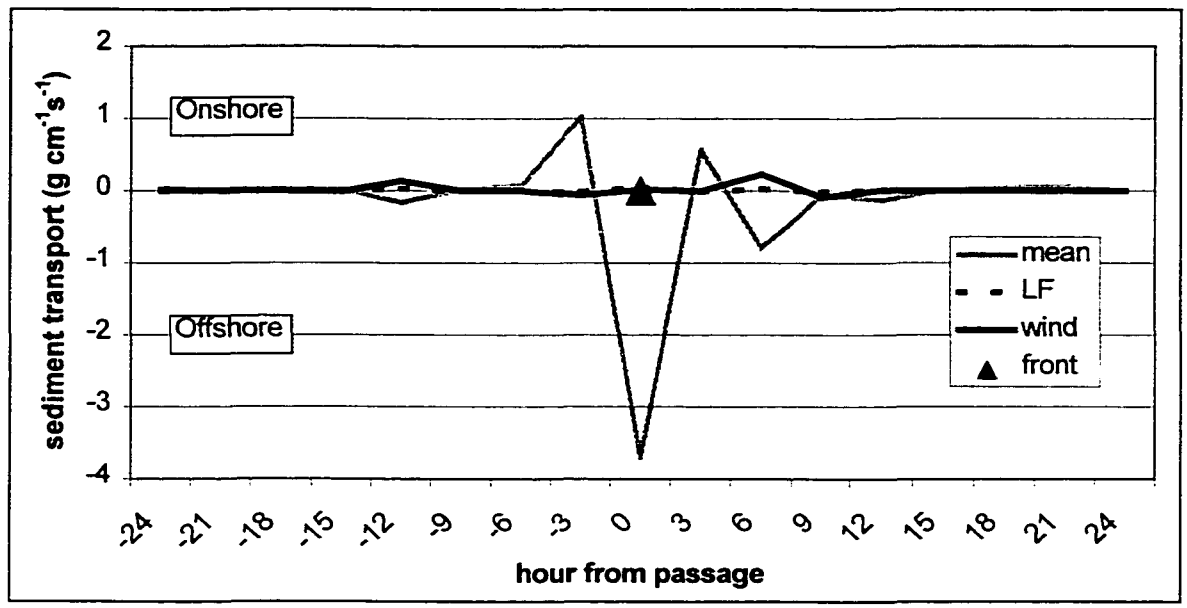

Figure 7.29: Across-shelf suspended sediment transport during a Type 2 storm (Storm 6), at mean, low (LF), and wind-wave frequencies, as predicted for Site 2 on the basis of the co-spectrum of flow and concentration measured by System 2A.

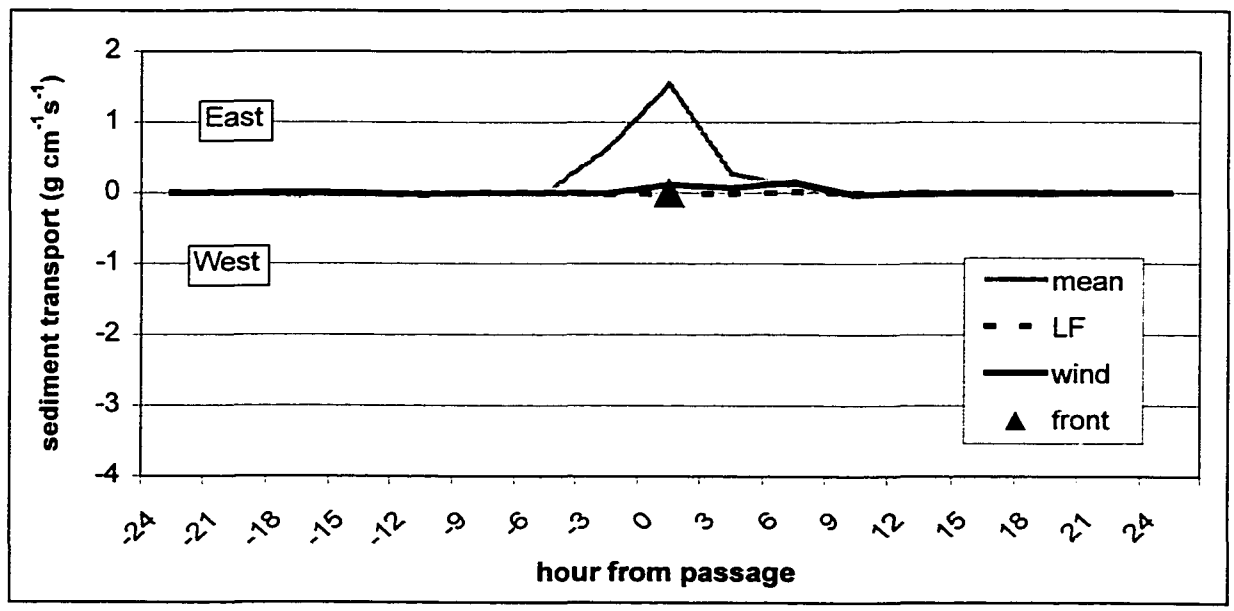

Figure 7.30: Along-shelf suspended sediment transport during a Type 2 storm (Storm 6), at mean, low (LF), and wind-wave frequencies, as predicted for Site 2 on the basis of the co-spectrum of flow and concentration measured by System 2A.

During Storm 6, a Type 2 storm (Figs. 7.29 and 7.30), maximum mean transport coincided with the frontal passage, when it was directed toward the southeast, as was the case for the majority of the storm. The only exceptions were two minor episodes of onshore flux that occurred three hours before, and three hours after, the frontal passage. Low-frequency transport was uniformly low during the storm, with southwesterly transport occurring prior to the frontal passage, and south- to northeasterly transport occurring subsequently. There were two peaks in transport at wind-wave frequencies, both directed toward the northeast, one prior to, and one following, the frontal passage.

It is not surprising that mean transport direction for the storm types predicted using the SCP method was similar to the results calculated using the GMR and MPM models. However, wind-wave and low frequency contributions to transport were highly variable and are difficult to explain since similar wave characterstics were sometimes associated with widely differing trends in oscillatory transport during the storms.

Figures 7.31 and 7.32 show the across-shelf component of sediment transport at low and wind-wave frequencies relative to the mean wave direction during the two types of storms, as well as bed level change. The first point to note is that the sediment transport patterns are surprisingly similar during the different storms. Second, as was the case with geographical transport direction, transport direction relative to waves fluctuated a great deal during the course of the storm. In other words, the highly variable direction of transport at wind-wave and low frequencies was not simply a function of a shift in the direction of the waves, but also of a shift in the transport direction relative to the waves themselves. Generally speaking, low-frequency transport occurred in the same direction as wave propagation during two main peaks, one prior to the frontal passage, and one

subsequent to it. During the majority of the storm's remainder, low-frequency transport was directed against the waves. The largest peaks in wind-wave transport were aligned with the direction of wave propagation, except during two episodes of transport, one immediately prior to the frontal passage, and the second several hours subsequent to it.

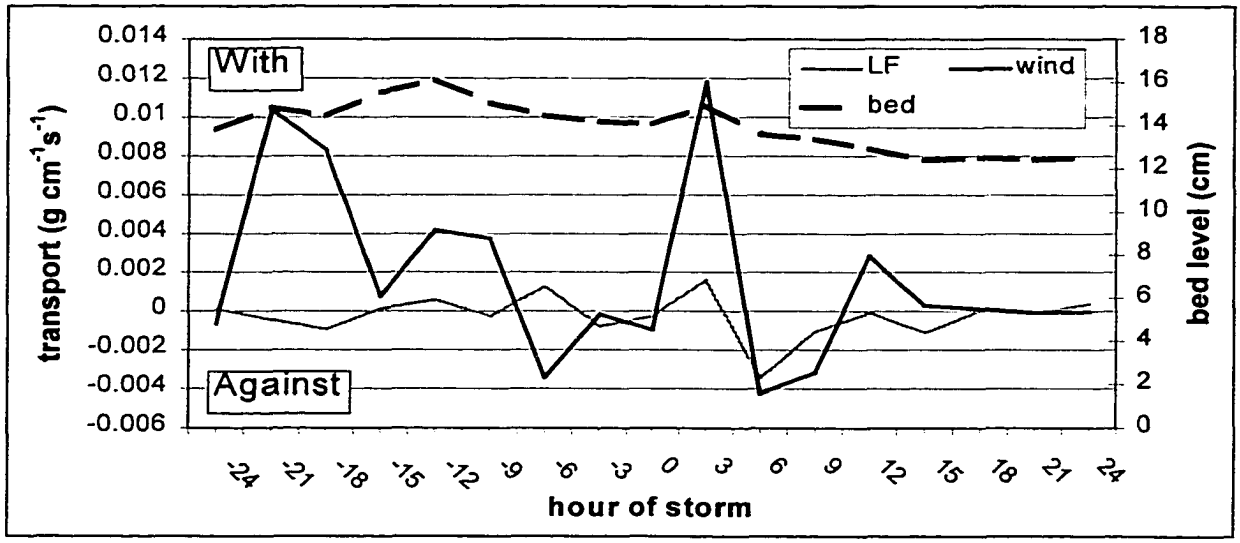

Figure 7.31: Bed level and across-shelf suspended sediment transport at Site 2, relative to mean wave direction, during a Type 1 storm (Storm 7), at low (LF), and wind-wave frequencies.

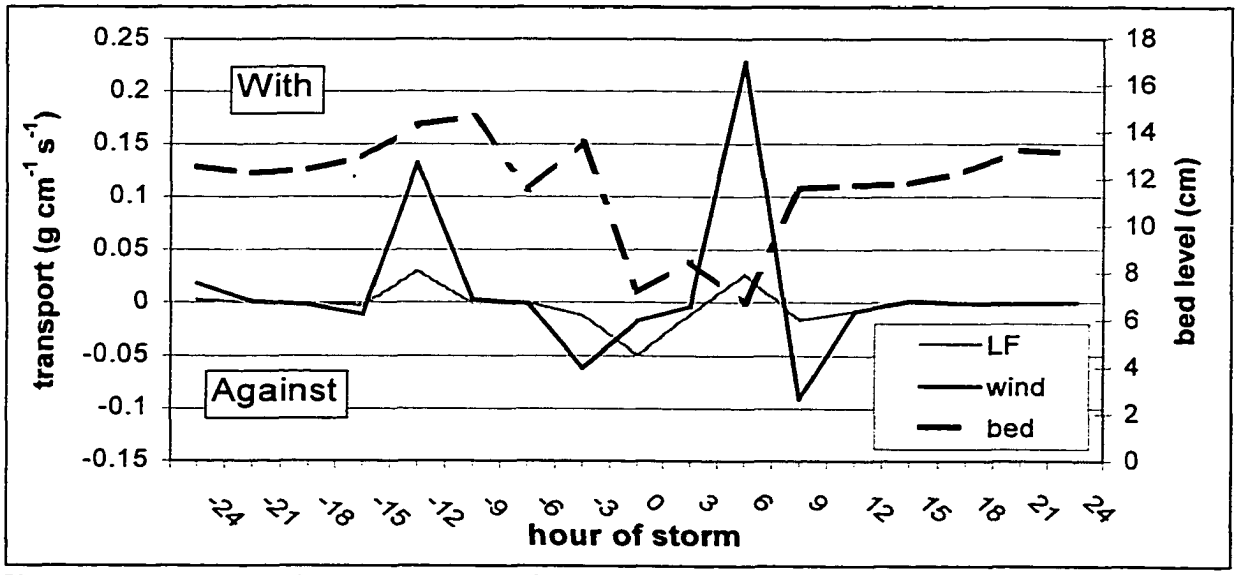

Figure 7.32: Bed level and across-shelf suspended sediment transport at Site 2, relative to mean wave direction, during a Type 2 storm (Storm 6), at low (LF) and wind-wave frequencies.

The causes associated with these directional shifts cannot be positively identified from the data set since the possible factors responsible for generating the necessary phase differences are numerous and include wave asymmetry, vortex generation by bed forms, sensor location relative to the bed (and individual bed forms), and the interaction of various wave trains. As stated in Chapter 6, wave characteristics alone did not seem to account for these differences, and as such, the most likely explanation must incorporate changes in the bed beneath the instrumentation. As shown in Figs. 7.31 and 7.32, large changes in bed level accompanied directional shifts in sediment transport during storms. Similar results were apparent for the wave event, as will be shown in Chapter 8. It is likely that as bed level varied, the lag-time of sediment reaching the sensor following its suspension by oscillatory flow was altered, as was demonstrated by Vincent et al. (1991), Osborne and Greenwood (1993), and Osborne and Vincent (1996). In addition, the influence of wave vortices may have changed depending on the size, shape and spacing of bed forms; Davies (1985), for example, showed that vortex shedding occurs only when wave orbital excursion length exceeds the spacing of bed ripples. Finally, the position of the sensor in relation to bed forms is important (Osborne and Vincent, 1996; Vincent et al., 1999). These explanations remain a matter of speculation, since bed observations are not available; however, it should certainly be investigated in the future. Despite the intriguing nature of the problem of oscillatory flux, the fact remains that it accounted for a much smaller portion of overall suspended sediment transport than mean flux.

7.5 Summary

The purpose of this chapter was to examine extratropical storm passages in detail and to introduce an extratropical storm classification system for the Louisiana inner shelf. It is

clear that extratropical storm passages are characterized by a fairly typical sequence that involves one or more of the following: 1) a pre-frontal period of elevated, northerly, long-period waves, weak to moderate northerly currents, increased shear velocity, and increased sediment transport; 2) a frontal period of reduced waves, currents, shear velocity, and variable sediment transport; 3) a post-frontal period of high waves that includes a short-period southerly component, strong southerly current flow, increased shear velocity, and very high, and generally offshore, sediment transport.

Despite these similarities, it is also clear that all extratropical storms are not identical, and as such, a classification system including three storm types was developed. Type 1 and 2 storms are essentially end-members on a continuum of relative cyclonic/anticyclonic influence, and intermediate types can undoubtedly be identified. Type 1 storms are dominated by an anticyclone to the north, and have a very weak pre-frontal phase followed by a fairly powerful post-frontal phase during which northeasterly winds dominate. Type 1 storms had a somewhat lower average significant wave height than Type 2 storms and were dominated by short-period southerly waves subsequent to the frontal passage. Currents were weak and northerly during the pre-frontal phase, but became very strong (the highest of all storm types) and southwesterly following the frontal passage. Shear velocity calculated for Type 1 storms was almost identical to that during Type 2 storms, although elevated values were confined primarily to the post-frontal phase. Sediment transport rate during Type 1 storms was not as high as during Type 2 storms, and the mean and overall direction tended to be southwesterly at Site 1 and westerly at Site 2, with low-frequency flows producing easterly transport, and wind-wave flows producing southeasterly transport.

Type 2 storms are dominated by a strong, nearby low-pressure cell, and have fairly strong southerly winds prior to the frontal passage, and strong northwesterly winds subsequent to it. Type 2 storms had the most energetic waves of any storm type, with peaks in significant wave height occurring during both the pre- and post-frontal phases. The wave field during Type 2 storms tended to be more complex than during Type 1 storms, with an energetic, northerly swell band gradually giving way to a southerly sea-band as the post-frontal phase progressed. Currents during Type 2 storms were moderate and northerly during the pre-frontal phase, but became much stronger and southeasterly during the post-frontal phase. Shear velocity was high during both the pre- and post-frontal phases of the storm, although sediment transport was highest following the frontal passage. Mean and overall sediment transport was directed southeasterly during Type 2 storms, with low-frequency and wind-wave flows producing northerly transport.

Finally, Type 3 storms are distinguished chiefly by the fact that they are weak, attaining a Power-V value of less than 2000. Most of their characteristics resemble those of either Types 1 or 2 storms, although they obviously tend to be much reduced in magnitude, particularly with regard to sediment transport. The characteristics of all storm types are shown in Table 7.9.

Table 7.9: Summary of storm characteristics associated with the three storm types.

Characteristic	*Type 1*	*Type 2*	*Type 3*
Primary Synoptic Feature	Anticyclone (High)	Cyclone (Low)	Variable
Storm Stages Experienced	Post-Frontal	Pre- and Post-Frontal	Post-Frontal
Wind Speed (Rank)	1	2	3
Dominant Wind Direction	NE	NW	NE-NW
Wave Height (Rank)	2	1	3
Wave Characteristics	S Sea	N swell becomes S sea	Variable
Current Speed	High	High	Low
Dominant Current Direction	SW	SE	SE-SW
Sediment Transport (Rank)	2	1	3
Sediment Transport Direction	SW-W	SE	SW-W

CHAPTER 8

DISTANT STORM WINDS IN THE GULF OF MEXICO AND THEIR INFLUENCE ON PROCESSES ON THE LOUISIANA INNER SHELF: THE WAVE EVENT

It is well-known that waves are capable of propagating thousands of kilometers from their source and influencing coasts an "ocean away". Komar (1998), for example, cited copious research in which it was demonstrated that waves reaching the Pacific coastline of North America were generated by storm activity in the South Pacific or East Indian Oceans. By comparison, the Gulf of Mexico is a fairly closed system with a much more limited fetch and lower hydrodynamic energy regime. It is not surprising that during this deployment, therefore, strong winds at the study site were directly correlated with high-energy hydrodynamic and sedimentary responses locally.

On the other hand, it was also noted in Chapter 6 that a conspicuous deviation from this pattern occurred during the "fair weather" interval between (approximately) 20:00 on Dec. 18, and 21:00 on Dec. 20, UTC. This interval was called a "wave event" and labeled "Event W" since its primary distinguishing characteristic was the occurrence of higher than average waves. During this time, mean hourly wind speed at the study site met the storm criterion for only one hour, and according to national weather maps, no cold fronts actually crossed the Gulf Coast. Nonetheless, between December 18 and December 20, significant wave height increased dramatically, reaching its second-highest level of the deployment (1.98 m at Site 1) at 11:00 UTC on December 19. In addition, energetic bottom boundary layer and sedimentary responses occurred, suggesting that the event exerted a significant influence on the inner shelf. The purpose of this chapter is to present data from this event and to discuss its possible causes and its significance.

8.1 Hydrodynamics

The morning of December 18, 1998 UTC was the least energetic interval of the entire deployment in terms of wave activity, with a significant wave height at Site 1 of less than 0.1 m. Between 16:00 and 19:00 on December 18, 1998, however, significant wave height quadrupled, eventually reaching 1.98 m at 11:00 UTC on December 19. During this time, peak wave period, which had been approximately 3.5 seconds, increased to 8 seconds. Near-bed orbital velocity also increased dramatically, to a maximum value of 41.3 cm s^{-1}. The trends measured at Site 2 were similar to those at Site 1, although wave characteristics were modified predictably by attenuation across Ship Shoal, an effect discussed previously in this dissertation.

A time series of color-coded frequency spectra for the 48-hour period surrounding this wave event, named Event W in Chapter 6, is shown in Fig. 8.1. It illustrates the coherent structure of the frequency distribution during the time period and the rapid, but regular, increase and subsequent decline in wave energy. The spectra making up this time series were obviously very narrow-banded, with wave energy tightly concentrated around 7-8 s periods, which is essentially the swell-band in this high-frequency wave environment. Similarly, Fig. 8.2, which is a directional spectrum for 11:00 UTC on December 19 (the peak of the wave event), illustrates the compactness of spectral energy distribution, not only in terms of frequency, but also in direction. Again, energy was heavily concentrated around the 8-s period band, and in addition, waves at all frequencies propagated toward the northwest (mean wave direction was 319°). These data clearly seem to indicate that a coherent wave group from offshore propagated northward through the study area during this 48-hour period.

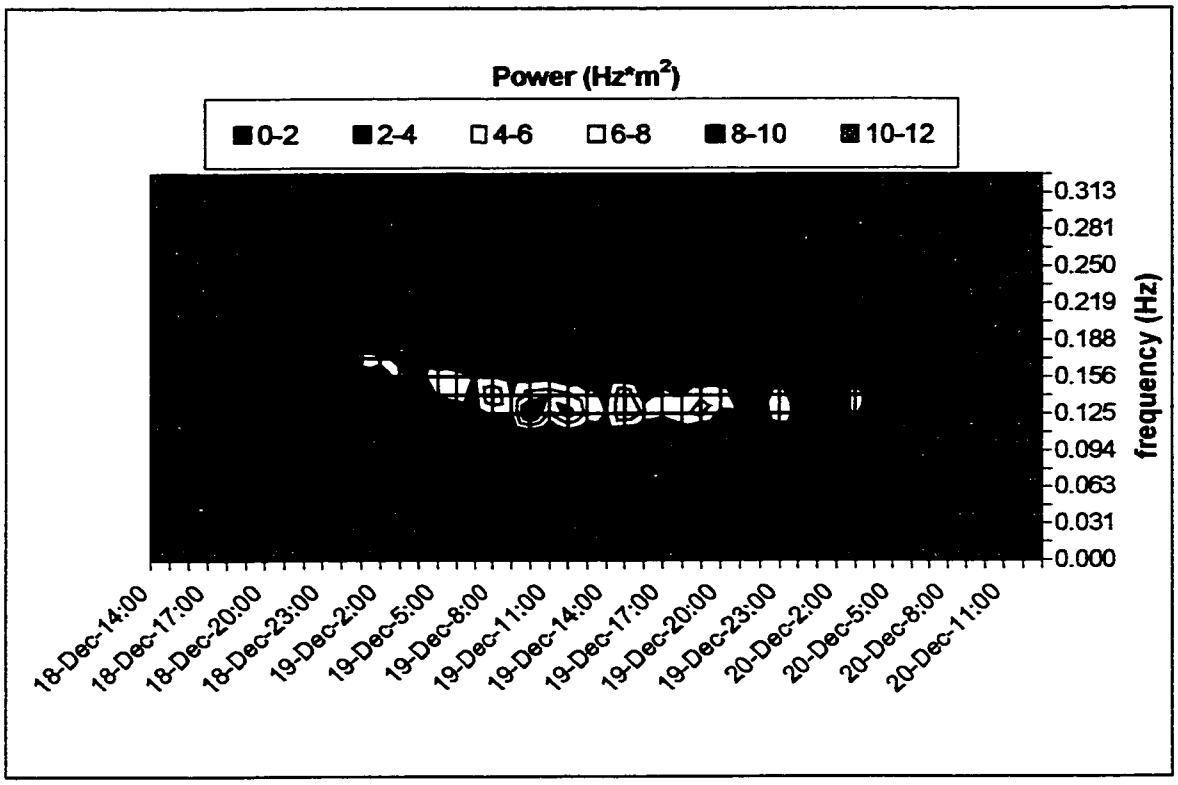

Figure 8.1: Color-coded time series of energy spectra for the wave event.

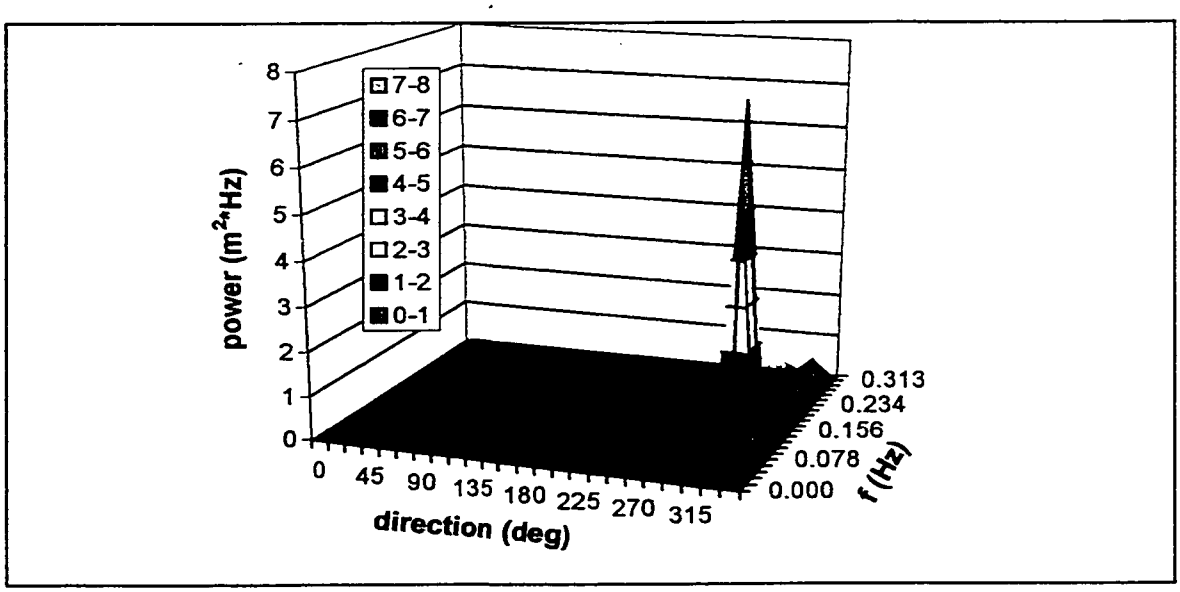

Fig. 8.2: Directional wave spectrum at Site 1 at 11:00 UTM on December 19, 1998, during the wave event.

Figure 8.3, which shows significant wave height at Site 1 as well as at NDBC buoy 42002, approximately 300 km to the south-south west, provides further verification of this hypothesis. Trends at the two sites were nearly identical with the time series at Site 1 lagging that of the buoy by a few hours. Linear wave theory would suggest a wave group travel time of just over six hours in deep water between the sites, and as such, it appears that the same wave group probably influenced the two sites a few hours apart.

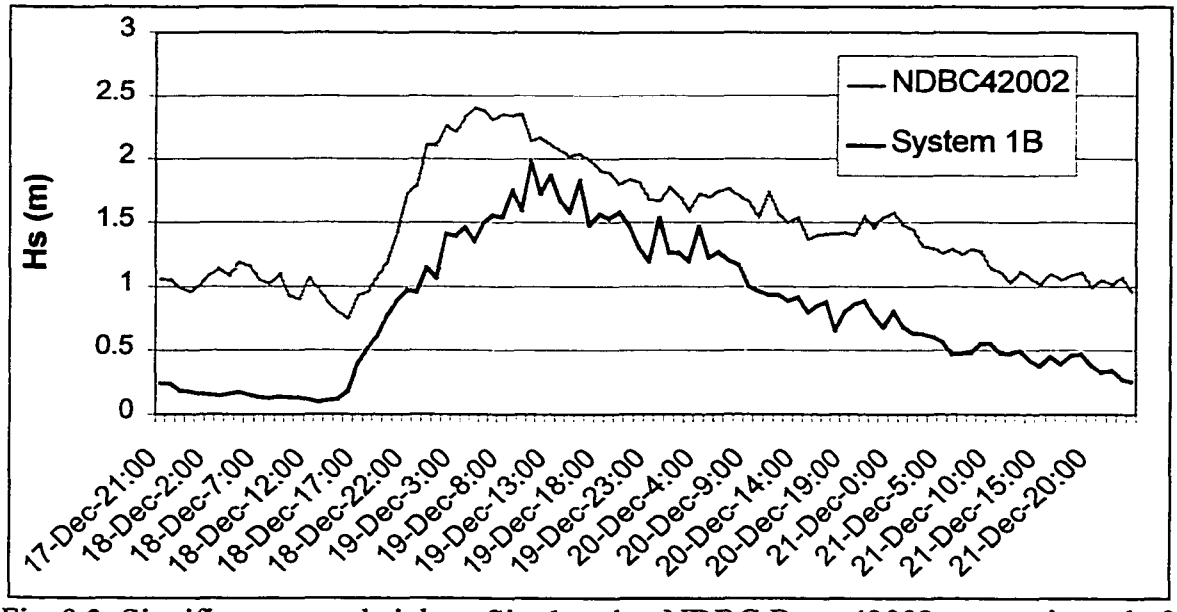

Fig. 8.3: Significant wave height at Site 1 and at NDBC Buoy 42002, approximately 300 km offshore, during Event W.

Current velocity during Event W is shown in Fig. 8.4. As discussed in Chapter 6, current speed during Event W was, for the most part, elevated only slightly above fair weather levels, although a brief (approximately 6 h) interval of increased mean current flow began approximately 24 h after the maximum significant wave height. During this interval, a peak current (at 100 cm above the bed) of 19.5 cm s^{-1} was measured at Site 1, 29 hours subsequent to the occurrence of maximum significant wave height. The current direction at the time was westerly, but it should be noted that the current direction during

the wave event rotated clockwise over time, with a frequency of approximately 24 hours. This suggests that although this occurrence was labeled a wave event, inertial currents were also present. Apparently, therefore, remote atmospheric storm activity may affect mean currents in the study area in a similar way that a local extratropical storm would.

8.2 Bottom Boundary Layer Parameters and Sediment Transport

Bottom boundary layer and sediment transport data for Event W are presented for Site 2, since instrument burial at Site 1 resulted in gaps in the data. Current- and wave-current shear velocity increased during the Event W, remaining noticeably elevated for approximately 48 h. Maximum shear velocity occurred at 10:00 on December 19 UTC, coincident with peak significant wave height (Fig. 8.5). It is clear, therefore, that high wave energy during Event W generated high shear velocity, despite weak mean currents.

Figures 8.6 and 8.7 show the across- and along-shelf flux of sediment calculated for Site 2 using the GMR and MPM methods, respectively. In both cases, periods of offshore flux occurred at the storm's onset and again during its later phases, separated by several hours of onshore transport. Both bed and suspended load transport were predominantly to the east and therefore, overall transport was toward the northeast. Across- and along-shelf suspended sediment transport at different frequencies, as calculated using the SCP method, are shown in Figs. 8.8 and 8.9, respectively. Mean transport provided the largest contribution to sediment flux, with northeasterly transport occurring throughout the majority of the storm. Transport was high and onshore at the "peak" of the storm, with comparatively minor intervals of offshore transport occurring both prior and subsequently. Along-shelf transport fluctuated a great deal, with several intervals of easterly transport and weaker westerly transport occurring during the storm.

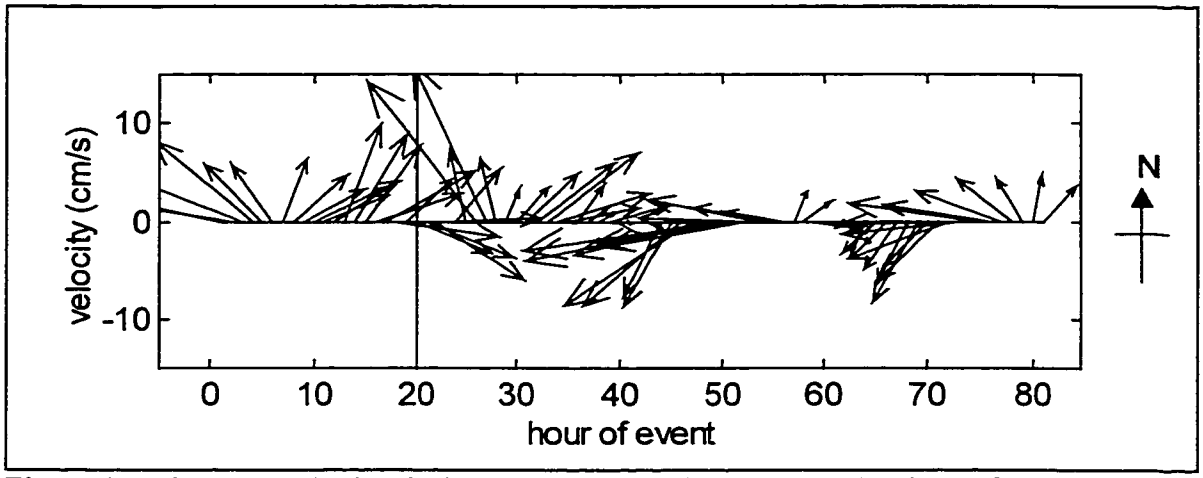

Figure 8.4: Current velocity during the passage of Event W. The time of peak wave energy of the storm is indicated by the vertical line.

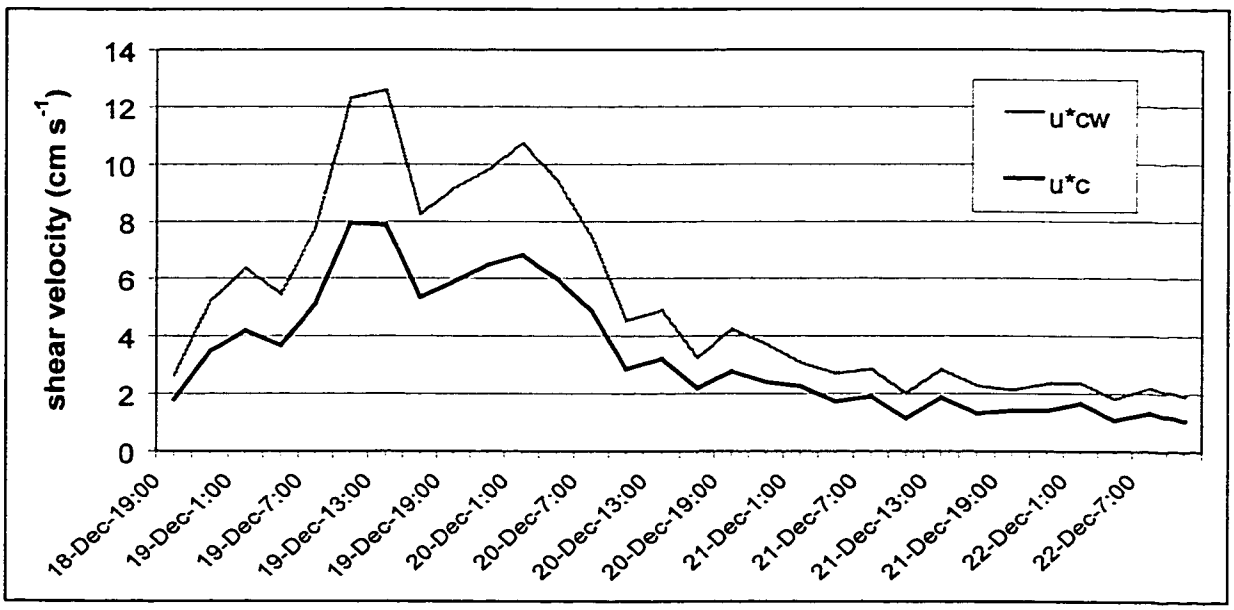

Figure 8.5: Current- and wave-current shear velocity (u*c and u*cw, respectively) during Event W at Site 2, as calculated using the Reynolds Stress (RS) method.

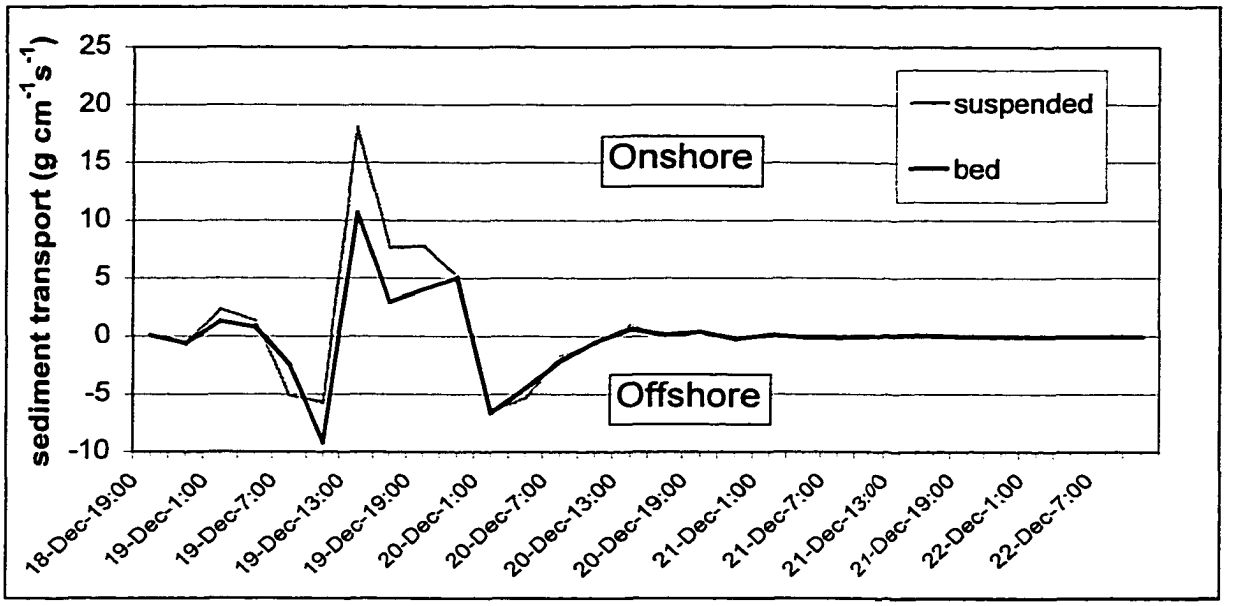

Figure 8.6: Across-shelf suspended and bed load transport at Site 2 during Event W, calculated using the GMR and MPM methods, respectively.

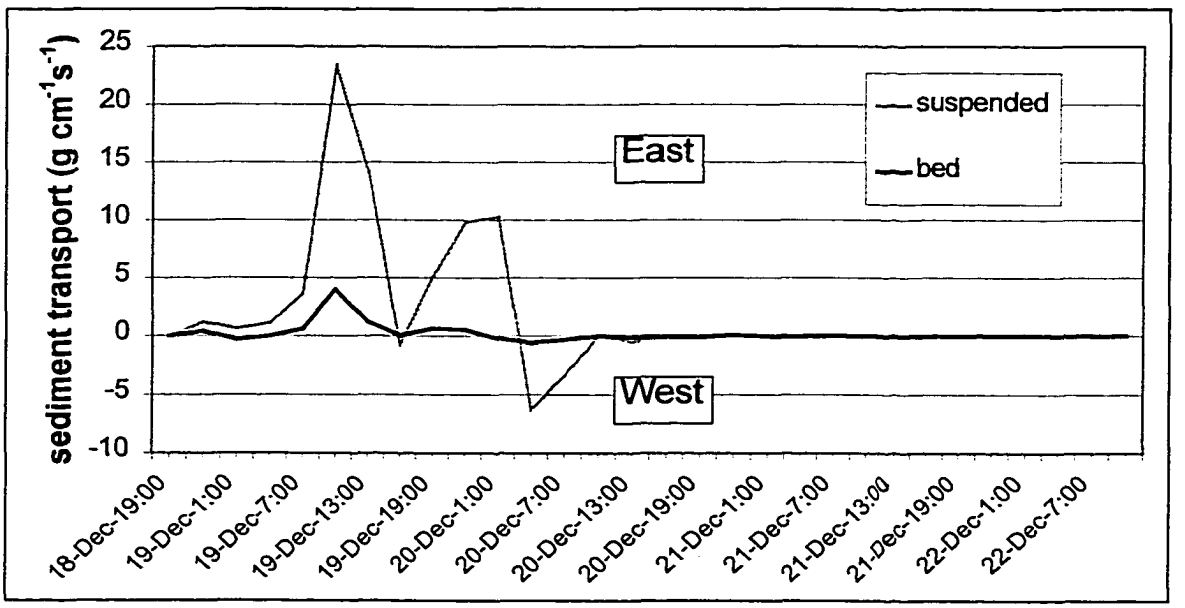

Figure 8.7: Along-shelf suspended and bed load transport at Site 2 during Event W, calculated using the GMR and MPM methods, respectively.

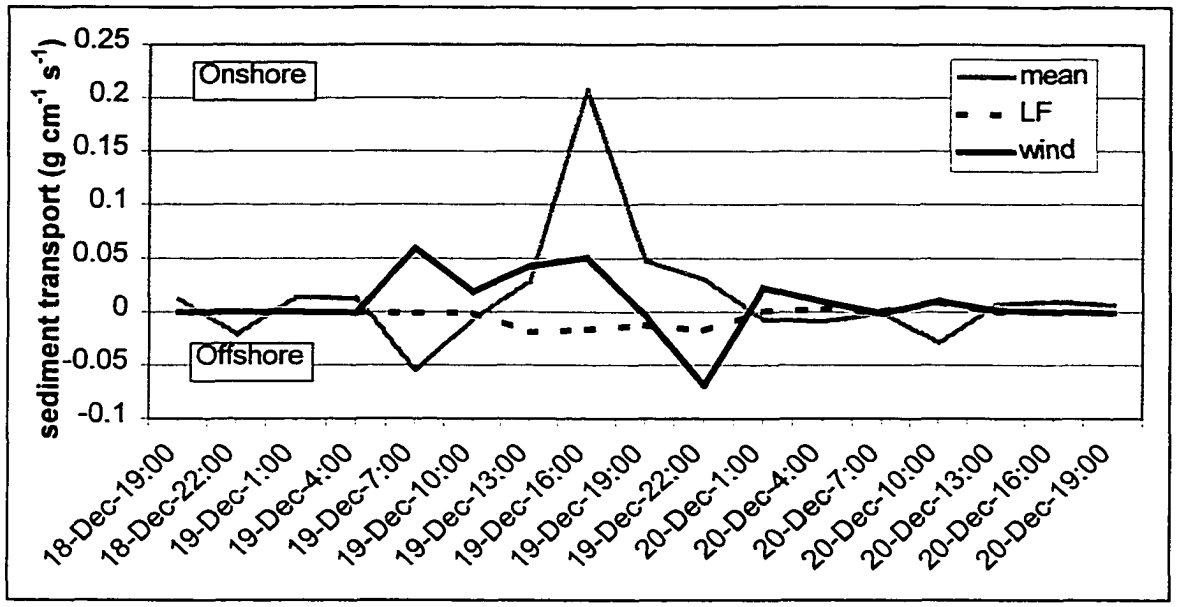

Figure 8.8: Across-shelf sediment transport at mean, low (LF), and wind-wave frequencies at Site 2 during Event W.

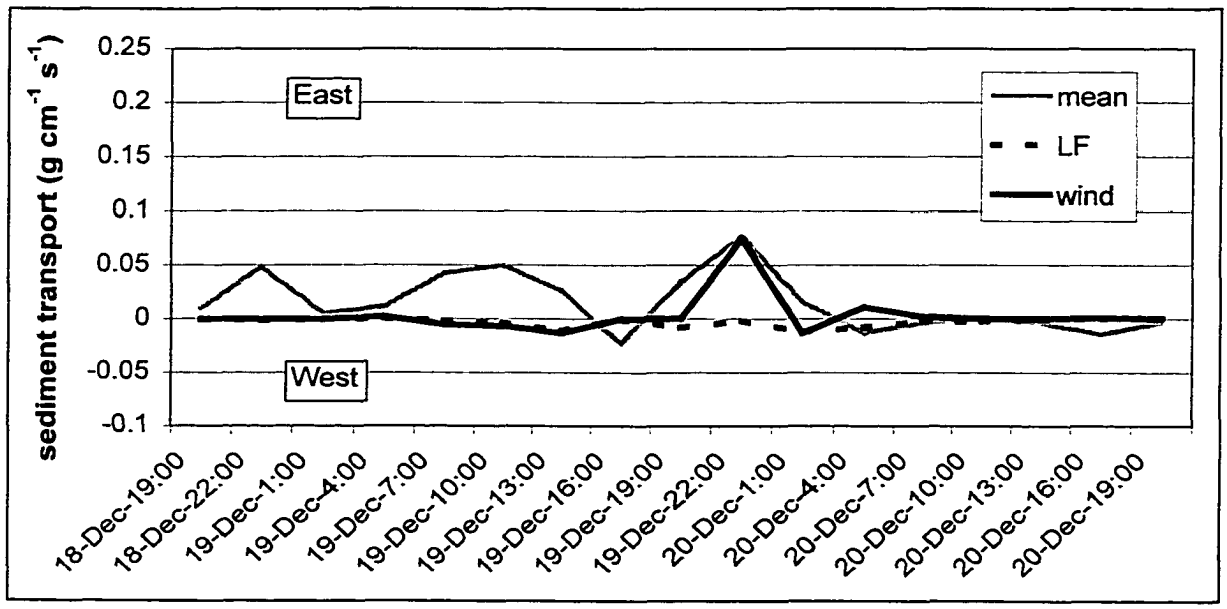

Figure 8.9: Along-shelf sediment transport at mean, low (LF), and wind-wave frequencies at Site 2 during Event W.

Oscillatory transport, especially at wind-wave frequencies, was much higher in comparison to mean transport than it was during most extratropical storm conditions, and was likely much higher still at Site 1, where wave activity was more energetic. This is not surprising, given the increased importance of wave activity in relation to current flow that characterized Event W. There were two roughly equivalent peaks in wave height during the storm, the first on December 19 at 16:00, and the second on December 19 at 22:00 UTC. A shift in transport direction at wind-wave frequencies occurred following the first of these peaks—prior to it, transport was toward the north-northwest, while subsequently, the storm's highest peak in wind-wave transport was directed toward the southeast. Transport at low frequencies was offshore and westerly throughout the storm.

As has been discussed previously, the cause of changes in transport direction in the wind-wave band is difficult to identify, given that there was little change in wave characteristics during this interval. Figure 8.10 depicts the across-shore component of wind-wave and low-frequency transport relative to the mean wave direction, which was nearly onshore during much of the storm, as well as the bed level change at Site 2. Low-frequency flux opposed the wave direction throughout much of the storm, suggesting that reverse-modulation of sediment transport at low frequencies as discussed by Shi and Larsen (1984) and Hanes (1991) may have been important. On the other hand, transport in the wind-wave band suddenly shifted, at virtually the height of the wave event, from being with the direction of wave propagation, to opposing it. As with the extratropical storms, bed level change accompanied this shift in transport direction, providing further evidence that bed changes that occur during energetic hydrodynamic events on the Louisiana inner shelf are responsible for variations in sediment transport.

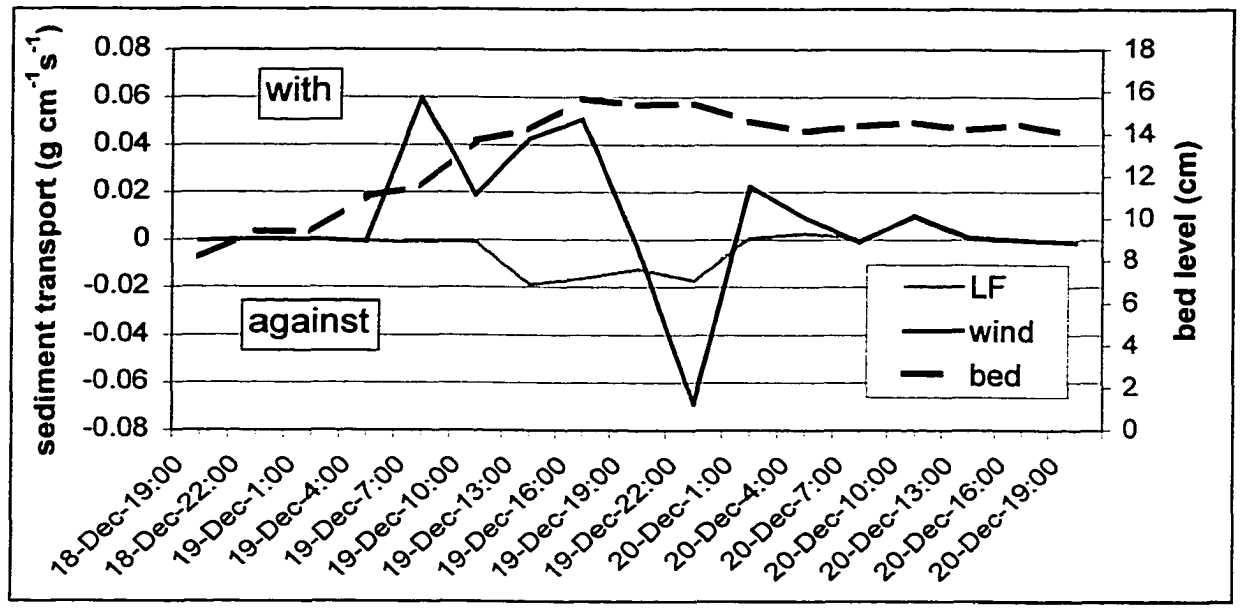

Figure 8.10: Across-shore component of wind-wave and low-frequency transport relative to the mean wave direction at Site 2 during Event W.

8.3 Summary

During a period defined as fair weather by the criteria outlined in this study, a group of very high, long-period waves propagated northward past the deployment sites. This was accompanied by rotational currents, which were qualitatively similar to those observed during local extratropical storms, although their magnitude was only slightly above the mean fair weather value. Shear velocity and sediment transport increased dramatically during this time as well, with northeasterly transport occurring as a result of mean flows, which were dominant overall. Transport at low frequencies was offshore, opposing the wave direction, while at wind-wave frequencies onshore transport occurred during the early phases of the storm and offshore transport occurred during its later stages, possibly of a result of bed form changes. It is clear from this chapter that, despite the importance of local extratropical storms during the winter, distant storms may also be responsible for increases in hydrodynamic and bottom boundary layer energy, and sediment transport on the Louisiana inner shelf.

CHAPTER 9

SEDIMENT FLUXES ACROSS SHIP SHOAL

9.1 Introduction

It is apparent that Ship Shoal exerts a significant influence on regional hydrodynamic and sediment transport patterns, and that processes on the seaward and landward sides of the shoal therefore differ. This presumably results in convergences and divergences (i.e. fluxes) of sediment across the shoal during certain conditions. Estimating these fluxes may provide an indication of the short-term evolution of the shoal in response to atmospheric forcing during the winter since convergences and divergences indicate potential accretion and erosion of the shoal, while transport at the two sites suggests the direction of shoal migration. Furthermore, as has been discussed throughout this dissertation, extratropical storms exert an important influence on coastal environments in the region, and as such, calculation of flux may provide an indication of the role of at least one factor in the long-term evolution of Ship Shoal.

The issues discussed above are important for both theoretical and practical reasons. First, as noted earlier, Ship Shoal is a conspicuous and influential bathymetric feature on the Louisiana inner shelf that reduces wave energy and modulates current velocity. Changes to its morphology are therefore closely linked with regional changes in hydrodynamics and sediment transport. Furthermore, its sandy sedimentary composition is somewhat anomalous in the regional context of the otherwise muddy Louisiana coast, and it may therefore serve as an important source of sandy sediment to adjacent barrier islands, either through natural processes or by means of human nourishment projects. Globally, the shoal is distinctive in terms of inner-shelf geology, since it formed recently

as a result of exceptionally rapid rates of coastal transgression and barrier island submergence (Penland et al., 1988). In a sense, therefore, Ship Shoal may serve as a "laboratory" in which transgressive responses over short time scales reflect long-term barrier island responses to relative sea level rise on more "typical" coasts. In light of these regional and more universal considerations, this chapter is devoted to discussing the sedimentary fluxes across Ship Shoal associated with meteorological forcing, and to speculating on the long-term fate of the shoal on this basis.

A few notes of strong caution are appropriate prior to a discussion of the results. First, it should be mentioned once again that considerable uncertainty was involved in calculating sediment transport rates at each site individually, an effect amplified when comparing two sites. Hopefully, this effect has been minimized since identical instrumentation and computational methods were used in both cases. Second, there is an inherent danger in estimating flux from instruments that are located a considerable distance away from each other, as is the case here, since sediment transport in the area between the two sites, which is unknown, may be quite different from that at the sites themselves. Despite these considerable shortcomings, sediment flux across the shoal obviously has a great deal of importance, and is therefore worthy of at least brief consideration in this dissertation.

9.2 Results

There was considerable variability in mean current and sediment flux across the shoal during the deployment, which is not surprising, given the short-term variability observed in these parameters at each site individually. Figure 9.1 represents the current flux throughout the deployment, which appears to have been predominantly divergent, aside

from a few convergent peaks, such as those accompanying Storms 2 and 6. The mean tendency toward divergence was the result of the persistent seaward current component at Site 1 and landward current component at Site 2, the cause of which was postulated in Chapter 6 to be bathymetric steering of along-shelf currents by gravity. The current convergence during Storms 2 and 6, on the other hand, occurred when flows were seaward at both sites, but were comparatively stronger at Site 2.

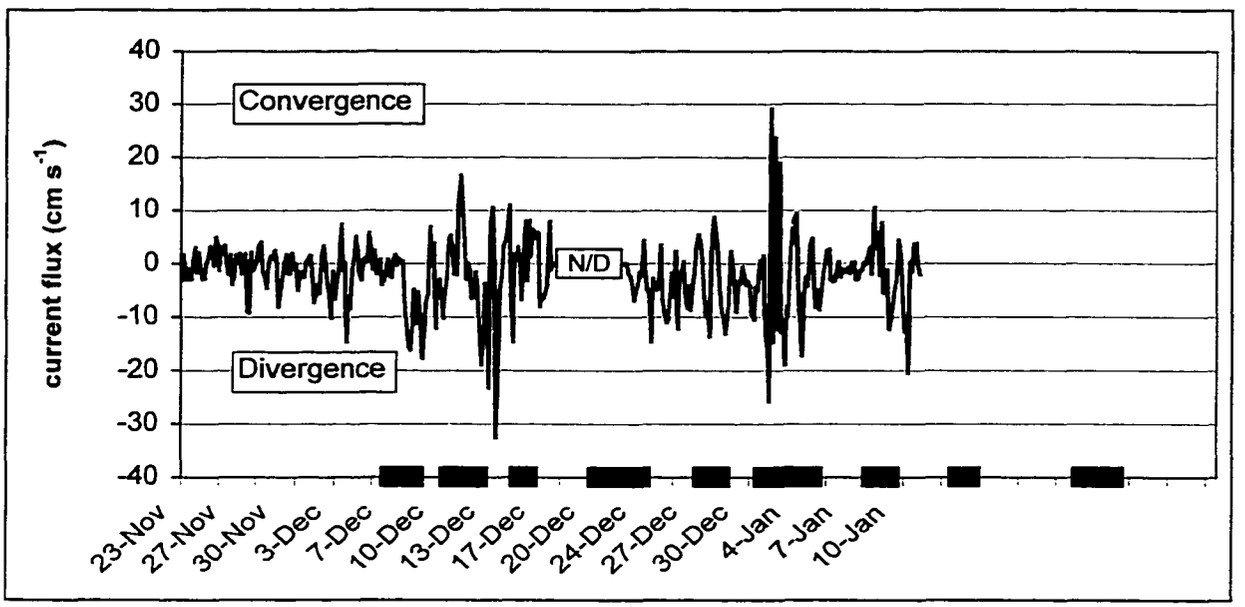

Figure 9.1: Current flux over Ship Shoal. The occurrence of storms is indicated with black arrows, and N/D represents a time for which no data are available, owing to sensor burial.

Figure 9.2 shows the flux of sediment across the shoal as calculated using the GMR and MPM methods. The pattern is similar in both cases—fairly low mean values were punctuated by high levels of episodic convergence or divergence. High-volume events often occurred in response to extratropical storms, as well as during the wave event, although storms did not always trigger large fluxes. Storms were sometimes characterized by alternating periods of convergence and divergence, and, as will be demonstrated subsequently, net storm flux was therefore much lower in volume than

might be expected. This pattern was similar to that of sediment transport at each location individually, where storms were often associated with 180° shifts in transport direction over a short time scale. Overall, therefore, sediment flux across the shoal, like sediment transport at a particular point, was highly episodic and strongly associated with atmospheric forcing.

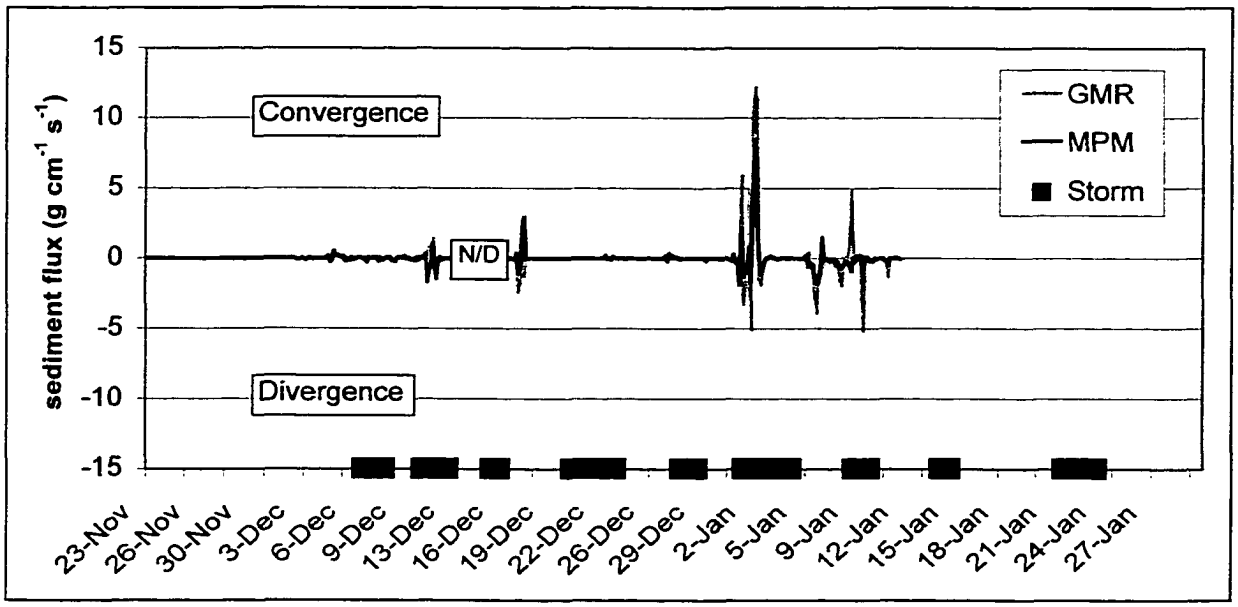

Figure 9.2: Flux of suspended and bed load sediment across Ship Shoal as calculated using the MPM and GMR methods, respectively.

Table 9.1 shows sediment flux across Ship Shoal during the deployment for all extratropical storms, fair weather, and the wave event. As expected, regularities in sediment flux over the shoal mirrored those in sediment transport at the individual sites and thus, there was considerable variation in flux depending upon both the individual storm and the computational method used. Despite these sources of variability, however, the data clearly indicate that overall, extratropical storms were associated with convergence of sediment over the shoal (accretion), while fair weather conditions were related to divergence (erosion). Unfortunately, results from the wave event are difficult to interpret, owing to missing data.

Table 9.1: Sediment flux (in mg cm^{-1} s^{-1}) across Ship Shoal during storms and fair weather as predicted from Systems1A and 2A using spectral methods and the GMR and MPM models. Negative values indicate a divergence of sediment from the shoal while positive values indicate a convergence. **As with previous data, it should be noted that data for the Storms W and 4 were incomplete, owing to sensor burial.

	Spectral				*Time-Averaged*	
	Mean	*Infragravity*	*Wind-wave*	*Sum*	*Model*	*MPM*
Storm 1	-8.6	2.8	3.0	-2.9	[illegible]	3.1
Storm 2	-7.6	1.2	7.9	17.0	31.3	-186.8
Storm 3	0.2	-0.1	-0.1	0.1	1.9	0.5
Storm 4	-5.0	4.1	-12.8	-13.0	4.4	0.2
Storm 5	-0.9	0.3	0.9	0.3	0.5	-0.3
Storm 6	36.6	4.5	-8.2	54.7	1307.9	263.5
Storm 7	25.0	-2.9	-11.2	11.2	-588.9	37.7
All Storms	13.5	**2.0**	-0.9	**16.4**	281.3	**3.0**
Fair Weather	-2.4	**0.9**	1.0	**-0.6**	-55.6	**-65.0**
Wave Event	-14.8	**-6.1**	-29.5	**-50.6**	-436.4	**540.1**

Table 9.2 shows the flux of sediment across the shoal during the extratropical storm types introduced in Chapter 7. Despite the overall tendencies noted in the previous paragraph, it is apparent that convergence tended to be associated specifically with Type 2 storms, while overall, Type 1 storms were associated with divergence. Particularly strong flux convergence occurred during Storms 2 and 6 (both Type 2 storms), apparently as a result of differences in the sediment transport rate, rather than direction, between the two sites. Specifically, although seaward transport occurred at both locations, the rate was highest at the nearshore site, suggesting that these storms may have caused seaward migration of the shoal as well as accretion. The overall flux divergence that occurred during Type 1 storms was largely the result of a single event—Storm 7. In this case, divergent flux occurred for just the opposite reason—a higher rate of seaward transport at Site 1 than at Site 2, which would also cause seaward migration. It is not clear why these different extratropical storms were associated with different transport rates at the two sites. As mentioned previously, fair weather conditions were characterized by flux

divergence over the shoal, as a result of landward transport at the nearshore location, accompanied by lower, and largely westward, transport at the seaward site. Thus, it seems that fair weather conditions cause erosion and landward migration of the shoal.

Table 9.2: Sediment flux across Ship Shoal during the three storm types.

	Spectral				Time-Averaged	
Storm Type	Mean	Low Frequency	Wind-wave	Sum	GMR	MPM
1	0.14	2.37	-8.16	-5.24	-121.83	8.67
2	29.22	3.88	10.65	47.58	867.12	165.16
3	-0.17	0.10	0.25	0.20	0.31	-6.81

9.3 Summary

In summary, sediment flux across Ship Shoal during fair weather tended to be divergent, due largely to high rates of onshore transport on its landward side, potentially resulting in shoal erosion and landward migration. In contrast, during most extratropical storms, and particularly Type 2 storms, convergent sediment transport occurred, chiefly due to strong offshore transport on the shoal's landward side, potentially resulting in shoal accretion and seaward migration. Furthermore, the sediment flux initiated by individual storms was highly variable, suggesting that a single "typical" pattern of flux due to storms may not be a realistic paradigm for the shoal. Although it appears that the annual-scale evolution of Ship Shoal may include the opposing effects of fair weather erosion/landward migration and extratropical storm accretion/seaward migration, geologic evidence indicates that the shoal has been migrating landward over the past few decades (Penland et al., 1988). Therefore, fair weather, and probably summer tropical storms, rather than winter extratropical storms, are most likely the dominant meteorological influences on Ship Shoal's long-term evolution.

CHAPTER 10

CONCLUSIONS

This dissertation research has produced numerous conclusions that relate to three general themes: 1) the nature and causes of temporal variability in hydrodynamic, bottom boundary layer, and sedimentary processes during the winter; 2) the influence of Ship Shoal on these processes; and 3) the resulting morpho-sedimentary response of Ship Shoal. Obviously, the first of these issues, which incorporates the influence of extratropical storms, the wave event, and fair weather conditions, has comprised the majority of this dissertation, a fact that will be reflected in the conclusions, subdivided by theme, which are as follows:

1. a) Hydrodynamic, bottom boundary layer, and sedimentary processes on the Louisiana inner shelf during the winter are characterized by episodic variability, largely as a result of the quasi-periodic cycle of recurring extratropical storm passages in the region.

b) Extratropical storms are generally characterized by increases in: wave height, near-bed orbital, and mean current speed, shear velocity, suspended sediment concentration, and sediment transport. Decreases in wave period and apparent bottom roughness are also apparent.

c) Typical extratropical storm phases include one or more of the following: i) a pre-frontal period of high, northerly, long-period waves, weak to moderate northerly currents, increased shear velocity, and increased sediment transport ii) a frontal period of low waves, currents, shear velocity, and variable sediment transport iii) a post-frontal period of high waves that include a short-period southerly component, strong southerly current flow, increased shear velocity, and very high sediment transport.

d) Despite these regularities, considerable variability between storms, as well as during storms themselves, is reflected in hydrodynamic, bottom boundary layer, and sedimentary processes. During strong storms, some indices were several orders of magnitude greater than during fair weather, while during weak storms they were lower.

e) As a result of this variability, the following extratropical storm classification, consisting of three storm types, has been proposed:

i) Type 1 storms are the result of strong anticyclonic activity and are characterized by weak southerly pre-frontal and strong northeasterly post-frontal winds. They generally result in strong post-frontal responses that

include high, short-period, southerly waves, strong, southwesterly currents, and moderately high sediment transport that is southwesterly overall.

ii) Type 2 storms are the result of the influence of nearby cyclonic activity, and include periods of both strong southerly pre-frontal winds and strong northerly post-frontal winds. Type 2 storms generate high, long-period northerly swell waves prior to the frontal passage that persist throughout most of the post-frontal phase, during which time energetic southerly storm waves develop, creating a complex, bimodal wave spectrum. Currents prior to the frontal passage are fairly strong and northerly, while subsequent to the frontal passage, they become rotational, likely as a result of inertial effects, but are southeasterly in direction overall. Shear velocity is elevated during both the pre- and post-frontal phases, while sediment transport occurs predominantly during the post-frontal phase, when mean sediment transport is directed southeasterly, and low-frequency and wind-wave flows produce northerly transport.

iii) Type 3 storms are weak and do not generally differ from fair weather.

f) Local extratropical storms are apparently not the only cause of high-energy responses on the Louisiana inner shelf. Distant storms, in this case referred to as wave events, apparently cause high, long-period waves, accompanied by moderate rotational currents, to impact the Louisiana inner shelf. These can create high sediment transport, which was, in the case of the example observed during this study, alongshore at mean frequencies, offshore at low-frequencies, and onshore at wind-wave frequencies.

g) Results from this study suggest that resuspension and transport of bottom sediment may sometimes occur during winter fair weather conditions, although it has previously been considered unlikely.

2. Differences between the seaward and landward sides of Ship Shoal are apparent. Waves tend to be higher and longer in period on the seaward side, while mean currents are generally higher landward, where they are directed onshore, unlike the offshore site, where seaward currents predominate. It is apparent, therefore, that Ship Shoal exerts a significant influence on regional hydrodynamics, reducing wave energy and modulating current velocity.

3. The short-term evolution of Ship Shoal appears to be the result of a balance between fair weather influences, which cause erosion and landward migration, and winter storm influences (particularly Type 2 storms), which cause accretion and seaward migration.

It is clear from this study, therefore, that although physical processes on the Louisiana inner shelf during the winter are dynamic and complex, largely as a result of extratropical storms, they are also somewhat predictable. This has implications for the long-term evolution of Ship Shoal itself as well as for the sediment budget of the

Louisiana coastal system, which is plagued by persistent land-loss problems. Much remains to be known, both in a regional context, and with respect to the universal mechanisms driving inner-shelf sediment transport.

In a regional sense, it is necessary to conduct a more comprehensive investigation of extratropical storms over the course of several years to fully assess the applicability of the proposed storm classification system, or alternatively, to develop a more quantitative scheme. In addition, greater spatial coverage of Ship Shoal would permit its influence on regional hydrodynamics to be better evaluated. More complete monitoring of bed forms in the area than was conducted during this study is necessary to better address questions of bed load sediment transport and physical bottom roughness. Finally, simultaneous measurement of morphological changes in the area as well as hydrodynamic and sedimentary process would allow causal relationships between process and response to be better described and quantified.

Study of inner-shelf processes is a fairly new field of interest, and as such, understanding is far from complete in many respects. However, a great deal of progress has been made recently, and ongoing work will undoubtedly prove to be very enlightening. The increasing sophistication of instrumentation will allow high-frequency, micro-scale measurements of flow, turbulence and sediment interaction to be made, while increasing sensor availability will allow greater spatial coverage, and a thus a better assessment of spatial variability. Ultimately, therefore, future inner-shelf research in Louisiana and elsewhere must seek to integrate microscale processes with their large-scale, long-term manifestations.

REFERENCES

Adams, C.E., Jr., D.J.P. Swift and J.M. Coleman (1987) Bottom Currents and Fluviomarine Sedimentation on the Mississippi Prodelta Shelf: February-May 1984. *Journal of Geophysical Research*, 92(C13): 14595-14609.

Adams, C.E., Jr. and G. Weatherly (1981) Suspended-sediment transport and benthic boundary-layer dynamics. *Marine Geology*, 42: 1-18.

Agrawal, Y.C. and D.G. Aubrey (1992) Velocity Observations Above a Rippled Bed Using Laser Doppler Velocimetry. *Journal of Geophysical Research*, 97(C12): 20249-20259.

Aguado, E. and J.E. Burt (1999) *Understanding Weather and Climate*, Prentice-Hall, Upper Saddle River, N.J., U.S.A: 505 p.

Amos, C.L., A.J. Bowen, D.A. Huntley, J.T. Judge and M.Z. Li (1999) Ripple Migration and Sand Transport Under Quasi-Orthogonal Combined Flows on the Scotian Shelf. *Journal of Coastal Research*, 15(1): 1-14.

Amos, C.L. and J.T. Judge (1991) Sediment transport on the eastern Canadian continental shelf. *Continental Shelf Research*, 11: 1037-1068.

Armbruster, C.K., G.W. Stone and J.P. Xu (1995) Episodic Atmospheric Forcing and Bayside Foreshore Erosion: Santa Rosa Island, Florida. *Gulf Coast Association of Geological Societies Transactions*, 45: 31-37.

Biocourt, W.C., W.J. Wiseman Jr., A. Valle-Levinson and L.P. Atkinson (1998) Continental Shelf of Southeastern United States and Gulf of Mexico. In: Robinson, A.R and K.H. Brink (eds.) *The Sea*. Vol. 11, Wiley and Sons, New York, U.S.A.: 135-182.

Boon, J.D., M.O. Green and K.D. Suh (1996) Bimodal wave spectra in lower Chesapeake Bay, sea bed energetics and sediment transport during winter storms. *Continental Shelf Research*, 16(15): 1965-1988.

Cacchione, D.A. and D.E. Drake (1982) Measurements of Storm-Generated Bottom Stresses on the Continental Shelf. *Journal of Geophysical Research*, 87(C3): 1952-1960.

Cacchione, D.A. and D.E. Drake (1990) Shelf Sediment Transport: An Overview with Applications to the Northern California Shelf. In: *The Sea*. Vol. 9, D. Hanes and B. LeMehaute (eds.) Wiley and Sons, New York, U.S.A.: 729-773.

Cacchione, D.A., D.E. Drake, J.T. Ferreira and G.B. Tate (1994) Bottom stress estimates and sand transport on northern California inner continental shelf. *Continental Shelf Research*, 14(10/11): 1273-1289.

Cacchione, D.A., W.D. Grant, D.E. Drake and S.M. Glenn (1987) Storm-Dominated Bottom Boundary Layer Dynamics on the Northern California Continental Shelf: Measurements and Predictions. *Journal of Geophysical Research.* 92(C2): 1817-1827.

Chaney, P.L. (1999) *Extratropical Storms of the Gulf of Mexico and their Effects along the Northern Coast of a Barrier Island: West Ship Island, Mississippi.* Unpublished Dissertation, Louisiana State University: 211p.

Chaney P.L. and G.W. Stone (1996) Soundside erosion of a nourished beach and implications for winter cold front forcing: West Ship Island, Mississippi. *Shore and Beach*, 64(1): 27-33.

Chuang W.S. and W.J. Wiseman, Jr. (1983) Coastal Sea Level Response to Frontal Passages on the Louisiana-Texas Shelf. *Journal of Geophysical Research*, 88(C4): 2615-2620.

Coleman, J.M., H.H. Roberts and G.W. Stone (1998) Mississippi River Delta: an Overview. *Journal of Coastal Research.* 14(3): 698-716.

Crout, R.L. and R.D. Hamiter (1981) Response of Bottom Waters on the West Louisiana Shelf to Transient Wind Events and Resulting Sediment Transport. *Transactions of the Gulf Coast Association of Geological Societies*, 31: 273-277.

Daddio, E. (1977) *Response of coastal waters to atmospheric frontal passage in the Mississippi Delta region.* Technical Report 234, Coastal Studies Institute, Center for Wetland Resources, Louisiana State University: 38p.

Davidson, M.A., P.E. Russell, D.A. Huntley and J. Hardisty (1993) Tidal asymmetry in suspended sand transport on a macrotidal intermediate beach. *Marine Geology.* 110: 333-353.

Davies, A.G. (1985) Observations of the stability of oscillatory flow above the seabed and of sand ripple formation. *Continental Shelf Research*, 4(5): 533-580.

Davies, A.G. (1995) Effects of unsteadiness on the suspended sediment flux in co-linear wave-current flow. *Continental Shelf Research*, 15(8): 949-979.

Davies, A.G. and Z. Li (1997) Modelling sediment transport beneath regular symmetrical and asymmetrical waves above a plane bed. *Continental Shelf Research*, 17(5): 555-582.

DiMego, G.J., L.F. Bosart and G.W. Endersen (1976) An Examination of the Frequency and Mean Conditions Surrounding Frontal Incursions into the Gulf of Mexico and Carribean Sea. *Monthly Weather Review*, 104: 709-718.

Dingler, J.R. and T.E. Reiss (1990) Cold-Front Driven Storm Erosion and Overwash in the Central Part of the Isles Dernieres, a Louisiana Barrier-Island Arc. *Marine Geology*, 91: 195-206.

Dingler, J.R., T.E. Reiss and N.G. Plant (1993) Erosional Patterns of the Isles Dernieres, Louisiana, in Relation to Meteorological Influences. *Journal of Coastal Research*, 9(1): 112-125.

Dolan, R. and R.E. Davis (1992a) Rating Northeasters. *Mariners Weather Log*, 36(1): 4-11.

Dolan, R. and R.E. Davis (1992b) An Intensity Scale for Atlantic Coast Northeast Storms *Journal of Coastal Research*, 8(4): 840-853.

Drake, D.E. and D.A. Cacchione (1986) Field observations of bed shear stress and sediment resuspension on continental shelves, Alaska and California. *Continental Shelf Research*, 6(3): 415-429.

Drake, D.E. and D.A. Cacchione (1992) Wave-current interaction in the bottom boundary layer during storm and non-storm conditions: observations and model predictions. *Continental Shelf Research*, 12(12): 1331-1352.

Dyer, K.R. and R.L. Soulsby (1988) Sand Transport on the Continental Shelf. *Annual Review of Fluid Mechanics*, 20: 295-324.

Earle, M.D., D. McGehee, and M. Tubman (1995) *Field Wave Gaging Program, Wave Data Analysis Standard.* U.S. Army Corps of Engineers Instruction Report CERC-95-1: 33p.

Frazier, D.E. (1967) Recent deltaic deposits of the Mississippi River, their development and chronology. *Transactions of the Gulf Coast Association of Geological Societies*, 17: 287-315.

Fredsoe, J. and Deigaard (1992) *Mechanics of Coastal Sediment Transport.* World Scientific, New Jersey, U.S.A.: 369 p.

Glenn, S.M. and W.D. Grant (1987) A Suspended Sediment Stratification Correction for Combined Wave and Current Flows. *Journal of Geophysical Research.* 92(C8): 8244-8264.

Grant, W.D. and O.S. Madsen (1979) Combined Wave and Current Interaction with a Rough Bottom. *Journal of Geophysical Research.* 84(C4): 1797-1807.

Grant, W.D. and O.S. Madsen (1982) Movable Bed Roughness in Unsteady Oscillatory Flow. *Journal of Geophysical Research.* 87(C1): 469-481.

Grant, W.D. and O.S. Madsen (1986) The Continental-Shelf Bottom Boundary Layer. *Annual Review of Fluid Mechanics*, 18: 265-305.

Green, M.O, J.D. Boon, J.H. List and L.D. Wright (1988) Bed Response to Fairweather and Storm Flow on the Shoreface. *Coastal Engineering*, 112: 1508-1521.

Green, M.O., J.M. Rees and N.D. Pearson (1990) Evidence for the Influence of Wave-Current Interaction in a Tidal Boundary Layer. *Journal of Geophysical Research.* 95(C6): 9629-9644.

Green, M.O, C.E. Vincent, I.N. McCave, R.R. Dickson, J.M. Rees and N.D. Pearson (1995) Storm sediment transport: observations from the British North Sea shelf. *Continental Shelf Research*, 15: 889-912.

Green, M.O. (1992) Spectral Estimates of Bed Shear Stress at Subcritical Reynolds Numbers in a Tidal Boundary Layer. *Journal of Physical Oceanography*, 22: 903-917.

Gross, T.F., A.E. Isley and C.R. Sherwood (1991) Estimation of stress and bed roughness during storms on the Northern California Shelf. *Continental Shelf Research*, 12: 389-413.

Gust, G. and J.B. Southard (1983) Effects of Weak Bedload on the Universal Law of the Wall. *Journal of Geophysical Research.* 88(C10): 5939-5952.

Halper, F.B. and D.W. McGrail (1988) Long-term measurements of near-bottom currents and suspended sediment concentration on the outer Texas-Louisiana continental shelf. *Continental Shelf Research*, 8(1): 23-36.

Halsey, S.D. (1986) Proposed classification scale for major Northeast storms; East Coast, U.S.A. based on extent of damage. *Geological Society of America-Abstract with Programs*, 18(1): 21.

Hanes, D.M. and D.A. Huntley (1986) Continuous measurements of suspended sand concentration in a wave dominated nearshore environment. *Continental Shelf Resesarch*, 6(4): 585-596.

Hanes, D.M. (1991) Suspension of Sand Due to Wave Groups. *Journal of Geophysical Research*, 96(C5): 8911-8915.

Henderson-Sellers, A. and P.J. Robinson (1986) *Contemporary Climatology*, Longman Scientific and Technical, U.K.: 439p.

Hill, P.S., A.R.M. Nowell and P.A. Jumars (1988) Flume Evaluation of the Relationship Between Suspended Sediment Concentration and Excess Boundary Shear Stress. *Journal of Geophysical Research*, 93(C10): 12,499-12,509.

Huntley, D.A. and D.G. Hazen (1988) Seabed Stresses in Combined Wave and Steady Flow Conditions on the Nova Scotia Continental Shelf: Field Measurements and Predictions. *Journal of Physical Oceanography*, 18: 347-362.

Huntley, D.A., R.J. Nicholls, C. Liu and K.R. Dyer (1994) Measurements of the semi-diurnal drag coefficient over sand waves. *Journal of Geophysical Research*, 14(C5): 437-456.

Hsu, S.A. (1993) The Gulf of Mexico—A Breeding Ground for Winter Storms. *Mariners Weather Log*, 37(2): 4-11.

Jaffe, B.E., J.H. List and A.H. Sallenger, Jr. (1997) Massive sediment bypassing on the lower shoreface offshore of a wide tidal inlet–Cat Island Pass, Louisiana. *Marine Geology*, 136: 131-149.

Jenkins, G. M. and D. G. Watts (1968) *Spectral Analysis and its Applications*. Holden-Day, San Francisco, CA., U.S.A.: 525 p.

Kim, S.-C, L.D. Wright and B.-O. Kim (1997) The combined effects of synoptic scale and local-scale meteorological events on bed stress and sediment transport on the inner shelf of the Middle Atlantic Bight. *Continental Shelf Research*, 17(4): 407-433.

Kitaigorodskii, S.A., M.A. Donelan, J.L. Lumley and E.A. Terray (1983) Wave-Turbulence Interactions in the Upper Ocean. Part II: Statistical Characteristics of Wave and Turbulent Components of the Random Velocity Field in the Marine Surface Layer. *Journal of Physical Oceanography*, 13: 1988-1999.

Kolb, C.R. and J.R. Van Lopik (1958) *Geology of the Mississippi deltaic plain-southeastern Louisiana*. U.S. Army Corps of Engineers Technical Report 2: 482p.

Komar (1998) *Beach Processes and Sedimentation*, Prentice-Hall, Upper Saddle River, N.J., U.S.A: 544 p.

Komar and Miller (1975) On the comparison between the threshold of sediment motion under waves and unidirectional currents with a discussion of the practical evaluation of the threshold. *Journal of Sedimentary Petrology*, 43: 362-367.

Larsen, L.H., R.W. Sternberg, N.C. Shi, M.A.H. Marsden and L. Thomas (1981) Field investigations of the threshold of grain motion by waves and currents. *Marine Geology*. 42: 105-132.

Lesht, B.M. (1980) Benthic Boundary-Layer Velocity Profiles: Dependence on Averaging Period. *Journal of Physical Oceanography*, 10: 985-991.

Li, M.Z. and C.L. Amos (1999) Sheet flow and large wave ripples under combined waves and currents: field observations, model predictions and effects on boundary layer dynamics. *Continental Shelf Research*, 19: 637-663.

Li, M.Z., C.L. Amos and D.E. Heffler (1997) Boundary layer dynamics and sediment transport under storm and non-storm conditions on the Scotian Shelf. *Marine Geology*, 141: 157-181.

Li, M.Z., L.D. Wright and C.L. Amos (1996) Predicting ripple roughness and sand resuspension under combined flows in a shoreface environment. *Marine Geology*, 130: 139-161.

Long, C.E, and J.M. Oltman-Shay (1991) *Directional characteristics of waves in shallow water*. U.S. Army Corps of Engineers Instruction Report CERC-95-1: 130 p.

Longuet-Higgins, M.S. (1980) On the distribution of the heights of sea waves: Some effects of nonlinearity and finite bandwidth. *Journal of Geophysical Research*, 85: 1519-1523.

Lynch, J.F., T.F Gross, C.R. Sherwood, J.D Irish and B.H. Brumley (1997) Acoustical and optical backscatter measurements of sediment transport in the 1988-1989 STRESS experiment. *Continental Shelf Research*, 17(4): 337-366.

Lyne, V.D., B. Butman and W.D. Grant (1990a) Sediment movement along the U.S. east coast continental shelf—I. Estimates of bottom stress using the Grant-Madsen model and near-bottom wave and current measurements. *Continental Shelf Research*, 10(5): 397-428.

Lyne, V.D., B. Butman and W.D. Grant (1990b) Sediment movement along the U.S. east coast continental shelf—II. Modelling suspended sediment concentration and transport rate during storms. *Continental Shelf Research*, 10(5): 429-460.

Madsen, O.S., L.D. Wright, J.D. Boon and T.A. Chisolm (1993) Wind stress, bed roughness and sediment suspension on the inner shelf during an extreme storm event. *Continental Shelf Research*, 13(11): 1303-1324.

Manighetti, B., and L. Carter (1999) Across-shelf sediment dispersal, Hauraki Gulf, New Zealand. *Marine Geology*, 160: 271-300.

Meyer-Peter, E. and R. Muller (1948) Formulas for bed-load transport. *International Association for Hydraulic Structural Research*, Meeting 2, Stockholm, Sweden.

Moran, J.M. and M.D. Morgan (1994) *Meteorology-The Atmosphere and the Science of Weather, 4th Edition*. MacMillan College Publishing Company, N.Y., U.S.A.: 517 p.

Muller, R.A. (1977) A Synoptic Climatology for Environmental Baseline Analysis: New Orleans. *Journal of Applied Meteorology*, 16: 20-33.

Murray, S.P., N.D. Walker, and C.E. Adams, Jr., 1993, Impacts of winter storms on sediment transport within the Terrebonne Bay Marsh Complex. *Coastlines of the Gulf of Mexico, Proceedings of the 8th Symposium on Coastal and Ocean Management, ASCE*: 56-70.

National Atmospheric and Atmospheric Administration (2000) Website Address: http://www.ndbc.noaa.gov/station_history?$station=gdil1.

Neumann, C.J., B.J. Jarvinen, C.J. McAdie, and J.D. Elms (1993) *Tropical Cyclones of the North Atlantic Ocean: 1871-1992*. National Climate Data Center: Asheville, N.C., U.S.A., 193 p.

Niedoroda, A.W. and D.J.P. Swift (1981) Maintenance of the Shoreface by Wave Orbital Currents and Mean Flow: Observations from the Long Island Coast. *Geophysical Research Letters*, 8(4): 337-340.

Niedoroda, A.W., D.J.P. Swift, T.S. Hopkins and C.-M. Ma (1984) Shoreface Morphodynamics on Wave Dominated Coasts. *Marine Geology*, 60: 331-354.

Niedoroda, A.W., D.J.P. Swift and T.S. Hopkins (1985) The Shoreface. In: Davis, R.A. (ed.) Coastal Sedimentary Environments. Springer: New York, U.S.A., p. 533-624.

Nielsen, P. (1992) *Coastal Bottom Boundary Layers and Sediment Transport*. World Scientific Publishing, New Jersey, U.S.A., 324 p.

Nittrouer, C.A. and L.D. Wright (1994) Transport of Particles Across Continental Shelves. *Reviews of Geophysics*, 32: 85-113.

Osborne, P.D. and B. Greenwood (1993) Sediment suspension under waves and currents: time scales and vertical structure. *Sedimentology*, 40: 599-622.

Osborne, P.D. and C.E. Vincent (1996) Vertical and horizontal structure in suspended sand concentrations and wave-induced fluxes over bedforms. *Marine Geology*, 131: 195-208.

Penland, S., R. Boyd and J.R. Suter (1988) Transgressive depositional systems of the Mississippi Delta Plain: a model for barrier shoreline and shelf sand development. *Journal of Sedimentary Petrology*, 58(6): 932-949.

Penland S. and K. Ramsey (1990) Relative Sea Level Rise in Louisiana and the Gulf of Mexico: 1908-1988. *Journal of Coastal Research*, 6(2): 323-342.

Pepper, D.A., G.W. Stone, and P. Wang (1998) A Preliminary Assessment of Wave, Current, and Sediment Interaction on the Louisiana Shoreface Adjacent to the Isles Dernieres. *Recent Research in Coastal Louisiana*: 35-45.

Pepper, D.A., G.W. Stone, and P. Wang (1999) Bottom Boundary Layer Parameters and Sediment Transport on the Louisiana Inner-Shelf During Cold Front Passages. *Transactions of the Gulf Coast Association Geological Societies*, 49: 432-439.

Pond, S. and G.L Pickard (1983) *Introductory Dynamical Oceanography, 2nd Ediiton.* Butterworth-Heinemann: U.K., 329 p.

Ritchie, W. and S. Penland (1988) Rapid dune changes associated with overwash processes on the deltaic coast of south Louisiana. *Marine Geology*, 81: 97-122.

Roberts, H.H., O.K. Huh, S.A. Hsu, L.J. Rouse, Jr. and D. Rickman (1987) Impact of Cold-Front Passages on Geomorphic Evolution and Sediment Dynamics of the Complex Louisiana Coast. *Proceedings of Coastal Sediments '87, ASCE*, 2: 1950-1963.

Roberts, H.H., O.K. Huh, S.A. Hsu, L.J. Rouse, Jr. and D. Rickman (1989) Winter storm impacts on the chenier plain coast of southwestern Louisiana. *Transactions of the Gulf Coast Association Geological Societies*, 39: 515-522.

Rouse, H. (1937) Modern conceptions of the mechanics of fluid turbulence. *Transactions of the American Society of Civil Engineers*, 102: 463-554.

Scruton, P.C. (1960) Delta Building and the Deltaic Sequence. *Recent Sediments, Northwest Gulf of Mexico—AAPG Symposium*: 82-102.

Shauer, U. (1987) Determination of bottom boundary layer parameters at two shallow sea sites using the profile method. *Continental Shelf Research*, 7(10); 1211-1230.

Shi, N.C. and L.H. Larsen (1984) Reverse sediment transport induced by amplitude modulated waves. *Marine Geology*, 54: 181-200.

Smith, J.D. and S.R. McLean (1977) Spatially Averaged Flow Over a Wavy Surface. *Journal of Geophysical Research*, 82(C12): 1735-1746.

SonTek (1997) *ADV Operation Manual, Firmware Version 4.0.* SonTek: San Diego, CA., U.S.A., 45 p.

Soulsby, R.L. (1987) The Bottom Boundary Layer of Shelf Seas. In: Johns, B. (ed.) Physical Oceanography of Coastal and Shelf Seas. Elsevier: Amsterdam, NDLS, p.189-266.

Stone, G.W., J.M. Grymes III, J.R Dingler and D.A. Pepper (1997) Overview and Significance of Hurricanes on the Louisiana Coast, U.S.A. *Journal of Coastal Research*, 13(3): 656-659.

Stone and Wang (1999) The Importance of Cyclogenesis on the Short-Term Evolution of Gulf Coast Barriers. *Transactions of the Gulf Coast Association Geological Societies*, 49: 478-487.

Stone, G.W. and J.P. Xu (1996) *Wave climate modeling and evaluation relative to sand mining on Ship Shoal, offshore Louisiana, for coastal and barrier island restoration.* Coastal Morphodynamics Laboratory Final Report, Louisiana State University.

Villaret, C. and J.H. Trowbridge (1991) Effects of Stratification by Suspended Sediments on Turbulent Shear Flows. Journal of Geophysical Research, 96(C6): 10,659-10,680.

Vincent, C.E. and A. Downing (1994) Variability of suspended sand concentrations, transport and eddy diffusivity under non-breaking waves on the shoreface. *Continental Shelf Research*, 14(2/3): 223-250.

Vincent, C.E. and M.O. Green (1990) Field Measurements of the Suspended Sand Concentration Profiles and Fluxes and of the Resuspension Coefficient γ_0 Over a Rippled Bed. *Journal of Geophysical Research*, 95(C7): 11,591-11,601.

Vincent, C.E., D.M. Hanes and A.J. Bowen (1991) Acoustic measurements of suspended sand on the shoreface and the control of concentration by bed roughness. *Marine Geology*, 96: 1-18.

Vincent, C.E., S.W. Marsh and M.P. Webb (1999) Spatial and temporal structures of suspension and transport over megaripples on the shore face. *Journal of Geophysical Research*, 104(C5): 11,215-11,224.

Vincent, C.E., D.J.P. Swift and B. Hillard (1981) Sediment transport in the New York Bight, North American Atlantic Shelf. *Marine Geology*, 42: 369-398.

Wiberg, P.L. and J.D. Smith (1983) A comparison of field data and theoretical models for wave-current interactions at the bed on the continental shelf. *Continental Shelf Research*, 2(2/3): 147-162.

Wiberg., P.L., D.E. Drake and D.A. Cacchione (1994) Sediment resuspension and bed armoring during high bottom stress events on the northern California inner continental shelf: measurements and predictions. *Continental Shelf Research*, 14(10/11): 1191-1219.

Worzel J.L. and C.A. Burk (1978) The Margins of the Gulf of Mexico. *American Association of Petroleum Geologists*: 403-419.

Wright, L.D., J.D. Boon, III, M.O. Green and J.H. List (1986) Response of the Mid Shoreface of the Southern Mid Atlantic Bight to a "Northeaster". *Geo-Marine Letters*, 6: 153-160.

Wright, L.D., J.D. Boon, III, S.C Kim and J.H. List (1991) Modes of cross-shore sediment transport on the shoreface of the Middle Atlantic Bight. *Marine Geology*, 96: 19-51.

Wright, L.D. (1995) *Morphodynamics of Inner Continental Shelves*. CRC Press Inc., Boca Raton, FL, USA, 241 p.

Wright, L.D. and C.A. Nittrouer (1995) Dispersal of River Sediments in Coastal Seas: Six Contrasting Cases. *Estuaries*, 18(3): 494-508.

Wright, L.D., C.R. Sherwood and R.W. Sternberg (1997) Field measurements of fairweather bottom boundary layer processes and sediment suspension on the Louisiana inner continental shelf. *Marine Geology*, 140: 329-345.

Wright, L.D., J.P. Xu and O.S. Madsen (1994) Across-shelf benthic transports on the inner shelf of the Middle Atlantic Bight during the "Halloween storm" of 1991. *Marine Geology*, 118: 61-77.

Xu, J.P. and L.D Wright (1998) Observations of Wind-generated Shoreface Currents off Duck, North Carolina. *Journal of Coastal Research*, 14(2): 610-619.

VITA

David Alton Pepper was born on April 19, 1970, in West Palm Beach, Florida, the son of Barry and Lorraine Pepper. In July, 1970, he moved to Windsor, Ontario, Canada, where he grew up, graduating from M.S. Hetherington Elementary School in 1984, and Riverside Secondary School in 1989. He enrolled at the University of Windsor in 1989, where he studied as an undergraduate for four years, excepting one year spent traveling and working in the South Pacific, graduating with a bachelor of arts in geography/environmental resource management in 1994. He returned to the University of Windsor in September, 1994 to pursue a master of arts degree in geography, specializing in coastal processes, which he obtained in June, 1996. In August, 1996, he became a candidate for the degree of Doctor of Philosophy in the Department of Geography and Anthropology at Louisiana State University. In August of 1998, David transferred to the Department of Oceanography and Coastal Sciences, from which he graduated in December, 2000. As of October, 2000, he had accepted a position as an Assistant Professor of Research in the Coastal Studies Institute at Louisiana State University.

DOCTORAL EXAMINATION AND DISSERTATION REPORT

Candidate: David A. Pepper

Major Field: Oceanography and Coastal Sciences

Title of Dissertation: Hydrodynamics, Bottom Boundary Layer Processes and Sediment Transport on the South-Central Louisiana Inner Shelf: The Influence of Extratropical Storms and Bathymetric Modification

Approved:

Major Professor and Chairman

Dean of the Graduate School

EXAMINING COMMITTEE:

Date of Examination:

October 9, 2000